The Roles of Non-polar Oil in Froth Flotation of Fine Particles

by

Hao Li

A thesis submitted in partial fulfillment of the requirements for the degree of

Doctor of Philosophy

in

Materials Engineering

Department of Chemical and Materials Engineering
University of Alberta

Abstract

Oil-assisted flotation is one of the most promising techniques in fine mineral particle recovery in the beneficiation of low-grade finely-disseminated ores. However, literature reports show that when non-polar oil is used in conjunction with different types of collectors, the flotation response is often unpredictable and does not always lead to improved fine mineral recovery. In this research, a systematic study was carried out to examine the balance of the hydrophobicity enhancing effects and the antifoaming functions of neutral oil in froth flotation. Fine hematite (-20 μm) and quartz (-15 μm) were used as mineral samples; sodium oleate (NaOl), octyl hydroxamic acid (OHA), and oleoyl hydroxamic acid (OLHA) were used as typical anionic collectors; and kerosene was used as the non-polar oil.

In micro-flotation of hematite single mineral using a custom-made glass tube where a froth layer did not exist, all three tested collectors were effective to float the hematite despite its fine size. The addition of emulsified kerosene showed a beneficial effect, particularly at high collector dosages, regardless of the type of collectors used. However, in batch flotation of either single hematite or hematite-quartz mixtures in a mechanically agitated stainless steel cell where a froth layer existed, kerosene behaved differently when used in conjunction with the three collectors. When NaOl or OLHA was used as a collector, kerosene emulsion improved the flotation performance as demonstrated by higher concentrate Fe_2O_3 grade and recovery. However, the addition of kerosene emulsion reduced concentrate weight yield, grade and recovery to a noticeable extent when OHA was used as a collector, especially at low OHA dosages.

Contact angle, particle size measurements and image analysis showed that the improved flotation recovery of the fine hematite in the absence of a froth layer was due to both the enhanced surface hydrophobicity and increased (hydrophobic) floc size after adding kerosene to a collector-treated hematite suspension. The effects

were most pronounced with the long chain collectors NaOl and OLHA, and much less in the case of the short chain collector OHA. Zeta potential distribution measurement coupled with an analysis of the interaction energies according to the extended-DLVO theory indicated that the hydrophobic interaction energies between hydrophobic hematite particles induced by NaOl or OLHA were stronger than by OHA. When kerosene was added, the hematite aggregates grew to a much larger size due to the stronger hydrophobic interaction between hematite particles and kerosene droplets when NaOl or OLHA was used, than when OHA was used.

Efficient froth flotation in a batch flotation machine, however, depends on both the mineral surface hydrophobicity and the presence of a stable froth layer. The froth stability of NaOl and OHA solutions was analysed using Bikerman method in the absence or presence of kerosene emulsion. The results showed that, in the absence of kerosene, the foamability of NaOl was much better than OHA. In the presence of kerosene, the oil droplets may stabilize or destabilize the froth layer depending on the concentration of the collector. In the batch flotation process, froth stability was related to water recovery into the froth phase. Water recovery measurements showed that froth destabilization by the addition of kerosene occurred at low collector dosages, especially when short chain collectors such as OHA was used. At higher collector dosages, the froth was generally stable. It is likely that the water drainage and froth destabilization effect by kerosene was counter-balanced by the higher hematite surface hydrophobicity, bubble surface tension gradient and stable pseudo-emulsion film, which led to more stable froth layer.

Therefore, a delicate balance exists when a neutral oil is used in froth flotation. The outcome depends on whether the beneficial effects of enhanced mineral surface hydrophobicity outweigh the detrimental effect of defrothing by the neutral oil. This study showed that when a short-chain collector such as OHA was used, the defrothing effects of neutral oil were predominant so that the combined use of neutral oil and OHA was counter-productive.

Acknowledgement

First of all, I acknowledge my sincere appreciation and deep respect to my supervisor, Dr. Qi Liu for guiding me throughout this research program. His guidance and encouragement was like a beacon lightening in the dark, showing me a way out of those confusions and difficulties. Thank you, Dr. Liu! It was my luck and honor to be his student.

My acknowledgement also extended to research associates of our research group: Dr. Xiaoli Tan and Dr. Kaipeng Wang for the discussions and suggestions on my research work. I would also like to appreciate mineral process lab instructor Dr. Mingli Cao, IOSI lab technicians Lisa Brant and Brittany Mackinnon for their assistance in lab instrument setup and training.

I would like to thank joint doctoral student Mingxia Liu from Central South University for the collaborations in the research.

I am also grateful to financial support to this research through a Collaborative Research and Development project sponsored by COREM and the Natural Sciences and Engineering Research Council (NSERC) of Canada.

Finally, I would like to thank my beloved wife Jing Xie, who married me while I am still a student and trusted me completely. This work could not been done without her patience and support. In addition, I am thankful to my dearest parents and my little sweetie Jiaqi. All my gratitude to them is beyond words. Thank you!

Table of Content

List of Tables

List of Figures

Chapter 1 Introduction

Since its invention in 1906, froth flotation has been the single most important technique used for the recovery and upgrading of value minerals. It has been used not only for the treatment of sulfide ores, but also for oxide ores of various metallic and nonmetallic minerals, rare earth minerals, salt-type minerals, coal, as well as oil recovery from oil sands and oil shales, and in waste treatment (Wills, 2011). Statistics data on froth flotation gathered by the United States Bureau of Mines show that millions of tons of ores were treated by froth flotation annually to satisfy market demands (Cooper, 1980; Varley, 1928).

As dictated by market and available technology, the rich and easy-to-treat ores are always processed first. After more than a century of intensive mining and mineral processing, the rich mineral resources are depleted and the minerals industry is facing a steady decline in ore grade, compounded by increasing complexity of mineral dissemination.

To recover value minerals from these ores, the ores have to be ground sufficiently fine to have a suitable degree of mineral liberation prior to further processing. The fine grinding produces large percentages of fine and ultrafine particles outside of optimal size range for ore dressing. As Gaudin (1957) pointed out, the flotation behaviors of fine and ultrafine minerals were very different from those of relatively larger mineral particles. Due to the unique characteristics of fine particles, i.e., small mass and high specific surface area, conventional flotation process has difficulty in recovering the fine value mineral particles with reasonable separation efficiency. The flotation performance of value minerals in terms of concentrate grade and value mineral recovery suffers a significant decline in this case. Therefore, the efficient recovery of fine minerals is becoming one of the major scientific and technological challenges in mineral processing.

Several methods have been proposed to promote fine mineral recovery. Electroflotation, dissolved air flotation and column flotation are examples based on air bubble size reduction to increase particle-bubble collision probabilities. Another school of thought focused on particle size enlargement, which can be accomplished by aggregation of fine minerals into floatable flocs by adding collectors, polymeric electrolytes and non-polar oils. The history of using non-polar oil to intensify flotation performance dates back to 1860s when bulk-oil was applied to concentrate hydrophobic sulfide from gangue minerals. Non-polar oil has since been used as a collector in the flotation of hydrophobic minerals, such as native gold, high-rank coal, molybdenite, sulfur, talc, etc. Later, in the flotation of hydrophilic oxide minerals or intermediate hydrophobic sulfide minerals, the addition of non-polar oil together or after collector addition was found to improve flotation performance in terms of higher flotation rate, lower degree of slime entrainment, lower collector consumption and most importantly, higher concentrate grade and value mineral recovery. Therefore, non-polar oil has been widely used as an auxiliary collector.

Despite its widespread applications in flotation, the effectiveness of using non-polar oil to enhance the flotation performance is still unclear. On the one hand, due to the intrinsic hydrophobicity of non-polar oil, oil droplets would preferentially attach and spread on the surface of hydrophobic particles, leading to a coverage of oil layer and higher hydrophobicity. Mineral flocs grow to form more close-fitted structure with larger floc size that can resist high shear rates by oil bridging effect. On the other hand, non-polar oil is known as an antifoaming agent that can destabilize the froths in the flotation cell. The defrothing ability of oil can be strengthened with synergistic hydrophobic particles. Therefore, when non-polar oil is added in conjunction with different types of collectors in froth flotation, the flotation response is often unpredictable.

For example, sodium oleate (NaOl), salt of long hydrocarbon chain fatty acid, is the most extensively used anionic collector in oxide mineral flotation due to its strong collecting capability. When used in conjunction with non-polar oils,

enhanced performances were observed in a number of studies. In addition to sodium oleate, long-chain petroleum sulfonates, amines, and tall oil are also widely used, alone or in combination with non-polar oils, to float fine oxide minerals. The application of another common and highly selective oxide collector, alkyl hydroxamic acids and related salts, in conjunction with non-polar oil however, was rarely discussed in the open literature. Due to their strong complexation capability with transition and rare earth metal ions, hydroxamic acids exhibited better performance than conventional fatty acids when it was used to float fine minerals. But the addition of kerosene in the batch flotation of a niobium oxide ore using octyl hydroxamic acid (OHA) was reported to have significantly deteriorated the flotation performance as recently reported in the mineral processing research group at the University of Alberta (Ni, 2013).

It is based on these controversies that the present PhD dissertation research is carried out, to systematically study the roles of non-polar oil in froth flotation of an oxide mineral using different oxide collectors.

Chapter 2 Research Objective and Approach

The main objective of this research is to understand and contrast the roles of non-polar oil in froth flotation using different collectors. To facilitate the comparison, collectors with the same polar (ionizable) groups but with different hydrocarbon chain lengths, and collectors with the same hydrocarbon chains but with different polar (ionizable) groups were studied. This rationale resulted in the selection of sodium oleate (NaOl), oleoyl hydroxamic acid (OLHA), and octyl hydroxamic acid (OHA) as collectors for the flocculation, micro-flotation and batch flotation of fine hematite (-20 μm) and hematite-quartz mixtures (1:1), using kerosene emulsion as the model oil. The differences of the three collectors in hematite floatability, concentrate yield, grade, recovery, flotation kinetics were assessed in the absence and presence of kerosene. In addition, zeta potentials and zeta potential distributions, contact angle and focused beam reflectance measurement (FBRM) particle/aggregate size measurement, as well as extended-DLVO theory calculations were used to understand the observed differences in the particle/oil droplet interactions. Froth stability studies were also conducted in the presence of oil and/or hematite particles to examine the influence of oil on froth stability.

Chapter 3 Literature Review

3.1 Fine Mineral Recovery

3.1.1 Fine Minerals

There is an optimum particle size range for maximum flotation recovery of a given mineral. In general, the optimum size range varies from 10 to 80 μm for oxide minerals and 5 to 200 μm for sulfide minerals (Trahar & Warren, 1976; Wills, 2011). Minerals with particle sizes below the optimum size range (generally below about 20 μm), which cause problems in conventional flotation, are defined as fine minerals or slimes.

The fine minerals can be divided into two categories: primary and secondary slimes. The former refers to the argillaceous mineral particles formed in mineral deposits under the action of internal geologic stress of earth or by natural erosion and weathering. Examples are limonite, chlorite and other clay minerals. The secondary slime is produced during mineral production operations such as mining, mechanical crushing, grinding, transportation and slurry conditioning.

3.1.2 Physical Aspects of Fine Minerals in Flotation

3.1.2.1 Flotation Kinetics

The particle size effect has an especially significant impact on the flotation of fine minerals. A large number of reports (Collins & Jameson, 1976; Miettinen et al., 2010; Pyke et al., 2003; Trahar & Warren, 1976) experimentally or theoretically confirmed that flotation rate decreases with decreasing particle size. The efficiency of collecting mineral particles is determined by the effects of particle size on three individual processes: (a) particle-bubble collision; (b) rupture of disjoining water

film between particle and bubble; (c) stability of particle-bubble aggregates. These factors are related by equation (1) (Derjaguin & Dukhin, 1961):

$$E_{Col} = E_C \times E_A \times E_S \quad (1)$$

Where E_{Col} is the overall efficiency of particle collection; E_C is particle-bubble collision efficiency; E_A is attachment efficiency; E_S is the probability of stabilizing particle-bubble aggregates.

Low particle-bubble collision efficiency under a given bubble size and agitation intensity is the primary reason for the low flotation rate of fine minerals in the conventional flotation process (Dai et al., 2000; Trahar & Warren, 1976; Yoon & Luttrell, 1989). As Hemmings (1980) pointed out, the efficiency of particle-bubble collision increased with increasing particle size and decreasing diameter of air bubbles,

$$E_c \propto (D_p/D_b)^n \quad (2)$$

Where D_p and D_b are the diameters of mineral particles and air bubbles, respectively; n equals to 2 in most cases.

For a successful collision, a particle has to deviate its movement trail under gravity forces, inertia forces and hydrodynamic drag forces to collide with a bubble. This involves four collision mechanisms depending on the particle size: inertia, gravity, interception and Brownian diffusion (Figure 3.1). In the case of coarse and high density particles where inertia forces dominate, decreasing particle size will perceptibly lower the efficiency of particle-bubble collision. On the contrary, for submicron particles, an increasing collision possibility between particles and

bubbles has been observed as a result of the Brownian motion (Derjaguin et al., 1984; Nguyen et al., 2006; Reay & Ratcliff, 1973; Yang et al., 1995). However, Brownian motion induced particle-bubble collision does not play a major role in froth flotation as the mineral particles of interest are usually not in the submicron range.

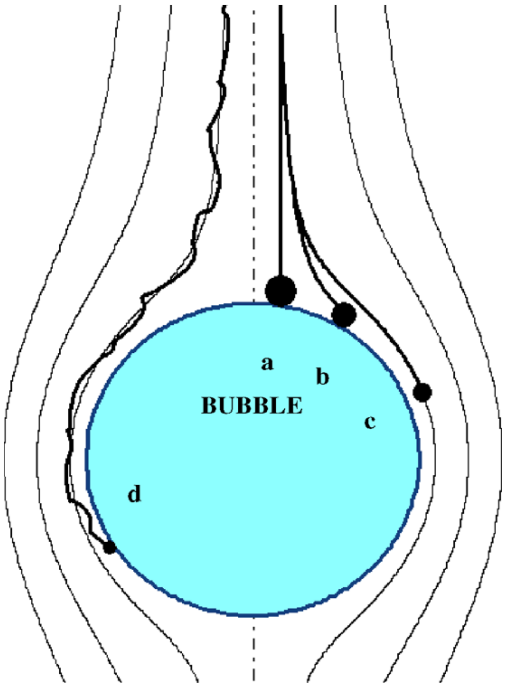

Figure 3.1 Schematic representation of inertia (a), gravity (b), interception (c) and Brownian movement (d) collision mechanisms between air bubble and particles with different sizes (Miettinen et al., 2010).

Attachment of a particle to a bubble is another physical process influenced by particle size. For a successful attachment, a particle has to a) achieve sufficient momentum to overcome the energy barrier and disrupt the intervening liquid film between particle and bubble (Whelan & Brown, 1956; Yoon & Mao, 1996); b) have a contact time (including the impact and sliding time of a particle to bubble) longer than the induction time (Schulze & Gottschalk, 1981; Sutherland, 1948). For a given particle size, experiments have confirmed higher probability of particle-bubble attachment with an increase in sliding time and decrease in induction time

of a particle (Glembotsky, 1953; Philippoff, 1952; Ye & Miller, 1988). Also, smaller air bubbles associated with shorter film drainage time also increases the particle-bubble attachment efficiency (Hewitt et al., 1995).

The stability of particle-bubble aggregates depends on the adhesion forces between particles and bubbles, disruptive shearing forces associated with the weight of aggregates and hydrodynamic conditions of agitating solutions (Gaudin, 1957). The equilibrium of the interacting forces determines the maximum size of the aggregates. The hydrophobicity of particles governs the formation of aggregates as well (Morris, 1950). It was estimated that the fine particle-bubble aggregates were much more stable than coarse particle-bubble aggregates. For submicron fine particles, the stability of aggregates is approximately equals to 1 when three phase line is formed even under turbulent environments (Derjaguin et al., 1984).

3.1.2.2 Mechanical Entrainment

Mechanical entrainment is another contributing mechanism to the fine particle recovery, in addition to the low rate of "true" flotation (Subrahmanyam & Forssberg, 1988). Entrainment is the process that fine particles entered the froth and transferred into concentrate through the inter-bubble water. It therefore has a direct link with the recovery of water (Smith & Warren, 1989). As shown in Equation (3), for fine particles, the gangue recovery by entrainment is proportional to water recovery (Engelbrecht & Woodburn, 1975):

$$R_g = e_g \times R_w \qquad (3)$$

Where R_g and R_w is the recovery of fine gangue of a given size and water respectively in a given time, e_g is entrainment factor, a constant under a given size and particle density. All particles finer than about 30 μm are affected by

entrainment (Warren, 1984). The finer the particles, the more likely they are entrained into concentrate, and less likely by true flotation (Johnson et al., 1974; Kirjavainen et al., 1991).

Therefore, from the physical point of view, with the reduction of particle size, the particle-bubble collision efficiency E_C decreases exponentially, resulting in lower flotation rate. On the other hand, decreasing particle sizes result in increased particle-bubble attachment efficiency E_A and more stable particle-bubble aggregates, so the particle size effect needs to be considered taking into account all three factors. The flotation performance can be further complicated by severe mechanical entrainment associated with an excess of stabilized froth by fine particles, and increased viscosity of mineral slurries, resulting in poor concentrate grade and value mineral recovery.

3.1.3 Chemical Aspects of Fine Minerals in Flotation

3.1.3.1 Surface Charge Effects

As the particles become increasingly finer, the effect of van der Waals force and electrical double layer force become more significant. The resulting forces can determine the tendency of aggregation/dispersion among particles. When the electrical double layer repulsion is strong, the mineral particles can stay dispersed; When the electrical double layer is thin or absent, or when the particles carry opposite charges, mineral particles can aggregate by the dominating attractive van der Waals forces. The most often seen surface charge interferences in flotation are heterocoagulation (Wang & Heiskanen, 1992; Xu et al., 2003) and slime coating (Somasundaran, 1980b), which is a phenomenon of coagulation of different mineral species. In flotation conditioning, the slurry containing multiple minerals bearing different surface charges will encounter heterocoagulation problem inevitably. Fine hydrophilic gangue would also attach to the surface of oppositely charged coarse

particles by slime coating (Parsonage, 1984), which would decrease the flotation selectivity and lower value recovery (Mitchell et al., 2005).

3.1.3.2 High Specific Surface Area and Surface Energy

The different behaviors of coarse and fine minerals in flotation mainly originate from the high specific surface areas of fine particles. Specific surface area, which is the surface area per unit volume or weight, is inversely proportional to particle size. As the particles become smaller, the ratio of edges, corners, cracks, dislocations and other crystallographic imperfections of particle surface increase, which results in high surface energy of particles (Welch, 1953). Several factors such as non-selective adsorption of reagents, fast surface oxidation in the case of sulfides, increased hydration and increased solubility of complex minerals are claimed to be the consequences of high surface energy of fine particles (Collins & Read, 1971; Klassen & Mokrousov, 1963). These results will inevitably influence the flotation performance.

3.1.3.3 High Solubility

The dissolution from the surface of fine particles can be predicted by modified Kelvin equation:

$$RT\ln\left(\frac{S_R}{S_O}\right) = 2\gamma_{sl}\frac{V}{R_P} \qquad (4)$$

Where R is the universal gas constant, which equals to 8.314 J/(K · mole); T is the absolute temperature in K; γ_{sl} is particle-liquid interfacial energy; V is molar volume; S_R is the solubility of particle of size R_P; S_O is the bulk solubility of coarse particle.

As can be seen from Equation (4), the solubility of particles depends on the magnitude of γ_{sl}, which is in the order of 0.1 J/m^2 for salt minerals (Walton et al., 1967) and 0.13-0.4 J/m^2 for silica (Iler, 1955). According to Trahar and Warren (1976), mineral particles with γ_{sl} of about 0.1 J/m^2 were unlikely to have an enhanced solubility when the particle sizes were larger than 0.1 μm. The differences in solubility between fine and coarse particles will be less than 10% (Rajagopalan & Hiemenz, 1997). Hence, the fine particles in the size range of 0.5-10 μm should have similar solubility as the coarse particles theoretically. But during the crushing and grinding processes, because of the generation of sharp edges and imperfections of particle surfaces, as well as the turbulent dynamic environment of slurry, the solubility of fine particles in water is significantly enhanced (Lidstrom, 1968; Rajagopalan & Hiemenz, 1997). The increased solubility will introduce undesired impurities in the flotation system, leading to increased concentration of ionic components, therefore, unavoidably affecting interactions between value minerals and collectors. For example, chemical transformations between dissolved components and mineral surfaces caused different minerals to possess similar surface potentials and similar flotation behaviors (Ananthapadmanabhan & Somasundaran, 1984). Also, dissolved metallic ions may activate gangue minerals, making flotation separation more difficult (Finkelstein, 1997; Finkelstein & Allison, 1976; Fornasiero & Ralston, 2005).

Overall, the relationship between the physical and chemical properties of fine particles and their behaviors in froth flotation is depicted in Figure 3.2, which elucidates the causes and effects of the above mentioned influences in flotation by fine particles.

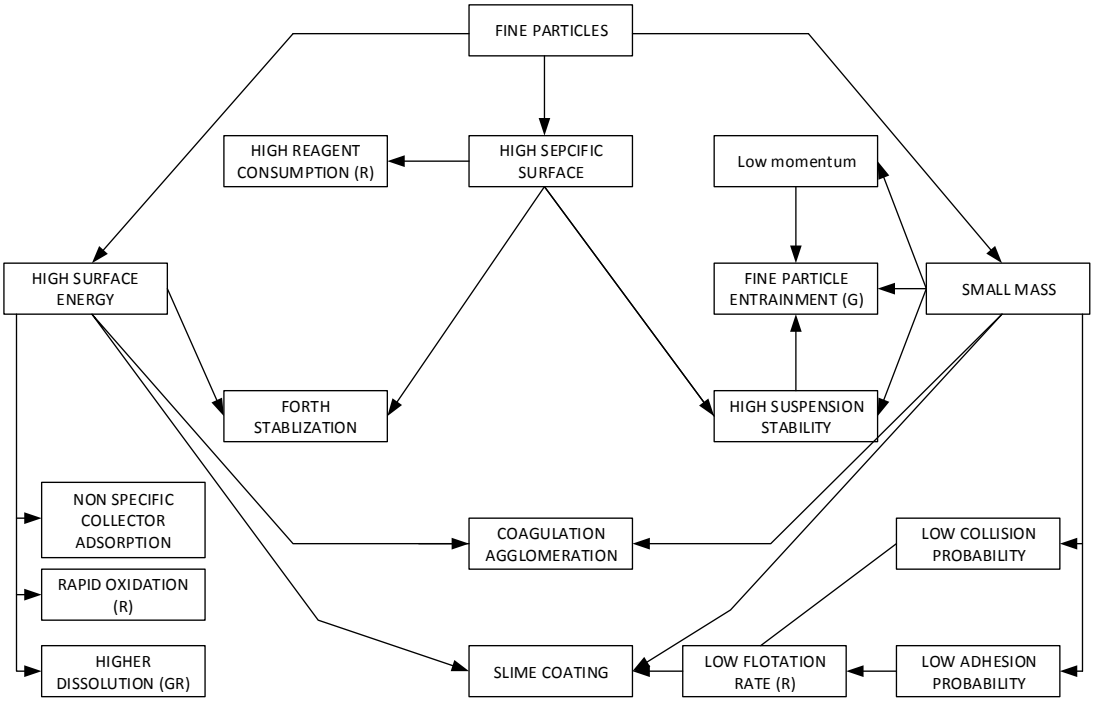

Figure 3.2 Schematic diagram showing the relationship between physical and chemical properties of fine particles and their behavior in flotation. (G) and (R) refer to whether the phenomenon affects the grade or recovery, separately (Fuerstenau, 1980).

3.1.4 Fine Particle Recovery Methods

It is seen from the foregoing discussion that fine mineral particles cannot be efficiently treated by conventional flotation techniques. Various methods have been proposed in the past to deal with the fine particle beneficiation problems. The major approaches in the fine particle flotation techniques can be summarized into two groups: those processes that are based on a reduction of bubble size to increase collision and adhesion probabilities; and those which are based on aggregation of fine particle to be floated using regular-sized bubbles (Miettinen et al., 2010; Somasundaran, 1980a).

3.1.4.1 Reduction of Bubble Size

Conventional industrial flotation machine with either self-aeration caused by mechanical agitation, or compressed air injection into the bottom of the flotation tanks is not efficient to collect particles less than 20 μm, as the bubble size distribution is not well controlled even with the use of strong frothers. Smaller bubbles help the flotation of fine particles. The generation of fine bubbles in flotation cells by electrolysis, or electroflotation, is the example of this approach. It improves collection of fine particles by the longer residence time of the smaller bubbles and increased collision probability. Column flotation technology was also employed by this mechanism to create counter current flow to help recover fine particles. Dissolved air flotation, by releasing the pressure of pre-pressurized slurry or by evacuating a flotation pulp, avoids the particle – bubble collision step by direct nucleation on hydrophobic particle surfaces. These are described in more details below.

Electroflotation

To recover fine particles, extremely fine bubbles are needed to help improve collision efficiency. Such bubbles can be generated by in situ electrolysis in a modified flotation cell. Electroflotation was originally utilized in the cleaning of wastewater to help remove fine particles that are difficult to remove by sedimentation tanks or conventional filters (Fukui & Yuu, 1980). It had its first application in mineral beneficiation in 1946 to recover fine minerals in the former Soviet Union (Matis & Backhurst, 1984). Direct current is passed through the slurry within the cell by two electrodes, generating a stream of oxygen (Equation (5)) on the anode and hydrogen bubbles (Equation (6)) on the cathode. The majority of bubbles are in the range of 10 – 60 μm, which is far smaller than bubbles in conventional mechanical flotation machines where bubble sizes range from 0.6 to 1 mm or larger (Wills, 2011). The bubble flux can be manipulated by changing

current density and the types of metal electrodes to yield optimum bubble size and distributions as well as froth depth (Bhaskar Raju & Khangaonkar, 1984).

$$H_2O \leftrightarrow 2H^+ + \frac{1}{2}O_2(g) + 2e^- \qquad (5)$$

$$2H_2O + 2e^- \leftrightarrow 2OH^- + H_2(g) \qquad (6)$$

These electrolytic gases can be used separately or together or in combination with air bubbles in the flotation (Miettinen et al., 2010). In the case of salt and oxide minerals, the flotation rate is mainly governed by bubble size and bubble flux. The types of generated bubbles does not have specific effect on the particle surface (Glembotskii et al., 1975; Ketkar et al., 1991). But in the case of sulfide minerals, the surface of these minerals go through physicochemical changes in the electroflotation cell, which can significantly influence the floatability. For example, collection of pyrite in the work of Glembotskii et al. (1975) can reach up to 98% without adding xanthate collector when using liberated oxygen bubbles during electrolysis. The author detected an increasing amount of Fe^{2+} and SO_4^{2-} ions in the solution and elemental sulphur on the surface of pyrite minerals, proving that oxidation-reduction reactions happened on the surface of mineral particles with the involvement of oxygen. Similar results were also found in the flotation of chalcopyrite using electrolytic oxygen (Raju & Khangaonkar, 1982, 1984) and cassiterite flotation using electrolytic hydrogen bubbles (Hogan et al., 1979; Mamakov et al., 1970).

Despite the observed advantages of electroflotation which is more effective in treating fine particles, it has significant shortcomings that prevented its widespread commercial application. The energy consumption of electroflotation per ton of ore treated is typically very high. For instance, in the flotation of sphalerite, the energy

consumption processing a ton by electroflotation is twenty times more than that of conventional flotation (Llerena et al., 1996). Besides, the control of pH is also problematic since hydroxyl and hydrogen ions are continuously released into the system (Bhaskar Raju & Khangaonkar, 1984). The higher the current density, the higher the variations of pH in the slurry. Un-adsorbed reagents could also be affected by liberated bubbles as well.

Dissolved Air Flotation

Dissolved air flotation, or DAF, is a mature technique in treating water, wastewater and domestic sewage, and now gradually entering in mineral processing area. A typical DAF unit is shown in Figure 3.3. Air bubbles are dissolved in recycled water stream through a tower type air saturator, and released from the diffuser nozzles into numerous tiny air bubbles. With the aid of microbubbles, the flocculated particles and suspended solids will concentrate in the froth layer as sludge and removed into desludging trough. The principle of DAF is based on Henry's law, where the solubility of air in water is proportional to the partial pressure of air at constant temperature. By releasing pretreated supersaturated slurry, the dissolved air molecules will precipitate out as tiny bubbles. Also, the bubbles can be precipitated by decreasing the pressure of slurry using vacuum evacuation (vacuum flotation). In treatment of fine particles, microbubbles will nucleate either on the surfaces of particles (Solari & Gochin, 1992) or be trapped physically inside the flocs (Carissimi & Rubio, 2005; Owen et al., 1999; Rubio et al., 2002); Thus, they can directly attach on the surface of particles and skip the step of particle-bubble collision.

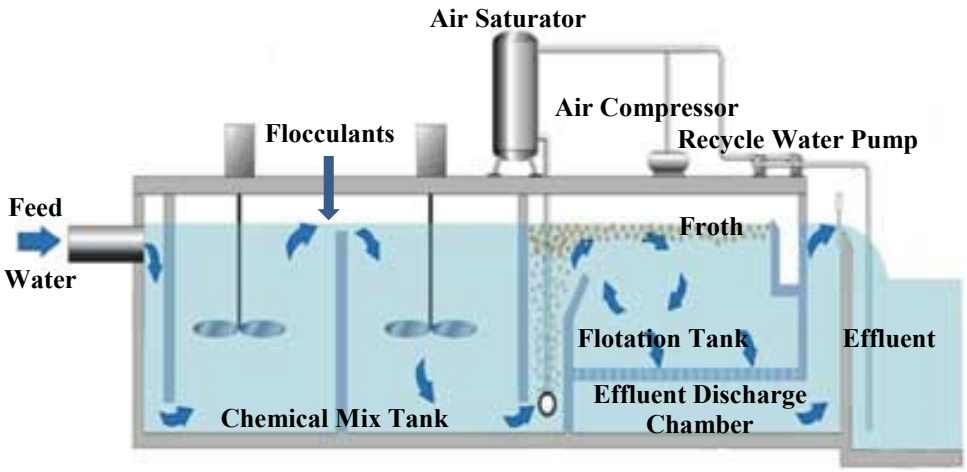

Figure 3.3 Process flow diagram of dissolved air flotation (DAF) (Wong, 2013).

Even though bubble nucleation or entrainment is independent of the nature of particles (Zhou et al., 1997), microbubbles will still preferably precipitate on the surface of hydrophobic particles (Rubio et al., 2003). The separation study of Solari (1980) indicated that fine cassiterite particles can be selectively collected from cassiterite/quartz mixtures by DAF. The main factor influencing the selectivity, besides operational parameters, is the surface chemical characteristics of both minerals in the presence of a collector.

However, the application of DAF in mineral processing was not very successful because of the low lifting power of the fine bubbles and the low air volume produced for coarse and heavy particles (Solari, 1980), and the problem was worse at high solid concentrations. Later, Yalcin et al. (2002) solved this problem by combing conventionally produced air bubbles from gas spargers at the bottom of the cell with microbubbles from dissolved air in the flotation pulp, where pressurized water was pre-mixed within. The separation efficiency was high, compared with dissolved air flotation or conventional flotation alone, especially for fine particles. This may be due to the presence of nucleated microbubbles on the surface of particles, leading to a promoted attachment efficiency between particle and regular-sized air bubbles (Mishchuk et al., 2002, 2006). However, Cotnoir et

al. (2005) noticed that a great amount of water along with slime as recovered into the concentrate. The microbubbles by DAF aggravated the problem of fine gangue entrainment during the flotation process. It is unlikely that DAF can find any practical application unless this entrainment problem is solved. So far, DAF is mainly utilized in wastewater treatment for suspended solids removal where no selectivity is needed (Matis, 1994).

Column Flotation

Column flotation technology was developed and commercialized in the 1980s to improve ultrafine particle recovery (Honaker & Mohanty, 1996). In a flotation column (Figure 3.4), fine bubbles are generated at the bottom of column and rise continuously upwards, and the mineral feed is introduced at approximately one third of the height from the top.

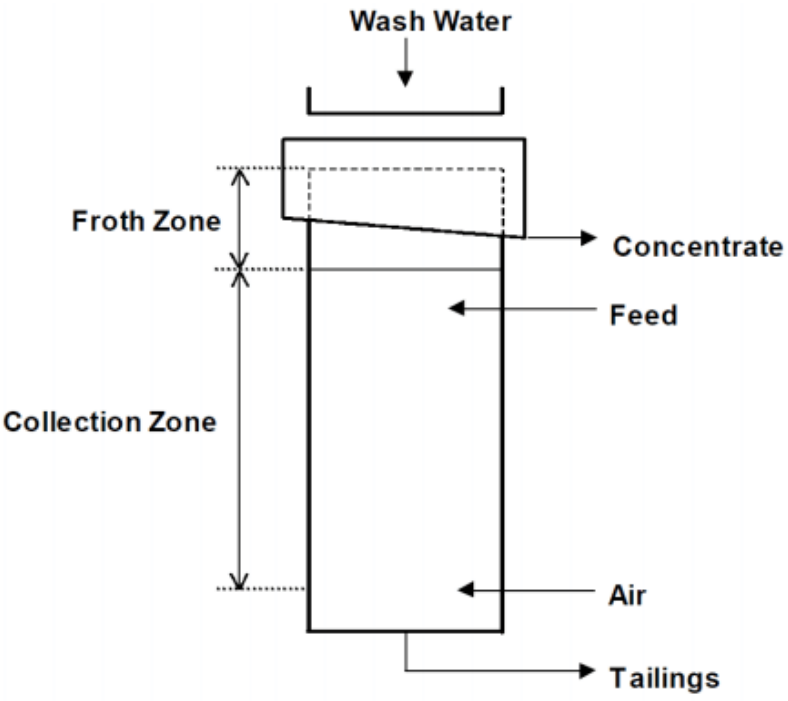

Figure 3.4 Schematic representation of a flotation column (Michaud, 2016).

Compared with conventional mechanical cell flotation, column flotation technology has many technical advantages. The countercurrent flow of the mineral and bubbles streams increases the contact time of fine minerals and bubbles, which improves the particle – bubble collision efficiency (Dobby & Finch, 1986; Yoon et al., 1989), leading to high recovery of value minerals. The hydraulic entrainment of gangue particles, which is inherent to mechanical cell flotation, is also reduced due to the rinsing of the mineralized bubbles by wash water (Falutsu & Dobby, 1989; Finch & Dobby, 1994). This leads to high froth product grade.

Narasimhan et al. (1972) used graphite and clay samples to verify the improved selectivity in column flotation compared with mechanical cells in laboratory testing. They showed that the grade of graphite concentrate after one rougher and four cleaner flotation in mechanical flotation cells is equivalent to one single stage rougher in a column cell. In addition to excellent metallurgical performance, low capital costs, easier operation and better adaptability to automatic control are other advantages of using column flotation technology (Rubio, 1996). However, poor results of column flotation were obtained when coarse particles exist in the feed (McKay et al., 1986; Somasundaran, 1986), mainly because of relatively low residence time of large particles and low lifting power of fine bubbles. In addition, the middling product has a high probability to report to the froth by the counter-current particle – bubble collision environment, especially for those small unliberated hydrophobic particles that can be recovered by bubble attachment. Improvements have been made by a multi-stage cleaning circuit to achieve better selectivity.

3.1.4.2 Fine Particle Enlargement

It is now theoretically and experimentally clear that flotation rate increases with increasing particle size. Trying to increase particle size and lower surface energy by particle aggregation has been studied for many years, and many techniques have been developed. Particle size enlargement can be accomplished by adding

collectors, polymeric electrolytes and non-polar oils. Depending on the subsequent particle separation method employed, the techniques can be divided into two major categories: selective aggregation, and floc flotation. These methods are reviewed below.

Selective Aggregation

Selective aggregation of ultrafine particles in suspension can be achieved by one of two major methods (Attia, 1982). The first method is selective coagulation, which causes aggregation by adding simple electrolytes to compress particle electrical double layer and the formed aggregates are known as coagula. It is based on the differences of slow coagulation rates of different particle components. In addition, all the particles should carry the same sign of surface charge to avoid heterocoagulation. The second method to aggregate fines is through adding long chain organic polymeric reagents that bind the fine particles of one component together from the mixture by a bridging mechanism. This method is named selective flocculation and the aggregates are known as flocs. It is controlled primarily by the interactions between polymer molecules and particles and potentially more selective than selective coagulation (Gaudin et al., 1942). Polymer flocculation has been claimed to be one of the most promising approaches in industrial separation of fine valuable minerals from run-of-mine ore as well as in non-mineral systems.

Generally, the flocculent polymers have a high molecular weight. Polyacrylamide, polyvinyl alcohol and polyethylene oxide are the major high molecular weight polymers. They can physically adsorb on many particles by electrostatic and/or hydrogen bonding forces, thus should be carefully controlled in the solution through adjusting pH and chemical compositions of the suspension. If functional groups are introduced into the polymer structure that can chemisorb on metallic sites at the mineral surface, the selectivity will be improved significantly. The cross-linked starches incorporated with carboxylate, diethanolamine, xanthate

groups are the typical cases of chemisorbing flocculants (Attia, 1977; Termes & Wilfong, 1985).

The selective flocculation involves the following four steps (Mathur et al., 2000). (1) stable dispersion of fine particles in the slurry by adding dispersants; (2) selective adsorption of polymer molecules on particles of choice; (3) floc growth under certain agitation speed; (4) separation of flocs from suspended slurries through flotation, sieving, sedimentation or other necessary separation methods. It is similar to conventional flotation in several ways. The selectivity of flocculation can be achieved by the functional groups incorporated in the polymer structure that was specific to the metallic site on the desired mineral surface (Clauss et al., 1976; Sresty & Somasundaran, 1977). This is very much like the role of functional groups in collectors. Also, the selectivity of flocculation may be controlled by using additives that can complex with dissolved interfering ions or adsorb on mineral particles selectively, acting in a manner similar to regulators in flotation (Attia & Kitchener, 1975). For example, by adding sodium hexametaphosphate and sodium fluoride, Read (1972) was able to successfully separate hematite/quartz mixtures selectively with anionic polyacrylamide. Similarly, Attia and Kitchener (1975) reported a case of selective flotation of copper oxide minerals. After pretreating the copper oxide minerals slurry with sodium sulfide and other surfactant, the induced hydrophobic particles were selectively flocculated and collected by polymeric xanthate. It is worth noting that these additives including the flocculant itself should not interfere with each other or with the following processing steps in order to achieve satisfactory results (Rubio & Kitchener, 1977).

Successful commercialization of selective flocculation processes in flotation has been reported previously (Colombo, 1980; Shi, 1986; Williams et al., 1997). However, not much development has been reported in recent years. The problem of finding truly selective organic polymers or effective reagent schemes is still the limitations of this process (Rubio & Kitchener, 1977; Rubio & Marabini, 1987). In addition, successful results of selective flocculation were often observed in

laboratories using single mineral suspension, but the selectivity is often lost with mineral mixture tests. Even when the mineral mixture tests are successful, the reagent schemes eventually fail in real ore testing or plant scale tests. This may be caused by heterocoagulation, interference from dissolved ions, slime coating, physical entrapment, mechanical entrainment, or cross-contamination during the size reduction process (Moudgil et al., 1987; Yu & Attia, 1988). Therefore, a correct choice of pretreatment as well as proper combination of the dispersants and flocculent polymers are the perquisite for a successful selective flocculation process.

Floc Flotation

If individual particles, with natural or induced hydrophobicity, are able to form aggregates in an aqueous suspension, their probability of being collected by froth flotation would increase significantly due to higher momentum of aggregates and high probability of particle/bubble collision and adhesion. Flotation procedures based on this concept is named as floc flotation (Rubin, 1972; Rubin & Haberkost, 1973). A prerequisite for floc flotation is that the floc formation should be selective. These flocs are generally held together through hydrophobic interactions between particles, sometimes supplemented by kinetic energy input through mechanical agitation (Koh & Warren, 1980; Warren, 1984, 1992). Non-polar oils are often added to the slurry to enhance the degree of hydrophobicity of particles. Compared with selective coagulation and flocculation, hydrophobized flocs are more close-fitted in froth flotation due to more compacted floc structure and higher strength that can resist shear forces that could otherwise break the flocs (Song et al., 2001b).

The floc flotation technique can be further divided into shear flocculation flotation, carrier flotation and oil assisted flotation (Fuerstenau, 1980; Hoover & Malhotra, 1976; Lai & Fuerstenau, 1968; Rao, 1997; Warren, 1992), as shown in Figure 3.5. The mechanism of shear flocculation flotation is not very different from that of carrier flotation. The only difference is that in carrier flotation, the flocs can be aggregated additionally by introduced foreign coarse particles acting as carrier

particles. For example, using coarse calcite minerals (approximately 60 μm in size) as carrier particles to aggregate with fine anatase from minus 2 μm kaolin suspension is the mostly studied example of carrier flotation (Wang & Somasundaran, 1980; YOON & SHI, 1986).

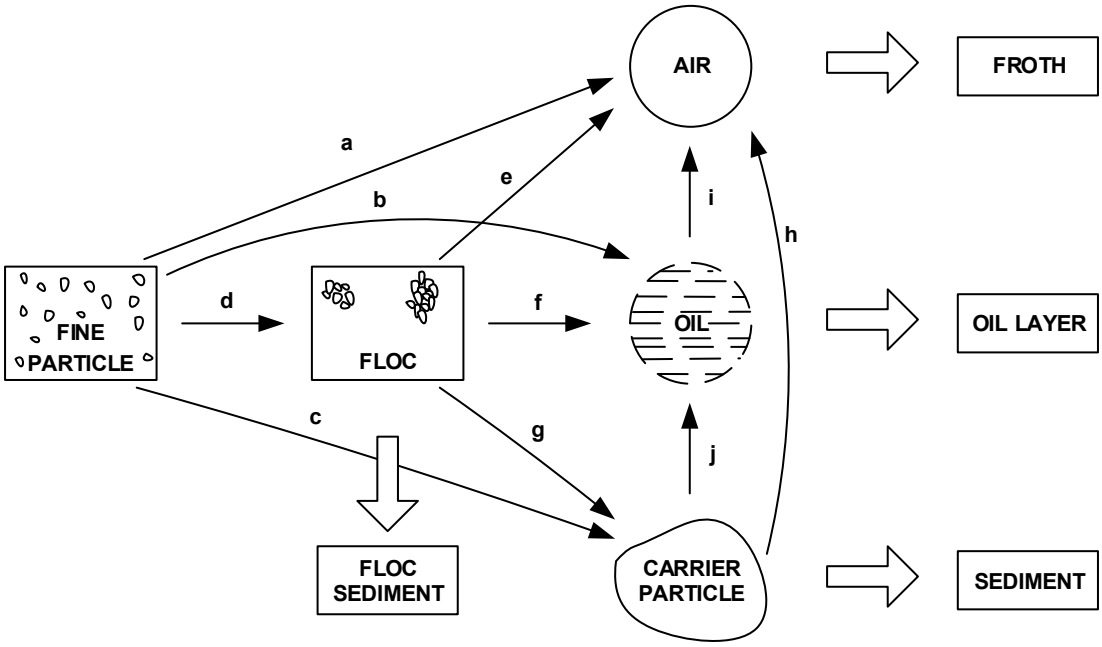

Figure 3.5 Schematic representation of separation methods based on surface activity and wettability. Froth flotation, a; Oil extraction and/or spherical agglomeration, b, d-f; Heterocoagulation, c; Selective flocculation, d; Flocculation flotation, d-e; Carrier flotation, c-h, c-j, c-j-i; Oil-assisted method, b-i, d-f-i (Somasundaran, 1980a).

Floc flotation has been used in a wide range of minerals and attracted a lot of attention due to its unique advantages. The compiled data of Table 3.1, obtained from Hu et al. (1987, 1988), gave the results of recoveries of several minerals by conventional flotation and carrier flotation, which shows that the latter is promising. However, like in conventional flotation, Attia (1982) observed high entrainment of fine gangue by floc flotation, which is an adverse aspect that needs to be addressed. Liu et al. (2004) proposed an idea of reducing hydraulic gangue entrainment by enlargement of fine hydrophilic gangue particles, by depressant polymers. They realized that it is not sufficient to control the amount of fine gangue in the concentrate only by the hydrophilizing effect of the depressant. The fine gangue

particles also need to be aggregated by hydrophilic polymers in order to lower their entrainment. Cotnoir et al. (2005) reported that by using depressant polymers, it is possible to flocculate hydrophilic fine gangue without affecting flotation recoveries of value minerals.

Table 3.1 Comparison between conventional flotation and carrier flotation (Hu et al., 1987, 1988).

Ore		Grade of feed (%)	Conventional flotation		Grade of feed (%)	Carrier flotation	
			Conc. Grade (%)	Conc. Rec. (%)		Conc. Grade (%)	Conc. Rec. (%)
Wolframite	WO_3	0.3	21.8	44.2	0.3	28.1	59.1
oxidized Pb-Zn sulfide ore slime	Pb	3.2	5.2	84.4	3.2	10.3	94.2
	Zn	5.6	10.1	96.7	5.5	21.0	98.2
Malachite	Cu	2.9	7.6	63.0	2.9	20.8	91.4
Cassiterite slime	Sn	0.4	0.6	64.0	0.4	2.8	57.5
Hematite	Fe	34.5	61.2	82.3	34.5	65.5	87.9
Slime-Fe	Fe	18.7	20.8	85.6	18.7	22.8	86.5
oxidized sulfide copper ore	Cu	2.3	15.0	35.0	2.0	24.9	81.2

Oil-assisted Techniques

The history of using oils in mineral processing can be traced back to a century ago even before the start of air bubble froth flotation. As a long known phenomenon, the use of non-polar oil in its native state or in emulsified state has been proven successful. Depending on the dosage of oil, slurry conditioning status and the separation techniques, oil-assisted flotation techniques, as shown in Table 3.2, can be classified into extender flotation, agglomeration flotation and emulsion flotation,

in addition to oil agglomeration and liquid/liquid extraction that use sizing and phase separation methods as a mineral separation technique (Finkelstein, 1979).

Table 3.2 Characteristics of oil-assisted mineral separation processes (Laskowski, 1992).

Technique	Ionic collector	Oil	Oil dosage (kg/t)	Conditioning	Method of separation
Extender flotation	Yes	Yes	0.05-0.5	Regular	Flotation
Agglomeration flotation	Yes	Yes	A few kg/t	Intense	Flotation
Emulsion flotation	No	Yes	Up to a few kg/t	Regular	Flotation
Oil agglomeration	Depends*	Yes	5-10%	Slow/intense shearing	Sizing
Liquid/liquid extraction	Yes	Yes	High	Intense	Phase separation

*Ionic collector is not required in the oil agglomeration of naturally hydrophobic minerals, but needed in treating hydrophilic minerals.

Extender flotation is used to improve the flotation performance of coarse particles by enhancing the surface hydrophobicity of minerals with some degree of aggregation (Laskowski & Dai, 1993; Laskowski & Wang, 1997). Small amount of hydrocarbon oils may be added together or after collector in the oil extender processing (Duong et al., 2000; El-Shall et al., 2000). These small oil droplets firstly collide with mineral particles. If the particle is hydrophobic, the oil droplets may spread out as a layer on the mineral surface that eventually leads to aggregation. The word “extender” generally refers to the spreading step of the oil film (Rubio et al., 2007).

Agglomeration flotation is considered a combination of agglomeration and froth flotation. It is mainly used to recover fine particles that are difficult to collect by conventional flotation. In order to enlarge the differences of surface properties of desired minerals and gangue minerals, oils are utilized to increase particle size by bridging particles together after surface hydrophobization with appropriate collectors. Meanwhile, gangue minerals remain dispersed in the slurry. The agglomerates are then recovered from the slurry by froth flotation.

Emulsion flotation, different from agglomeration flotation that recover both inherent (Jiangang et al., 2012; Sahinoglu & Uslu, 2008; Sen et al., 2005) and induced hydrophobic particles (Cebeci & Sönmez, 2004; Sönmez & Cebeci, 2003a, 2003b), can only be applied to treat inherent hydrophobic particles like gold, coal, talc, molybdenite, etc. (Laskowski, 1992). In this process, immiscible hydrocarbon oils take the role of ionic collectors and frothers and are utilized to improve the attachment of hydrophobic particles to bubbles in a way similar to oil agglomeration flotation (Laskowski & Yu, 2000).

The above oil-assisted techniques belong to a family of flotation techniques that recover minerals by attachment of air bubbles. Non-polar oils, from a very small amount up to a few kg/ton, depending on the characteristics of minerals, are utilized to help aggregate particles into optimized flotation sizes. If the dosage of oils is further increased, the agglomerates may become too heavy to be uplifted by air bubbles, making separation by flotation impossible. In this case, oil agglomeration can be used to separate the hydrophobic particle aggregates from slurry mixtures by selective settling (Capes & Germain, 1982; Mehrotra et al., 1983). If oil dosage continues to increase to the level that exceeds a few times the volume of mineral particles, a mineral-water-oil three-phase system can be formed. Natural or induced hydrophobic particles will be transferred into the oil phase from the water phase, and the hydrophilic gangue minerals remain dispersed in water. Particles with intermediate wetting ability accumulate at the oil/water interface. This process is

known as liquid/liquid extraction (Shergold & Stratton-Crawley, 1981; Stratton-Crawley & Shergold, 1981).

3.2 Oil-assisted Flotation

3.2.1 Non-polar Oils

Non-polar oils are water-immiscible hydrocarbon mixtures extracted from crude oil. Oil products generally do not have a defined chemical composition because of the differences in physical and chemical characteristics of the crude oil from which they are recovered (Srdjan, 2007). The major compositions of non-polar oil in terms of molecular structures can be classified as n-paraffins, C_nH_{2n+2}, iso-paraffins, C_nH_{2n+2}, naphthalene C_nH_{2n}, and aromatics, C_nH_{2n-6} (Hobson & Pohl, 1973).

The products of petroleum distillation fractions are divided into light distillates, intermediate distillates, heavy distillates and residues according to ASTM standard. Light distillates are the petroleum product at boiling range from 93°C to 204°C. Its fraction consists of C5-C6 hydrocarbons including liquefied petroleum gas, gasoline and naphtha. Intermediate distillates are the product at 204-343°C boiling range. The product mainly composed of jet fuel, kerosene, diesel and No. 2 fuel oil. Heavy distillates such as C20-C70 lubricating oils, heavy mineral oils, heavy flotation oils and waxes are produced at the highest boiling range of 343-566°C. Residues are the non-distillable pitch remaining after all the other distillates are removed. They include residual fuel oil, asphalt and petrolatum, which are the mixtures of very high molecular weight paraffins, polycyclic hydrocarbons, condensed polyaromatics and other impurities.

The most frequently used non-polar oils in mineral flotation are kerosene, diesel, transformer oil, synthetic hydrocarbon oil and other fuel oils characterized by the hydrocarbon chain length from C9 to C20 (Speight, 2014). The elements of the hydrocarbons are bonded by covalent forces and do not react with water diploes or

metallic sites on mineral surfaces, exhibiting prominently hydrophobicity, immiscibility and non-ionizing characteristics in aqueous solutions. Therefore, non-polar oil is often referred to as neutral oil although the oil droplets usually carry a negative charge. Unlike non-polar oils, hydrocarbons that contains sulphur, nitrogen, oxygen or metallic constituents exhibit powerful heteropolar "surface active" characteristics and can influence the flotation performances in different ways and are thus excluded from the discussion.

3.2.2 Basic Characteristics of Non-polar Oil

The density of hydrocarbon oil is closely related to the C/H ratio and the extent of cyclic and aliphatic compounds in petroleum (Seitz & Kawatra, 1986). Generally, the density of petroleum and its distillates are slightly lower than water and vary in the range between 0.75 and 1.0 g/cm^3, with a higher density fraction containing higher cyclic hydrocarbons. Oils of lighter or heavier density can be divided into two catalogues, depending on the flotation performances (Botsaris & Glazman, 1989; Song et al., 1999b). Oils such as solvent naphtha, hexane, refined paraffins, kerosene, No. 2 fuel oil and diesel have densities below 0.9 g/cm^3. Good selectivity or ash rejection is achieved when light oils are used in mineral flotation or coal cleaning. Conversely, oils with densities above 0.9 g/cm^3 showed good value mineral recovery but poor selectivity. Due to the existence of high levels of inorganic polar constituents, oils in the higher density category exhibit more erratic behavior, making them similar to the function of a flotation collector, which in turn results in uncertain wetting behaviors during oil-particle interaction.

Similarly, the viscosities of hydrocarbons are determined by the content of paraffins, naphthenes, aromatics and derivatives since each type of hydrocarbon has its unique temperature-density-viscosity relationships (Smit & Bhasin, 1985). In most cases, the viscosity of hydrocarbon increases with increasing molecular weight. The increasing branches in the compounds also lead to a higher viscosity. Due to the complicated closed-ring structures, heavy or residual oil products have much higher

viscosity than light or intermediate distillates. As Botsaris and Glazman (1989) pointed out, longer agitation and more vigorous hydrodynamics are required for denser and more viscous oils to achieve intimate oil-particle interaction for similar recoveries.

The surface tension or oil/water interfacial tension of petroleum distillates is very different from each other based on molecular weight, chemical composition, compound structures, functional polar groups and temperature. Demond and Lindner (1993) compiled hundreds of interfacial tension values between water and organic liquids including alkanes, branched alkanes, aromatics and other hydrocarbons with polar groups. Aveyard and Haydon (1965) and Zeppieri et al. (2001) reported the interfacial tension values of many n-alkanes as a function of temperature and observed a decrease of interfacial tension with increasing temperature. Under constant temperature, the longer n-alkanes have a higher oil/water interfacial tension. But for heavier hydrocarbons containing aromatics or hydrocarbons with polar groups, the interfacial tension decreases appreciably. In spite of the interfacial tension differences among oils, the oil/water interfacial tension was much lower than air/water interfacial tension under certain surfactant concentration. In most cases, the oil/solid interfacial tension was also much lower than the air/solid interfacial tension in mineral suspensions where surfactant was also added. When utilized in oil-assisted flotation, this feature played a significant role according to Young's equation, as more fine mineral particles preferentially concentrate on the oil/water interfaces (Laskowski, 1992).

The electrophoretic mobility of emulsified hydrocarbons is another important parameter in oil assisted flotation. A schematic diagram of the electrophoretic mobility of emulsified hydrocarbons in the presence of surfactants as a function of pH is summarized in Figure 3.6. The electrophoretic mobility of hydrocarbons generally increased with increasing pH, and it is strongly influenced by the type of surfactants used in the emulsification process. In the absence of any surfactants, the oil droplet surface charges remain negative in a wide pH range and an isoelectric

point (iep) exists at a very acidic pH. This phenomenon has been explained by preferential adsorption of hydroxyl ions rather than hydronium ions on the surface of emulsified oil droplets (Stachurski & MichaŁek, 1985). In recent years, an increasing body of evidence suggested that below its iep., the surface of oil droplets turned positive, presumably by the depletion of hydroxyl ions and the adsorption of hydronium ions (Creux et al., 2009; Knecht et al., 2010). Creux et al. (2009) measured the electrophoretic mobility of several hydrocarbons. Despite the large differences of the overall shape of the electrophoretic mobility curves, nitrobenzene, benzene and three alkanes were all found to have similar ieps between 2 and 3. This is in agreement with the results by Stachurski and MichaŁek (1985), Liu et al. (2002a) and Zhou et al. (2014).

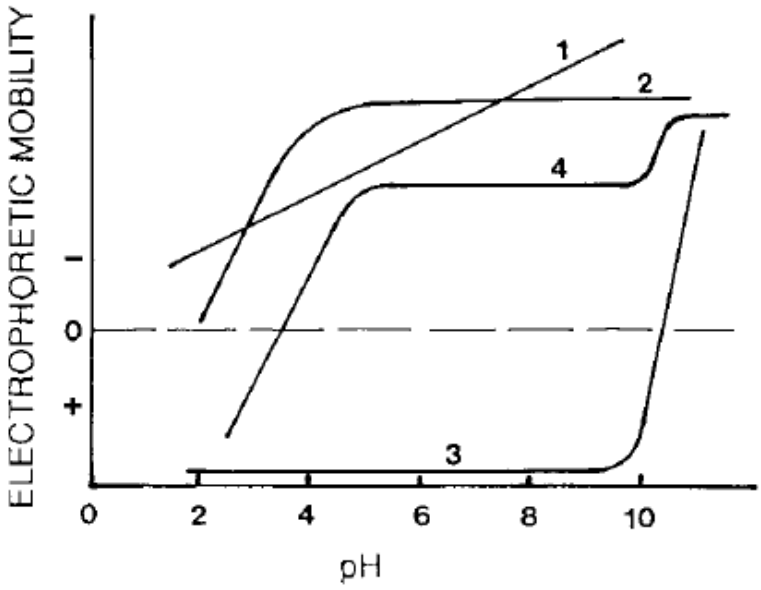

Figure 3.6 The schematic electrophoresis mobility of hydrocarbons as a function of pH (1, oil droplets; 2, oil droplets with anionic surfactants; 3, oil droplets with cationic surfactants; 4, oil droplets with amphoteric surfactants) (Good, 2012).

3.2.3 Applications of Non-polar Oil in Flotation

The intensifying effects of non-polar oil in the mineral separation process were observed in many reports. As shown in Table 3.3 below, non-polar oils can be used

in the flotation of not only naturally hydrophobic minerals such as coal, molybdenite and sulfur, but also hydrophilic minerals such as chalcopyrite, galena, sphalerite, hematite, talc, apatite, quartz, etc., in conjunction with an appropriate collector.

A number of benefits have been observed when non-polar oil was used as an auxiliary collector. These include larger floc size (Song et al., 1999a; Song et al., 2002), faster flotation rate (Rubio et al., 2007; Soto & Iwasaki, 1986), less slime entrainment (Ying et al., 2015), lower collector consumption (Liu et al., 2014), and higher concentrate grades and value recoveries (Song et al., 2001b).

Unless the oil droplets and mineral surfaces carry strong opposite charges, whether oil droplets attach to mineral particles or not is determined by the hydrophobicity of the mineral particle surfaces. Naturally hydrophobic minerals can be recovered by froth flotation simply with non-polar oils as collectors (Harris et al., 1995; O'Connor & Dunne, 1994; Zanin et al., 2009). For oxide minerals with hydrophilic surfaces, conventional collectors are necessary to induce particle-oil droplet interactions. The choice of collectors to alter mineral surface wettability is therefore important in the oil-assisted flotation separation process. Sodium oleate (NaOl), salt of long hydrocarbon chain fatty acid, is the most extensively used anionic collector in oxide mineral flotation due to its strong collecting capability. When used in conjunction with non-polar oils, enhanced performances were often observed. In addition, long-chain petroleum sulfonates, amines, and tall oil are also widely used, alone or in combination with non-polar oils, to float fine oxide minerals (Liu et al., 2014; Wang, 2016a).

As indicated by Pascoe and Doherty (1997), an increase in collector hydrocarbon chain length could produce larger and stronger mineral flocs. In the presence of non-polar oil, the enhancement of hydrophobic flocculation would be much more significant by collectors with longer hydrocarbon chain lengths (Ozkan et al., 2016). Considering this effect, collectors with short chain hydrocarbons were not

suggested when non-polar oil was used in the processes (Zollars & Ali, 1986). On the other hand, many researchers reported the beneficial effect of non-polar oil even with short-chain collectors (e.g. isopropyl or amyl xanthate in the flotation of partially hydrophobic sulfide minerals), provided that mineral surfaces were rendered sufficiently hydrophobic to induce a strong hydrophobic interaction (Rubio et al., 2007; Song et al., 2001a; Song et al., 2000).

However, the application of alkyl hydroxamic acids and related salts in conjunction with non-polar oil has been rarely discussed in the open literature. Due to their strong complexation capability with transition and rare earth metal ions, hydroxamic acids exhibited better performance than conventional fatty acids such as oleate when used to float fine minerals (Natarajan, 2013; Wang, 2016b). However, Ni (2013) observed that the addition of kerosene in the batch flotation of a niobium oxide ore using octyl hydroxamic acid (OHA) as a collector significantly deteriorated the flotation performance. In addition, many instances shown in Table 3.3 also reported a defrothing effect of non-polar oils during the flotation operation, which resulted in poor metal grade and recovery.

Table 3.3 Application of non-polar oil in the flotation of naturally hydrophobic minerals or hydrophilic minerals in conjunction with collectors with different hydrocarbon chain length.

Ore	Ionic collector	Non-polar Oil		General Effects of Non-polar Oil	Reference
		Type	Dosage (g/t)		
Coal fines	N/A	Kerosene	2000	Effective collector for coal flotation.	(Wojcik & Al Taweel, 1984)
Molybdenum	N/A	Diesel	80-200	Effective collector for Mo flotation.	(He et al., 2011)
Chalcopyrite and gold ore	Sodium ethyl xanthate	Fuel oils for trucks	500	Improved metallic grade at similar recoveries, *but the froth stability was detrimentally affected by higher dosage of fuel oil or heavy oils.*	(Bos & Quast, 2000)
Separation of CuS from ZnS	Potassium ethyl xanthate	Kerosene	*unk*	Grade and recovery of Cu mineral fines enhanced significantly at cleaner stage.	(Aruna & Shende, 2006)
Copper and molybdenite ore	Sodium isopropyl xanthate	Diesel, kerosene, or motor lubricant oil	30~120	Increased recovery of Cu by 2~3% and Mo by 3~5%, and flotation rate increased by 20~30%. Severe depletion of froth height would occur if non-emulsified oils were used.	(Rubio et al., 2007)
Lignite	Sodium diisobutyl Dithiophosphate	Kerosene	900	Content of sulfur ashes in lignite decreased with reverse flotation.	(Öztürk & Temel, 2013)
Galena and sphalerite ore	Potassium amyl xanthate	Kerosene	200~250 mg/L	The micro-flotation result of galena and sphalerite increased from 64% and 67% to near 100%, individually. The floc size also increased significantly.	(Song et al., 2001b)
Pyrochlore ore	Octyl hydroxamic acid	Kerosene	250~ 5000	*The Nb grade and recovery decreased drastically during the batch flotation where several froth depletion was observed.*	(Ni, 2013)
Silica	Dodecyl amine	Dodecane	0~2730	Oil did not have any effect on the stability of collector coated silica aggregates nor the bubble size in aqueous	(Ata & Yates, 2006)

				phase, but flotation efficiency can be improved when oil was added.	
Separation of francolite from dolomite	Octadecyl amine	Kerosene	1500	The rate of micro-flotation was 5 times faster when oil was added in conjunction with collector.	(Soto & Iwasaki, 1986)
Francolite	Sodium oleate	Fuel oil	180	The recovery of P_2O_5 increased from 0 to 80% with the addition of oil.	(Lu et al., 1997)
Florida phosphate	Mixture of fatty acids and fuel oil		1:1	*Significant reduction in recovery of P_2O_5 due to destruction of froth can occur when recycling water containing low dosage of collector was used with anionic frother during column flotation.*	(El-Shall et al., 2000)
Florida phosphate	Mixture of sodium oleate and dodecane		1:1	Help to reduce consumption of oleate and control the excess frothing.	(Sis, 2001)
Talc fines	Sodium oleate	Kerosene	0.5 g/L	The effect of sodium oleate with kerosene was better than sodium dodecyl sulfate and Aero 801 (petroleum sulfonate) with kerosene.	(Ozkan et al., 2016)
Hematite, rhodochrosite fines	Sodium oleate	Kerosene	0~150 mg/L	Hydrophobic flocculation of mineral fines can be strongly enhanced by kerosene addition	(Song et al., 1999b)
Rhodochrosite, cassiderite	Sodium oleate	Kerosene	0~100 mg/L	Both flocculation and flotation performance was positively intensified by non-polar oil. Hydrophobic interaction is the governing force during oil-particle attachment.	(Dai & Lu, 1991)
Mica	Tallow amine	Fuel oil	200~1500	Help to reduce consumption of collector. Frother was suggested to be used to maintain froth stability.	(Fenske, 1959)
Sericite	Coconut oil amine	Kerosene	600~1200	Significantly increase mineral recovery. Kerosene enhanced frothing stability, as indicated by higher air recovery and increased water recovery during flotation.	(Tian et al., 2017)

Italic texts show the adverse effects of flotation performance in presence of non-polar oil.

3.3 Oil-Particle Interaction Mechanisms

3.3.1 Thermodynamic Approach

The oil-assisted flotation environment is a complicated heterogeneous system compared with that of conventional flotation with soluble collectors, due to the existence of water immiscible oil phase, gaseous phase, minerals with or without adsorbed surfactant collector and aqueous phase that contains various regent molecules, ions, colloids, and so on.

The introduction of hydrophobic oil droplets in aqueous solution disrupts the hydrogen bonds formed among water molecules, resulting in an increase of orientational ordering and densification of ions at water/oil interfaces, and therefore a higher free energy of the system. In order to lower the overall free energy, the hydrophobic materials tend to be repelled from the system, leading to the aggregation of hydrophobic particles or oil droplets (Luzar et al., 1983). If an oil droplet was forced to be in contact with a mineral particle in the aqueous suspension, the change of free energy equals (Laskowski, 1992):

$$\Delta G = \gamma_{so} - \gamma_{sw} - \gamma_{ow} \qquad (7)$$

Where γ_{so}, γ_{sw} and γ_{ow} are the solid/oil, solid/water and oil/water interfacial tensions, respectively.

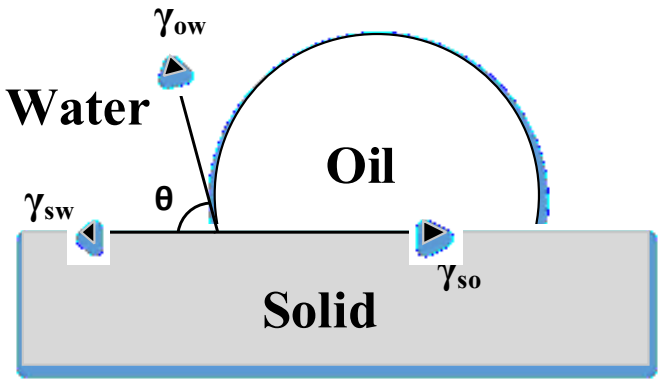

Figure 3.7 A schematic diagram of three-phase equilibrium of water, oil and mineral solids.

For a three-phase equilibrium contact line as shown in Fig. 3.7, according to Young's Equation:

$$\gamma_{so} = \gamma_{sw} + \gamma_{ow} \cdot cos\theta \qquad (8)$$

By substitute Equation (8) into (7), we have

$$\Delta G = \gamma_{ow}(cos\theta - 1) \qquad (9)$$

For a complete hydrophilic mineral particle where $\theta = 0$ and therefore $\Delta G = 0$, the stable attachment of an oil droplet onto mineral surface would not happen; But if the mineral is naturally hydrophobic or made hydrophobic by collectors, $\theta > 0$ and $\Delta G < 0$, indicating the spontaneous attachment of oil droplet on mineral surface from the thermodynamics standpoint.

In mineral flotation practice, a critical contact angle is necessary for a successful attachment between the mineral particle and air bubbles or oil droplets, which also

depends on the hydrodynamics and physicochemical characteristics of mineral particles and oil droplets (Shaw, 1992). Therefore, γ_{SO} should be minimized to obtain a large contact angle for desired mineral surface by surfactant adsorption. In addition, the value of γ_{ow} should not be neglected, because a high concentration of surfactant adsorbed on the surface of oil droplets tend to decrease γ_{ow} which decreases the tendency of oil-particle attachment (Iler, 1979).

The spreading of an oil droplet on a mineral surface is also examined using Harkins spreading coefficient (Harkins & Feldman, 1922):

$$S = \gamma_{sw} - \gamma_{so} - \gamma_{ow} \qquad (10)$$

If $S > 0$, the oil will spread on the mineral surface spontaneously and form an oil film between aqueous phase and solid phase; On the contrary, if $S < 0$, oil will form a stable three phase contact line on the solid/water interface.

After applying Young's Equation (8) into Equation (10), the spreading coefficient is given as:

$$S = -\gamma_{ow}(cos\theta + 1) \qquad (11)$$

Therefore, it is clear that if $\theta = 180°$ which is a case that has never happened in mineral processing, $S = 0$; Otherwise $S < 0$, and oil will attach and form a lens-like stable position on mineral surface. Spreading of oil drops on a mineral surface is not likely when the mineral surface possesses a finite contact angle.

3.3.2 Interaction Energy from Extended-DLVO Theory

Depending upon the separation distance, short range and/or long range forces between particles can take place at the interface (Lee, 2013). Within one or two atomic distances (< 0.3 nm), short range interactions by covalent, ionic, metallic or hydrogen bonds dominate (Israelachvili, 2011). If the separation distance is long (10~100 nm), interaction energies from extended Deryagin-Landau-Verwey-Overbeek (DLVO) theory should be taken into consideration. In oil-assisted flotation that involves the interaction between oil droplets and mineral particles, long range interactions that include van der Waals interaction, electrostatic double layer interaction, and hydrophobic interaction, are discussed in the following.

As an attractive intermolecular force, van der Waals force is a function that depends on the approaching distance between two particles, and the magnitude of van der Waals force is determined by the Hamaker constant. During the interaction of naturally hydrophobic mineral particles with oil droplets, the value of van der Waals force remains the same as long as there is no change in the physical characteristics of the oil droplets and the particles. However, when the hydrophobicity of the mineral particles is induced by the adsorption of collectors, van der Waals force between the collector coated minerals and oil droplets is expected to decrease slightly, because the Hamaker constant for coated collector is smaller than that for the underlying minerals (Parfitt, 1973). Hence, without considering the effect of the electric double layer, the collector coating on mineral surface will theoretically help disperse the mineral suspensions.

Electrical double layer interaction between a mineral particle and an oil droplet was determined by the charge signs and magnitude of the particle and the droplet. If both the mineral particle and oil droplet are negatively charged, a repulsive potential energy occurs. The larger the magnitude of surface charge of oil droplets, the stronger the repulsive energy. When the mineral particle and oil droplet carry opposite surface charges, a strong attractive potential energy arises. When added

into the mineral suspension, the surface charge property of oil droplets will be influenced by the chemical species present in the suspension (surfactants, pH, etc.). Therefore, by controlling the surfactant type and concentration, pH and other conditions, selective attachment of oil droplets to mineral particles could be achieved through hydrophobic interaction.

The total interaction energy by the sum of van der Waals interaction and electrostatic double layer interaction according to classic DLVO theory has its limitations and can only be applied for the suspension of colloids with contact angles in the range of 15º to 64º (Derjaguin & Churaev, 1989). Other non-DLVO forces can be present in both hydrophilic (smaller contact angles) and hydrophobic (larger contact angles) cases and could play important roles in the stability of the colloidal particles (Xu & Yoon, 1989; Yotsumoto & Yoon, 1993). For instance, when quartz surface was partially or completely hydroxylated by a water film, and the contact angle was small (less than 10~20º), a short-range repulsive hydration force was apparent when the separation distance was less than 3 nm (Churaev, 1995; Churaev & Zorin, 1992). Within the range of contact angles between 20~40º where classic DLVO theory was commonly applied, the non-DLVO force changes from repulsion to attraction. The magnitude of it is negligible, compared with van der Waals force and electrical double layer interactions. When the water contact angle was larger than 64º on hydrophobic mica or methylated quartz, long-range hydrophobic attraction was detected and the magnitude of it increased with the increasing degree of surface hydrophobicity (Churaev, 1995; Yoon et al., 1997). With direct force measuring techniques, the hydrophobic force between two hydrophobic mica surfaces was found to be ten to a hundred times stronger than the van der Waals force within a very short distance (approximately 8 nm) and decayed exponentially with separation distance (Israelachvili & Pashley, 1984).

Based on the foregoing review of the extended-DLVO theory, it can be seen that the energy barrier of the interaction between oil droplets and mineral particles can

be significantly lowered when the particle surface is made sufficiently hydrophobic, benefiting particle-oil aggregation.

3.3.3 Oil Bridging Effect

Hydrophobic mineral particles will be wetted by non-polar oil in aqueous suspension as a result of the hydrophobic interactions. The resulting oil-coated particles may form aggregates of oil-coated particles by the oil bridging effect (Mehrotra et al., 1983). A schematic representation of oil bridging aggregation process for particles that are naturally hydrophobic or made hydrophobic by collectors is shown in Figure 3.8.

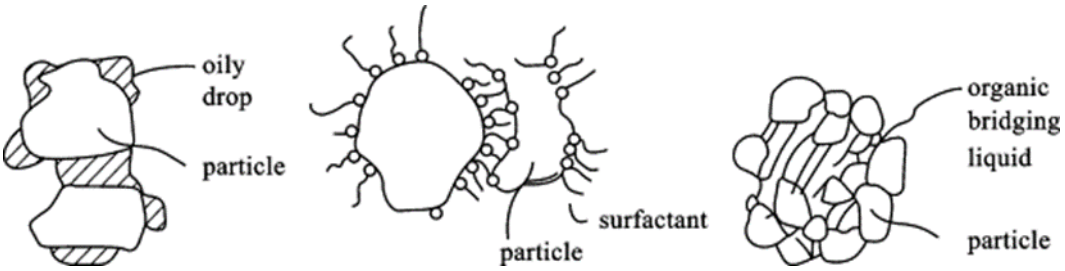

Figure 3.8 Oil bridging aggregation process (Somasundaran & Wang, 2006).

The structure of oily aggregates is closely associated with the volume of non-polar oil added. Figure 3.9 indicated the relationship between structure, size of oil aggregation and volume of oil addition.

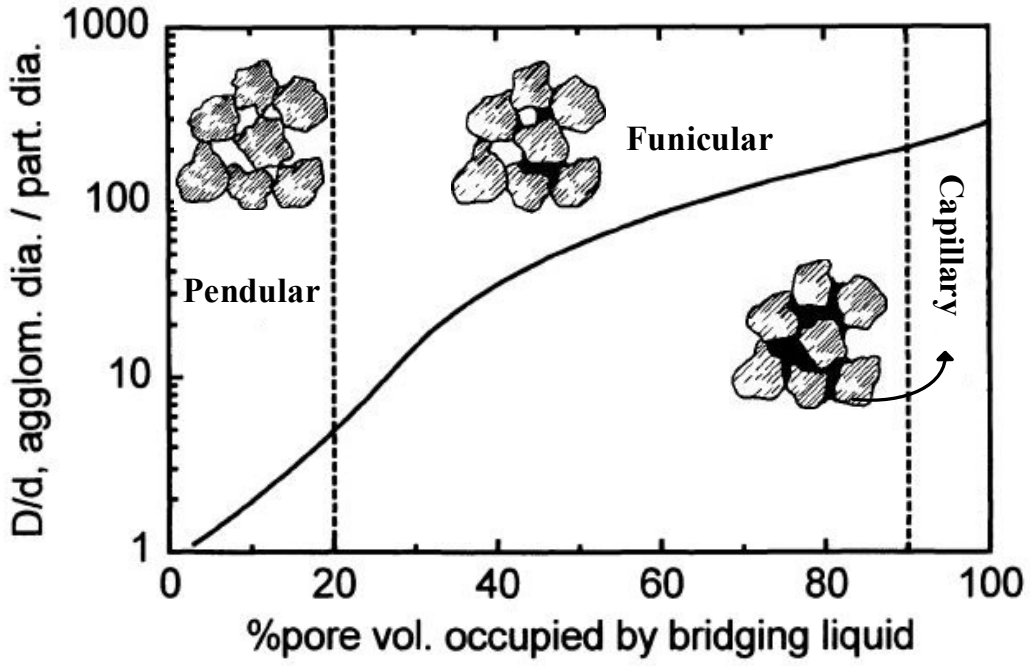

Figure 3.9 Structure and size of oily agglomerates as a function of oil content (Capes & Darcovich, 1997; Sadowski, 1998).

At pendular state where small volume of non-polar oil was added in the suspension, mineral particles are bound together by discrete lens-shaped oil rings at contact points. Assuming that the hydrophobic mineral surface was fully wetted by non-polar oil, the adhesive force between two symmetrical spherical particles can be calculated by Equation (12) (Capes & Darcovich, 1997).

$$\sigma_T = \frac{9}{4}\left(\frac{1-\tau}{\tau}\right)\frac{\gamma}{d} \qquad (12)$$

Where σ_T is the mean tensile strength per unit area, Pa; τ is the void fraction of the aggregates; γ is the surface tension of bridging oil in N/m; d is the diameter of assumed spherical particles in m.

With an increasing amount of oil addition, the discrete hydrocarbon rings start to merge into a continuous oil network (funicular state) until the aggregate voids are fully filled with oils when the capillary states dominates. The strength of wetted aggregate can be estimated using Equation (13):

$$\sigma_T = sC\left(\frac{1-\tau}{\tau}\right)\frac{\gamma}{d} \qquad (13)$$

Where s is the fractional filling by oils at aggregate voids; C is the parameter that equals 6 theoretically for spherical particles (Newitt, 1958). For irregular particles, C has a value ranging from 6.5 to 8 (Carman, 1941).

It is clear that the mean tensile strength of aggregate in capillary state is three times stronger than that in pendular state by comparing Equation (12) and (13). If the addition of oil increases further, hydrophobic particles will be immersed in hydrocarbon fluid and the size of it could increase to several millimeters, which may be too heavy to float by air bubbles, but could potentially be separated by screening.

The calculations of the aggregate strength discussed above are based on already established aggregates that are in a static state. In addition to oil dosage, it was demonstrated that the type and intensity of conditioning also play a significant role in the formation of aggregates (Mehrotra et al., 1983). Under intense agitation, the strong mechanical energy input brings oil-wetted particles to proximity and overcome the energy barrier, making the strength of aggregates ten-fold stronger compared with the static state strength (Ennis et al., 1990).

3.4 Flotation Froth Stability

In the mechanical flotation or column flotation where the recovery of hydrophobic particles relies ultimately on the survival probabilities of air bubbles, the froth stability plays a critical role in determining the flotation performance. The froth stability is the lifetime of the persistence of the froth (Subrahmanyam & Forssberg, 1988). Destabilized froth has a weak ability to provide sufficient carrying power and cleaning actions by water drainage within the bubble films, or to carry valuable mineral particles to the concentrate. On the contrary, a highly stabilized froth usually causes high degree of mechanical entrainment of gangue minerals (Nguyen & Schulze, 2004). Pugh (1996) catalogued them as unstable or meta-stable froth. It was considered that unstable froth is favorable for high grade and meta-stable bubbles for high recovery.

To quantify froth stability, characterization techniques such as dynamic and static froth stability measurements are typically used (Bikerman, 1973; Prud'homme, 1995). Dynamic froth stability tests measure the maximum froth height at the steady state during aeration, while the static stability tests measures the collapse rate of froth when aeration stops. From the point of flotation hydrodynamics, the dynamic froth stability test is tightly connected with froth flotation and therefore has been frequently used in froth stability research (Qu et al., 2013).

The factors influencing the froth stability were summarized by Farrokhpay (2011); Pugh (1996); Subrahmanyam and Forssberg (1988). Typical variables include the rate and time of aeration, type and concentration of frother, collector and other chemical reagents, pH, temperature, salt concentration, slurry conditioning, size and hydrophobicity of mineral particles, etc.

The dispersed oil droplets can stabilize or destabilize the froth phase, depending on the interactions between froth and oil. Four mechanisms were proposed in the open literature to explain the behavior of oil droplets at the air-water interface: (1) entry

of oil droplet into air-water interface; (2) spreading of oil droplet on the air-water interface to displace the adsorbed surfactant species; (3) formation of destabilizing oil bridge between two lamella surfaces; (4) stability of pseudoemulsion film. Therefore, the defrothing effect of neutral oil can be determined thermodynamically with the classical entry coefficient (E), spreading coefficient (S), and bridging coefficient (B). The expressions for E, S and B are given as:

$$\mathrm{E} = \gamma_{aw} + \gamma_{ow} - \gamma_{oa} \qquad (14)$$

$$S = \gamma_{aw} - \gamma_{ow} - \gamma_{oa} \qquad (15)$$

$$\mathrm{B} = \gamma_{aw}^2 + \gamma_{ow}^2 - \gamma_{oa}^2 \qquad (16)$$

Where γ_{aw}, γ_{ow} and γ_{oa} are the air/water, oil/water and oil/air interfacial tensions, respectively.

Two possible defrothing mechanisms by oil droplet are shown in Figure 3.10. Positive values of E mean oil may enter the air/water interface; Negative values of E indicate oil droplets are rejected from the film and can only stay in the aqueous phase. Similarly, positive values of S indicate that oil should spread on the surface of an air bubble, leading to a Marangoni-driven flow of liquid within the lamella to produce topical water film thinning, thus forming a duplex layer and finally ruptures. Positive values of B mean unstable bridges that leads to de-wetting of oil and film rupture.

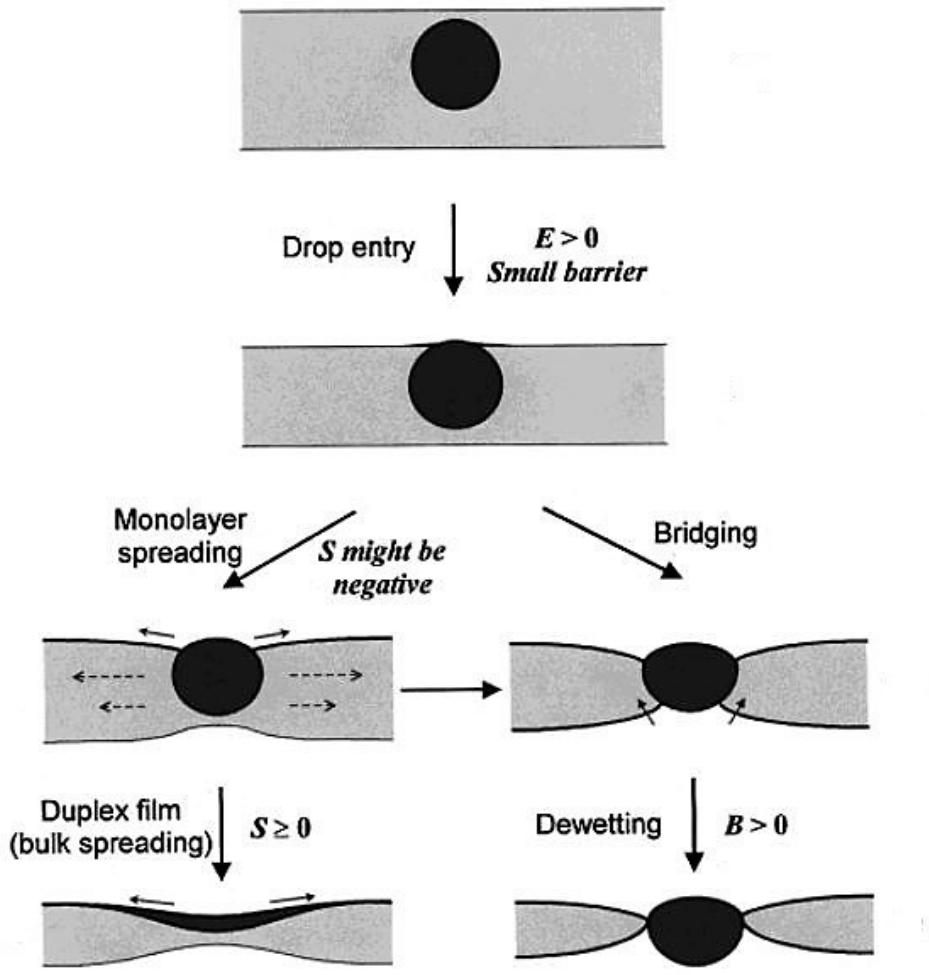

Figure 3.10 Possible defrothing mechanisms by an oil droplet (Denkov et al., 1999).

Therefore, it is apparent that the positive values of E are crucial for foam destruction. (Denkov et al., 1999; Garrett, 1992). However, the classical entry coefficient cannot correctly predict the real behaviors of froth stability in the presence of oil droplets. The expressions are calculated based on involved phases separately without considering the surface interaction forces when the separation distance between oil droplet and water film are getting close enough to form a pseudoemulsion film (Niewiadomski et al., 2001). The pseudoemulsion film provides a barrier for the oil droplet to enter into water lamella (Denkov et al., 2014). If the barrier is high enough (as shown in Figure 3.11), oil droplet cannot enter the film, oil spreading or bridging would consequently be suppressed (Koczo et al., 1992; Lobo & Wasan,

1993). Several reports indicated the foam stabilization effect by oil droplets because the non-entering oil droplets accumulated at Plateau-boarder and inhibited water drainage (Koczo et al., 1994; Koczo et al., 1992). In this case, the froth stability may be improved. Usually froth stability is influenced by oil volume fraction, droplet size and oil density.

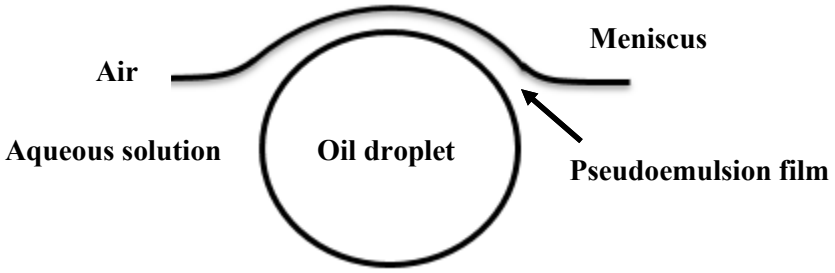

Figure 3.11 Configuration of oil droplet at water/air interface where a stable pseudoemulsion film existed (Koczo et al., 1992).

In addition to oil droplets, fine hydrophobic particles also play an important role in the stability of froth phase (Dippenaar, 1982a, 1982b). The work by Johansson and Pugh (1992) and Schwarz and Grano (2005) demonstrated that hydrophilic fine particles have no influence on froth stability. The maximum froth stability is achieved by particles with intermediate degree of hydrophobicity. However, froth phase is destabilized when mineral particles are very hydrophobic.

The mixture of hydrophobic particles and oil droplets exhibits a synergistic effect on destruction of froth stability (Pugh, 1996). The combination can easily destabilize the pseudoemulsion film, so that the neutral-oil enters the lamella and ruptures the foam, exhibiting a much higher antifoaming efficiency than oil droplets or hydrophobic particles alone.

Therefore, neutral oil plays a conflicting role in froth flotation. On one hand, it increases the mineral particle surface hydrophobicity, causing the formation of mineral-oil agglomerates, which benefits flotation. On the other hand, it can destabilize the flotation froths and adversely affect flotation. In practice, there may

be a delicate balance between the two roles. However, no systematic research has been performed to understand the conflicting roles and how to control their balances.

Chapter 4 Experimental Materials and Methods

4.1 Mineral Samples

4.1.1 High Purity Hematite and Quartz

The high purity hematite mineral used in this work was a spiral concentrate taken from an iron ore mine in eastern Canada. The hematite sample was wet ground in a laboratory 8" diameter ball mill, and wet screened to collect the -20 μm fraction for testing. Distilled water was used during the sample preparation. The sieved -20 μm fraction was filtered, dried and homogenized. A high purity -15 μm quartz sample was purchased from US Silica and used in flotation without any treatment. Table 4.1 shows the chemical composition of the two minerals determined by standard whole rock analysis.

Table 4.1 Chemical composition of hematite and quartz

Element in oxide form	Hematite (wt%)	Quartz (wt%)
SiO_2	4.44	99.52
Al_2O_3	0.11	0.19
Fe_2O_3	90.94	0.07
MgO	<0.01	<0.01
CaO	0.01	0.01
Na_2O	<0.01	<0.01
K_2O	0.03	<0.01
TiO_2	0.02	<0.01
P_2O_5	<0.01	0.01
MnO	3.65	<0.01

Scanning electron microscopy coupled with energy dispersive X-ray spectrometry (SEM/EDS) was used to image the mineral grains as well as to identify mineral species and elemental composition. For this analysis, the fine hematite sample was mounted on an aluminum pin stub using a carbon adhesive tab, and examined in a Zeiss EVO LS 15 scanning electron microscope using a beam voltage of 15.0 kV. An SEM image of the -20 μm hematite sample is presented in Figure 4.1, showing the morphology of the hematite sample. As can be seen, the majority of the particles were much smaller than 20 μm. EDS spectrum of a selected area scan, shown in a yellow rectangular box and labeled as hematite_1, indicated an overall composition of 54.36% Fe, 3.67% Si and 2.47% Mn (Table 4.2). The EDS spectra of the two points, hematite_2 and hematite_3, showed that these are possibly hematite and a mixture of hematite and pyrolusite, respectively.

Table 4.2 EDS analysis with elemental composition of hematite sample

Element, wt%	Fe	O	Si	Mn
Hematite_1	54.36	21.40	3.67	2.47
Hematite_2	60.41	18.97	0.80	0.11
Hematite_3	38.67	24.00	16.63	1.49

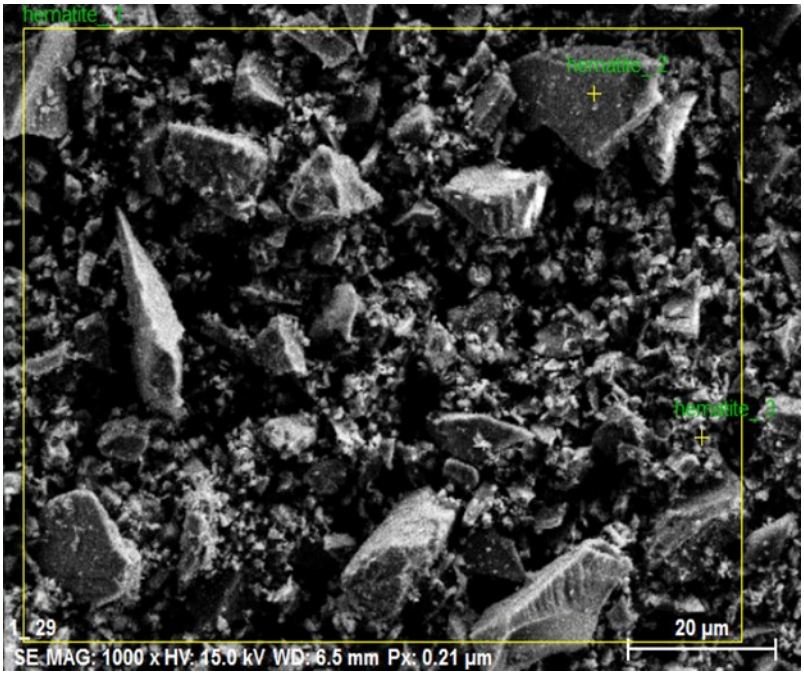

Figure 4.1 SEM secondary electron micrograph of the -20 µm hematite sample.

X-ray diffraction (XRD) was used for qualitative identification of the mineralogical composition of the hematite and quartz samples. The coupling XRD diffractometer (Bruker D8 XRD) was operated at 40 kV, 44 mA and 4 degree/min scan rate and the scanned results are shown in Figure 4.2. The hematite sample was predominantly hematite with minor impurity peaks for quartz and pyrolusite. The peaks of quartz sample completely match the quartz crystal peaks, indicating the sample is pure quartz with no impurity.

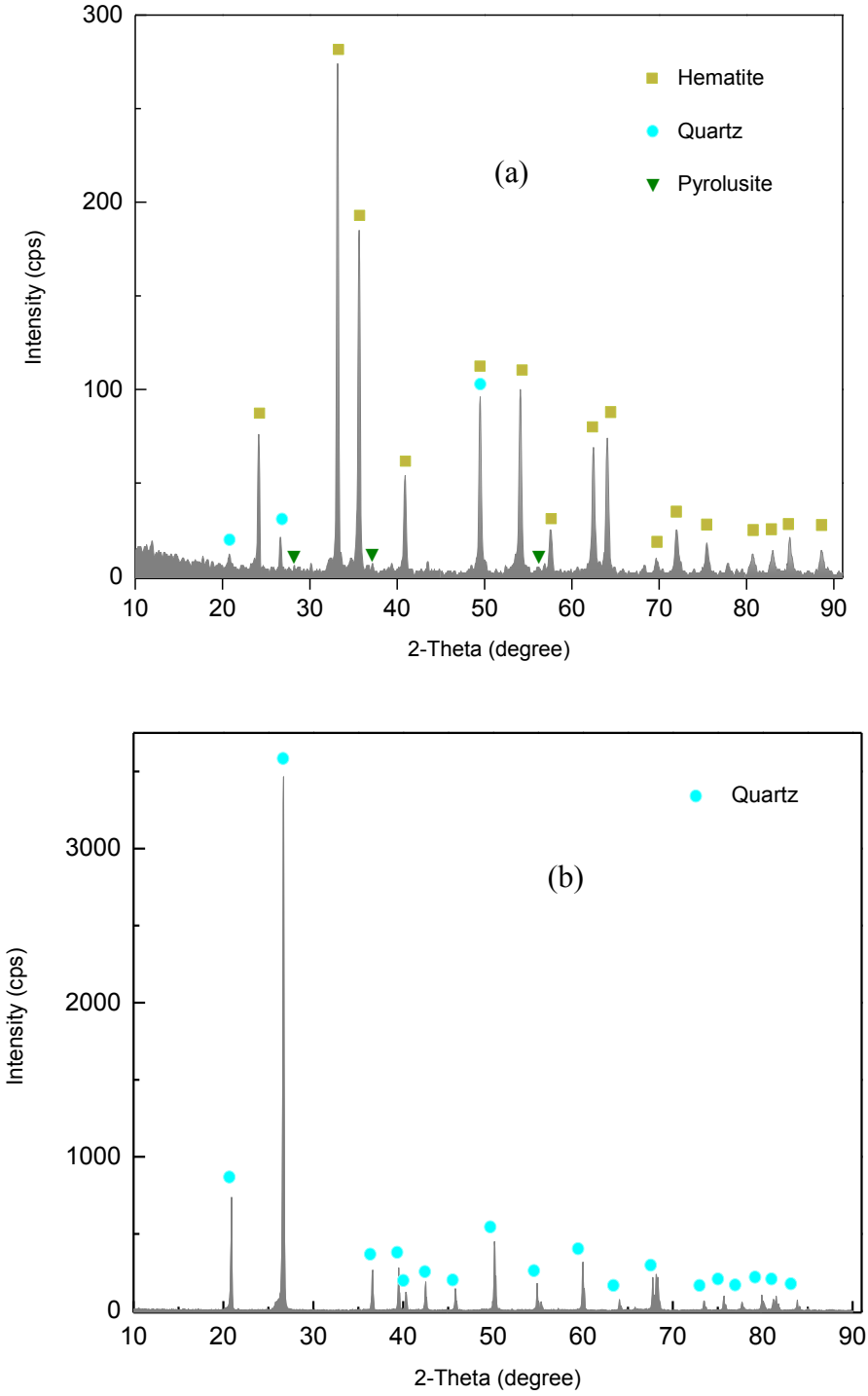

Figure 4.2 XRD patterns of hematite (a) and quartz (b) samples.

The particle size distribution of the -20 μm hematite and quartz samples was determined by a Malvern Mastersizer 3000 particle size analyzer using the

following operating parameters: Hematite: refractive index 2.42, absorptive index 0.003 (Cornell & Schwertmann, 2003); Quartz: refractive index 1.54, absorptive index 0.008 (Mitchell, 2004). The results are shown in Figure 4.3. As can be seen, the particle size of the -20 μm hematite sample ranged from 0.1 to 25 μm, with a mode of about 5 μm, and approximately 90% of the particles are between 1 and 12 μm. Quartz particles also have similar size distribution but slightly finer than hematite particles.

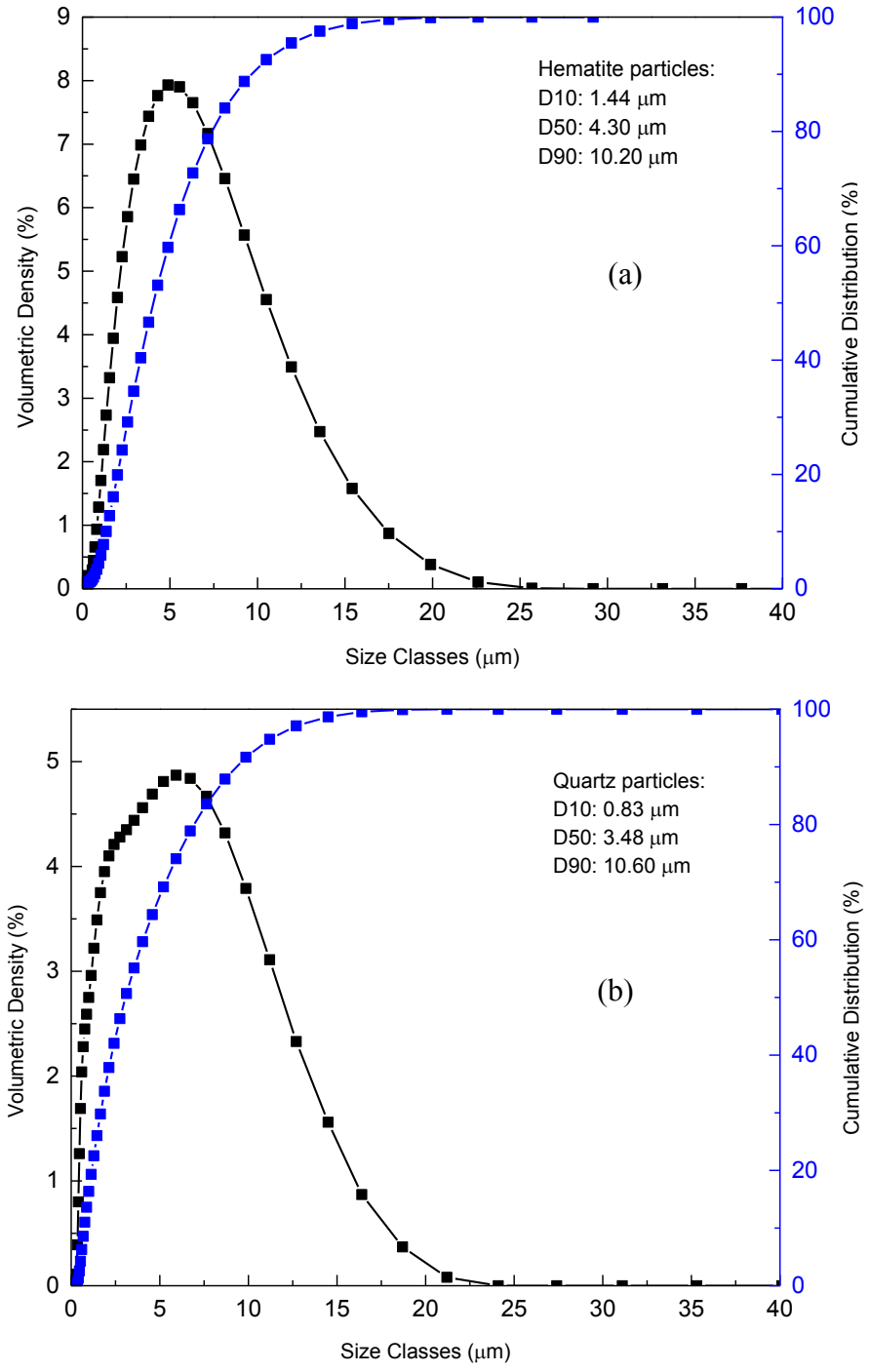

Figure 4.3 Particle size distribution of the hematite (a) and quartz (b) sample.

4.2 Reagents and Chemicals

Sodium oleate (NaOl) (≥82 % oleic acid basis) was purchased from Sigma-Aldrich and was used as a collector without further purification. The NaOl dosage was expressed on the basis of the active ingredient (i.e., 82%). High purity octyl hydroxamic acid (OHA) and oleoyl hydroxamic acid (OLHA) were synthesized in our labs by the hydroxylamine hydrochloride/sodium hydroxide method and prepared as hydroxamate solution in this study (Liu et al., 2015). The chemical structures are shown in Figure 4.4. OLHA has the same hydrocarbon tail as NaOl but has hydroxamic acid as the polar (ionizable) group. Thus, OLHA was used to decouple the effects of chain length and functional polar groups to understand the effect of non-polar groups on the flotation of hematite.

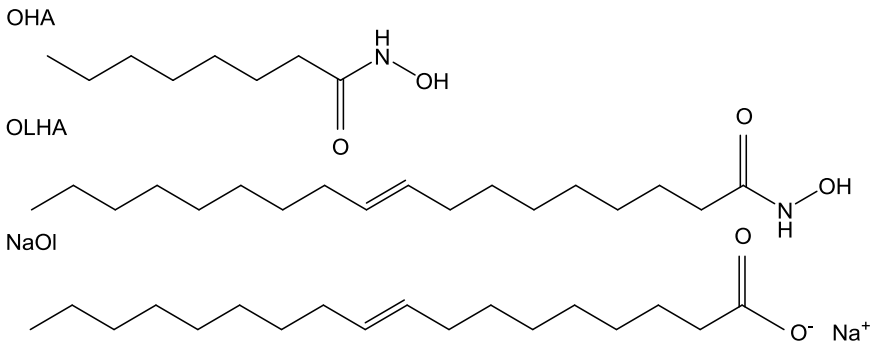

Figure 4.4 Structures of octyl hydroxamic acid, oleoyl hydroxamic acid and sodium oleate.

Analytical grade sodium hydroxide (NaOH) and hydrochloric acid (HCl) were purchased from Fisher Scientific and used as pH modifier.

4.3 Non-polar Oil

Odorless kerosene, purchased from Fisher Scientific, was used as the non-polar oil in this study. Kerosene is a mixture of C9~C16 hydrocarbons and has a density of 0.79 g/cm^3 with a viscosity of 1.8 mPa·s.

Kerosene emulsion was prepared by mixing 1 mL kerosene with 200 mL distilled water followed by shearing in a high-speed blender for 3 min. After standing for approximately 5 min, the kerosene emulsion was found to have a small D_{50} of 2.98 µm, and D_{90} of 6.94 µm, determined by the Malvern Mastersizer 3000 (operating parameters: refractive index 1.43, absorptive index 0.001 (Tummons, 2016)) (Figure 4.5).

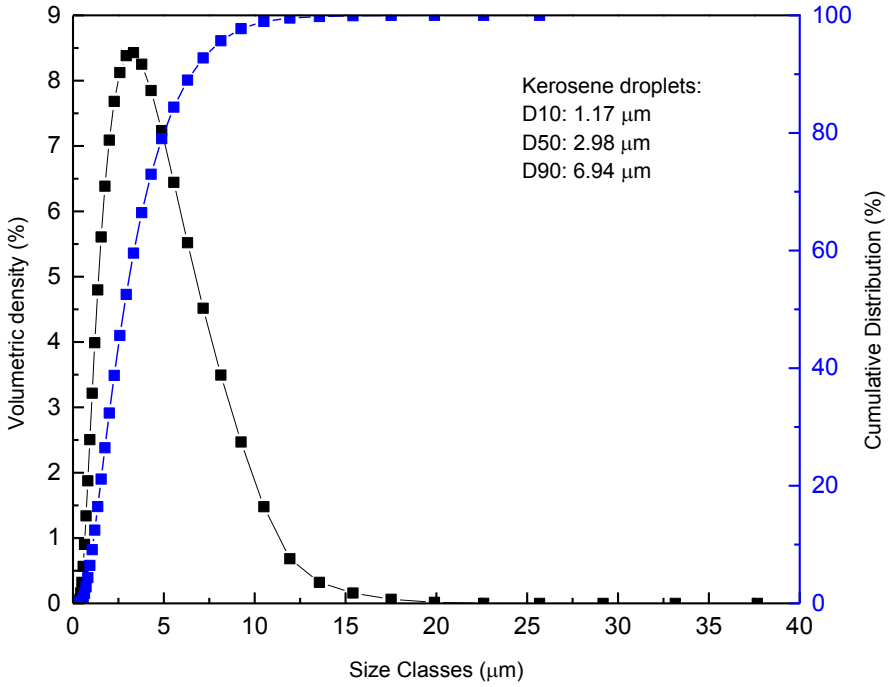

Figure 4.5 Droplet size distribution of kerosene emulsion (measured 5 minutes following high speed mechanical blending of 1 mL kerosene in 200 mL distilled water).

4.4 Experimental Methods

4.4.1 Infrared Spectroscopy

The chemical structure of synthesized reagents was identified qualitatively by infrared spectra with a Bruker Alpha FTIR spectrometer equipped with a vertical attenuated total reflection (ATR) sampling accessory. Scanning parameters and

data processing were controlled by the OPUS software suite. The spectra obtained by measuring in an atmospheric environment was chosen as a reference. About 10 μg of the reagent sample powder was deposited on the surface of the ATR crystal prior to scanning. The spectrum was acquired in the range of 500~4000 cm^{-1} with a resolution of 2 cm^{-1}. The crystal was carefully cleaned using methanol and distilled water and dried with paper wipes between measurements.

4.4.2 Micro-flotation Test

Micro-flotation tests were performed in a custom-made glass tube at ambient temperature (22°C). A schematic diagram of the micro-flotation tube is shown in Figure 4.6. The tube has a sintered glass disc at the bottom to allow the passage of gas while a magnetic stir bar can be placed on the sintered glass disc to agitate the mineral sample. The top of the microflotation tube was modeled after Siwek et al. (1981). One and a half (1.5) g hematite sample was conditioned in 170 mL distilled water in a 250-mL beaker under moderate magnetic agitation. A desired dosage of a collector was added and conditioned for 3 min. When used, kerosene emulsion was also added into the mineral suspension and conditioned for another 3 min. NaOH or HCl solution was added to adjust the pH of the pulp. After conditioning, the hematite suspension was transferred to the microflotation tube and agitated with a magnetic stirrer at 400 rpm. A 3-min flotation time was employed at 14 mL/min nitrogen gas flow rate. No frother was used during the flotation test. The concentrate and tailing were weighed separately after filtration and drying. Hematite recovery was calculated as the weight percentage of the concentrate against the original sample weight. The results were reproducible within ±5%. The stirring in both the beaker and the micro-flotation tube was intended to maintain the mineral particles in suspension rather than to cause intensive shear.

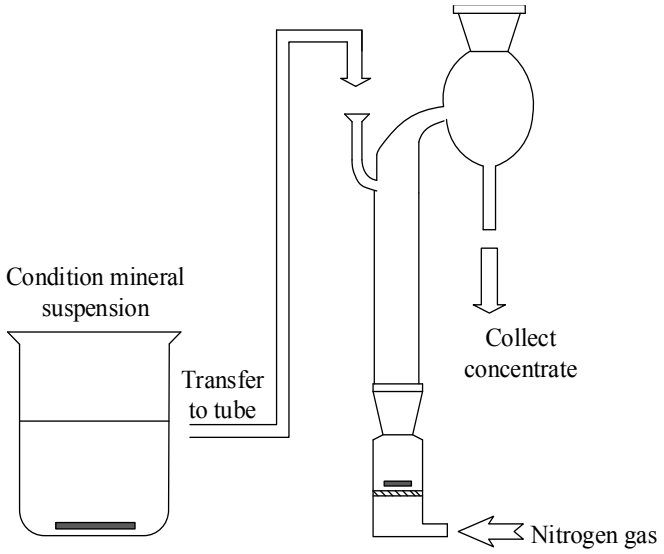

Figure 4.6 Schematic diagram of the microflotation tube used in this study.

4.4.3 Batch Flotation Test

Batch flotation tests of artificial mixed minerals (hematite:quartz = 1:1 weight basis) were conducted in a Metso D-12 laboratory flotation machine (Figure 4.7) under natural pH of 6.5~7.5. Two hundred grams of the hematite-quartz mixture and 1 L tap water were added into a 1.5-L stainless steel cell and stirred at 900 rpm for 2 min. A desired dosage of a collector was added and conditioned for another 2 min. When used, 1 kg/t emulsified kerosene was added subsequently and conditioned for 2 min. No frother was used. Following conditioning, air was turned on at an aeration rate of 2.5 L/min (equivalent to a superficial air velocity of 0.36 cm/s) and the flotation froth was scraped every 1 s until 5 min 30 seconds when the froth was barren. The temperature of batch flotation tests was ambient to room temperature, which was maintained at 22°C. The concentrate and tailing products were filtered, dried, weighed and sub-samples were assayed by Bureau Veritas Commodities Canada Ltd located in Vancouver, BC by whole rock analysis. To evaluate the selectivity and efficiency of the batch flotation, the separation efficiency E was calculated using the modified Hancock equation:

$$E = \frac{100(\beta - \alpha)\gamma}{(100 - \alpha)\alpha} \times 100\% \qquad (17)$$

where α, β are the Fe_2O_3 grade of the feed and the concentrate product, and γ is the weight yield of the concentrate (Hancock, 1918).

For batch flotation of single hematite minerals, the procedures were the same as above except that two hundred grams of the single mineral were used in each test, and that the rougher concentrates were collected every 30 seconds to study the kinetics of the flotation. The weights of both water and the mineral were recorded. In addition to mineral recovery, water recovery was also calculated, which was the ratio of recovered water against the total amount of water added to the flotation cell.

Two different approaches were used for single hematite mineral flotation, i.e., shear-agglomeration flotation and conventional batch flotation. For the shear-agglomeration flotation test, 200 g hematite sample was mixed with tap water to make a 600 mL mineral suspension in a baffled container (inner diameter: 10.3 cm; baffler width: 1.5 cm). After the addition of pre-determined concentrations of a collector or/and kerosene emulsion, the suspension was completely sealed with a lid and extra volume of tap water was added to remove air voids with the purpose of eliminating air vortex during the agitation. The resulting mineral suspension (25 wt%) was conditioned at 1200 rpm for 20 min at an average torque of 9.5 N·cm using a Rushton Turbine of 5 cm in diameter. Afterwards, the suspension was transferred to the mechanical flotation cell and diluted to 16.67 wt% solids. After 2 min conditioning in the flotation cell, the suspension was floated in the same manner as described above.

Conventional batch flotation of the hematite single minerals was carried out without the intensive shearing step. The hematite was slurried in the flotation cell and floated as described above.

Figure 4.7 Metso D-12 laboratory flotation machine.

4.4.4 Focused Beam Reflectance Measurement (FBRM) Particle Size Analysis

The study of the aggregation process was carried out using a Mettler-Toledo G400 FBRM probe to monitor the real-time evolution of aggregates after reagent addition. The FBRM technique is based on the pulses of backward light scattering, detected by the probe when a focused laser beam is intersected by particles and flocs (Sparks & Dobbs, 1993). The calculation of pulse width multiplied by the scanning rate gives chord length. Thousands of chord length data detected by the laser beam produces a chord length distribution (CLD) which was updated every 2 seconds during measurement (Kail et al., 2009). As a sensitive indicator, chord length data from FBRM was used to represent the aggregation or dispersion status of the suspension. Both “not weighted” and “square weighted” chord lengths were applied on chord length distribution, reflecting the linear and volumetric chord length of particles, respectively.

For the aggregation measurements, a 200 mL hematite suspension containing 0.5 wt% -20 μm hematite was transferred into a 250-mL glass beaker placed in the FBRM stand, and stirred at 400 rpm with a four-blade turbine impeller (each blade was 2.1×0.8 cm, angled at 45°, and the shaft diameter was 0.8 cm). The FBRM probe was submerged in the suspension. The suspension was maintained at pH 7 with HCl or NaOl solution. After 5 min conditioning, a desired dosage of collector was added to the slurry and conditioned for another 5 min to equilibrate floc growth. Then 100 mg/L kerosene emulsion was added subsequently followed by another 5 min conditioning. The aggregate size was monitored throughout the process.

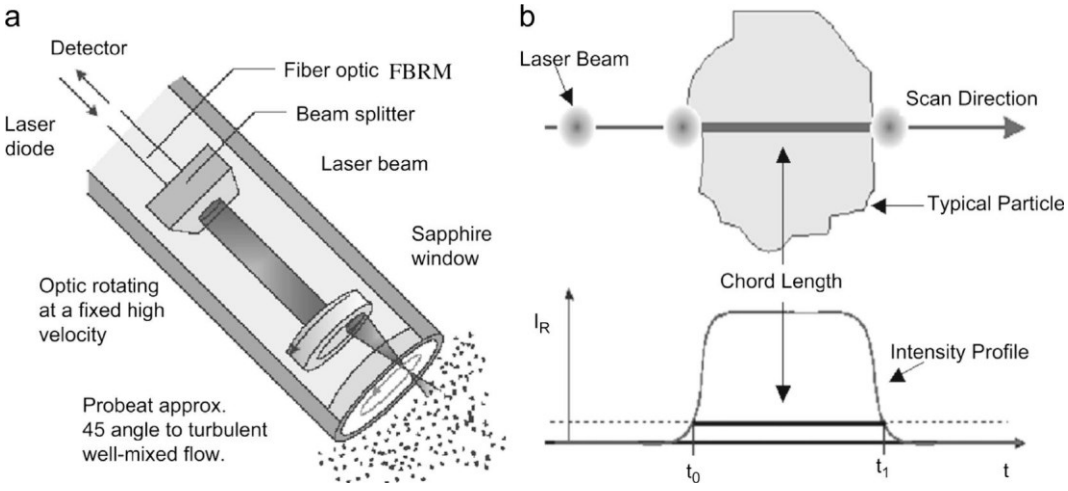

Figure 4.8 Schematic diagrams of focused beam reflectance measurements (FBRM) probe (a) and measured chord length by a beam of laser light through a particle (b) (Greaves et al., 2008).

4.4.5 Optical Microscopy

Direct observation of particle and aggregate structures was performed using a Zeiss Axioskop 40A optical microscope equipped with a digital camera. One drop of mineral slurry was pipetted onto the center of a glass slide and covered gently with a thin coverslip. The images of prepared samples were viewed and captured immediately. The mineral slurry was prepared following the procedure described previously in section 4.4.4.

4.4.6 Contact Angle Measurement

Static sessile drop contact angle method was employed to determine the wettability of the hematite surface after collector treatment. A high-grade hematite lump ore purchased from Ward's Science was cut into slices about 30 mm long, 20 mm wide and 10 mm thick. The surface of the hematite slice was wet polished using 200, 400, 600, 800, and 1200 grit silicon carbide papers sequentially, and then with 0.3 μm alumina gel on a polishing cloth. The polished surface of hematite was ultrasonically cleaned with distilled water to remove any traces of alumina impurities. The sample slice was treated in 100 mL aqueous solution with a desired dosage of collector at pH 7 for 5 min and then vacuum dried in a glass chamber.

Water contact angles were measured with a FTA-200 contact angle goniometer, with an accuracy of ±5°. About 4 μL distilled water was introduced onto the substrate using a micro-syringe. Special care was taken to avoid vibration of water droplets on the needle during the measurements. After 10 s equilibrium, the water drop image was captured and analyzed to determine the contact angle. The average of at least six measurements at different locations on the hematite surface was considered the final contact angle of the hematite surface. In this study, the contact angles of the -20 μm hematite powder surface were approximated to be the same as the hematite slice treated in the same batch of collector solution.

4.4.7 Zeta Potential Measurements

The zeta potentials of hematite particles and kerosene droplets in the presence of 10^{-3} mole/L KCl supporting electrolyte were measured using a Brookhaven ZetaPALS zeta potential analyzer at 22°C. To prepare the stock suspension, 1 g hematite was added to 200 mL 10^{-3} mole/L KCl solution and equilibrated for 24 hours. Kerosene suspension was prepared by emulsifying 1 mL kerosene with 200 mL KCl solution and standing for 24 hours. The kerosene suspension was re-emulsified prior to measurements. For each measurement, 10 mL stock hematite

slurry or 1 mL kerosene emulsion was diluted in 100 mL distilled water containing 10^{-3} mole/L KCl, adjusted to an appropriate pH and treated by collectors when needed. The diluted suspension was conditioned for at least 20 min before transferring to the sample cell for electrophoretic mobility measurements. The Smoluchowski model was utilized to calculate the zeta potentials of the tested suspension. Each measurement was repeated 10 times with 10 cycles for each run, and the average value was taken as the final recorded zeta potential.

The zeta potential distribution measurements of single hematite particles or kerosene droplets and their mixtures were carried out with a Zetaphoremeter (CAD instrumentation 2000 model), which was equipped with a laser illuminating microscope with a CCD camera on the top, a rectangular electrophoresis chamber with two palladium plated electrodes and a computerized viewing and operating system. The system was first calibrated for an accurate positioning of the camera by focusing the laser on the stationary layer near the surface of the viewing chamber walls prior to testing. About 30~50 mL of prepared suspension was introduced into the chamber. Extra attention was taken to avoid the existence of air bubbles in the cell. When the voltage was applied between two electrodes, the traced particles or droplets will migrate accordingly. An histogram of mobilities is then plotted and the related zeta potential distribution was computed.

4.4.8 Interfacial Tension Measurements

The determination of interfacial tension of air/surfactant solution, air/kerosene and kerosene/surfactant solution was conducted with a platinum plate measuring 20×10×0.1mm in a Krüss 100 tensiometer. The desired surfactant solution was prepared by successive dilutions using 10^{-3} mole/L KCl supporting electrolyte. The pH of surfactant solution was adjusted to 7 by adding KOH or HCl solution using a plastic pipette. Freshly prepared solution was measured within 30 min to avoid any possible alterations in the surfactant. Each measurement was carried out at

24±0.5°C and kept running until the standard deviation of 100 measured raw data was less than 0.1 mN/m to ensure equilibrium was achieved at the interface.

4.4.9 Froth Stability Measurements

The foam stability measurement setup was comprised of a nitrogen gas cylinder, digital mass flow controller and a 1-meter-tall graduated glass column with an inner diameter of 4.76 cm. A schematic setup is shown in Figure 4.9. Nitrogen gas flow rate was carefully controlled by the mass flow meter ranging from 150 mL/min to 750 mL/min. The measurement was conducted at room temperature 20±0.5°C. The glass column was washed with concentrated alkaline solution, methanol and distilled water sequentially and air dried in a fume hood between different measurements.

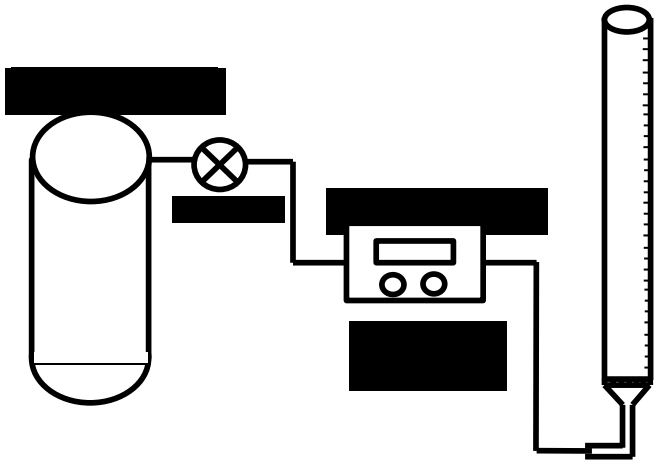

Figure 4.9 Schematic setup of foam stability measurement.

A 100-mL surfactant solution with or without kerosene emulsion was initially adjusted to pH 7. After stabilizing for 5 min, the solution was transferred into the glass column and aerated at a certain gas flow rate. The entire foaming process was recorded by digital camera.

The foam volume was calculated using Eq. (18).

$$V = \pi \times r^2 \times (H_0 - H_1) \quad (18)$$

Where, V is the foam volume at certain time; r is the inner radius of the glass column; H_1 is the average foam height at the top; H_0 is the foam height of the solution/foam interface at the bottom. Since there was no sharp boundary between gas emulsion below and true foam above, the height of 100 mL solution before gas injection was approximately considered as the level of the gas-liquid interface. Therefore, the reported froth height did not reflect the absolute froth volume, however, it was sufficient to study the effect of kerosene on the frothing behavior.

Chapter 5 Results and Discussion

5.1 Characterization of OHA, OLHA and NaOl

The synthesized octyl hydroxamic acid (OHA) was snow-white with flaky textures. The synthesized oleoyl hydroxamic acid (OLHA) was also white but showed a glutinous texture. Both OHA and OLHA were sparingly soluble in water at room temperature.

The infrared spectra of the synthesized OHA and OLHA, as well as commercially purchased sodium oleate NaOl (≥82 % oleic acid basis) are shown in Figure 5.1. A comparison of the observed peaks in the infrared spectra with the IR Database compiled by Yamaji et al. (2014) and Higgins et al. (2006) in Table 5.1 shows that they matched closely, indicating the high purity of the reagents synthesized. The spectra of the two hydroxamic acids have two absorption bands at 1663 cm^{-1} and 1624 cm^{-1}, corresponding to the amide Ⅰ band (C=O stretching). Other important bands including the N-H stretching vibration band at 3250 cm^{-1}, O-H stretching at 3066 cm^{-1} and amide Ⅱ band at 1560 cm^{-1} (Raghavan & Fuerstenau, 1975). Sodium oleate has its characteristic absorption bands of $–COO^-$ at 1711 cm^{-1}, 1560 cm^{-1}, and 1421 cm^{-1}, among which, 1711 cm^{-1} is the C=O stretching vibration, 1560 cm^{-1} and 1421 cm^{-1} are the asymmetrical and symmetrical stretching vibration of $–COO^-$, respectively. The bands at 1462 cm^{-1} and 1446 cm^{-1} are assigned to the asymmetrical stretching vibrations of $–CH_3$ and $–CH_2$, respectively. The bands between 2953 cm^{-1} and 2848 cm^{-1} representing the hydrocarbon chains are the asymmetrical $–CH_3$ stretching, asymmetrical and symmetrical $–CH_2$ stretching, respectively (Rao et al., 1991). The band at 722 cm^{-1} indicates that the reagent has an aliphatic tail with no less than 7 carbon atoms (Sayed & Zayed, 2006).

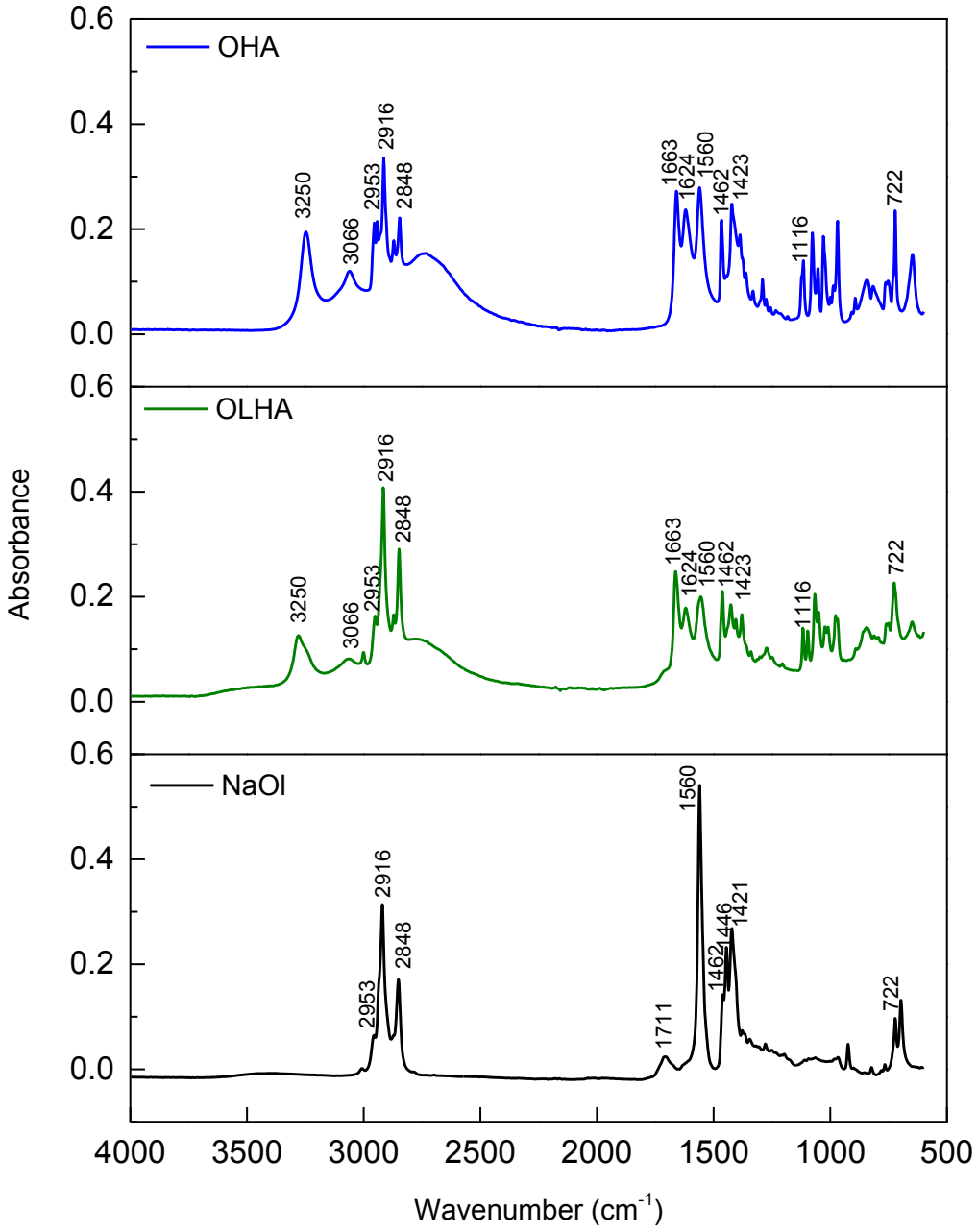

Figure 5.1 ATR-FTIR spectra of lab synthesized OHA, OLHA and commercially purchased NaOl (≥82% oleic acid basis).

Table 5.1 Comparison of FTIR absorption peaks (cm^{-1}) of lab synthesized hydroxamic acids through ATR mode and reference data using KBr method.

Lab synthesized	(Higgins et al., 2006)	(Yamaji et al., 2014)
3250	3254	3258
3066	3056	3059
2953	2955	2954
2916	2917	2915
2848	2849	2847
2750	2758	2769
1663	1663	1664
1624	1625	1623
1560	1567	1566
1462	1468	1463
1423	1425	1425
1386	1378	1388
1116	1116	1116
1077	1079	1079
1030	1031	1032
969	970	970
722	723	723
650	649	649

5.2 Oil-assisted Micro-flotation

The micro-flotation tests were performed to examine the flotation responses of fine -20 μm hematite with or without kerosene when different collectors were used. The effect of pH, collector concentration, kerosene concentration were investigated. The kerosene was either added directly in its liquid form, or emulsified by a mechanical blender prior to addition to flotation. The results are shown in Figures 5.2 to 5.5 and discussed in the following.

5.2.1 The Effect of Flotation pH

To investigate the effect of pH, experiments were carried out with 40 mg/L NaOl, OHA or OLHA as a collector in the presence or absence of 100 mg/L kerosene emulsion at pH 6 to 10. As seen in Figure 5.2, the floatability of hematite varies significantly within the tested pH range. The optimum flotation without kerosene occurs in the vicinity of 6.5 to 8.5 for NaOl, 6 to 8 for OHA, and 6 to 7 for OLHA, respectively. With the addition of kerosene, the flotation recoveries of hematite was positively influenced regardless of the type of collector, and the maximum flotation recoveries were also observed at the optimum flotation pH range.

When hydroxamic acid was used, the hematite recovery dropped with increasing pH. This was likely caused by the poor solubility of the hydroxamic acid at the high pH, which is especially true for the OLHA.

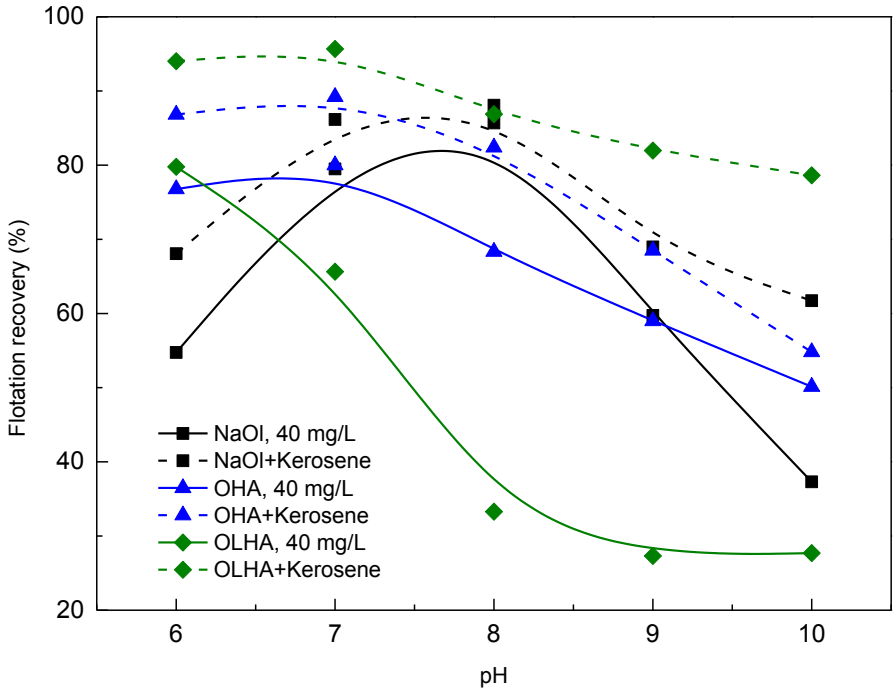

Figure 5.2 Micro-flotation recovery of -20 μm hematite as a function of pH with or without 100 mg/L kerosene. Solid curves are for collector only, and dashed curves are for collector + kerosene.

5.2.2 The Effect of Collector Concentration

The micro-flotation tests were performed at room temperature to examine the effect of kerosene on hematite flotation when different collectors were used. As seen in Figure 5.3, in the absence of kerosene, NaOl, OHA and OLHA were effective collectors for the fine hematite. The flotation recovery increased steadily with higher collector dosages. It was found that the NaOl displayed the strongest collecting ability over the two hydroxamic acids, especially at low concentrations. Of the two hydroxamic acids, OHA showed a much better flotation performance than OLHA. This is in good agreement with previous reports in terms of flotation performance using NaOl or OHA as a collector (Hughes, 2006; Pattanaik et al., 2000; Pavez et al., 1996). The flotation performance of hematite using OLHA as a collector was inferior to NaOl or OHA. This is mainly because OLHA has limited

solubility in water (Vaysse et al., 1997), leading to a low concentration of functional collector molecules to float hematite.

The addition of 100 mg/L kerosene generally increased the flotation recovery of the -20 μm fine hematite, especially at high collector dosages, but the responses were different between oleate and hydroxamic acids. At low NaOl dosages (below 30 mg/L), the addition of kerosene did not seem to have any effect on hematite flotation. At intermediate concentrations of 40-50 mg/L NaOl, the addition of the 100 mg/L kerosene led to a 5 percentage point increase in hematite recovery. On the other hand, the addition of 100 mg/L kerosene caused an increase in hematite recovery for both hydroxamic acids OHA and OLHA at all collector dosages tested, and the increase was more pronounced at high collector concentrations. In fact, the addition of 100 mg/L kerosene together with 50 mg/L OLHA caused a 28 percentage point increase in hematite recovery from about 60% to about 88%, on par with the other two collectors NaOl and OHA. It seems that the addition of kerosene counter-balanced the negative effects of the low solubility of OLHA, making it behave similarly to soluble collectors.

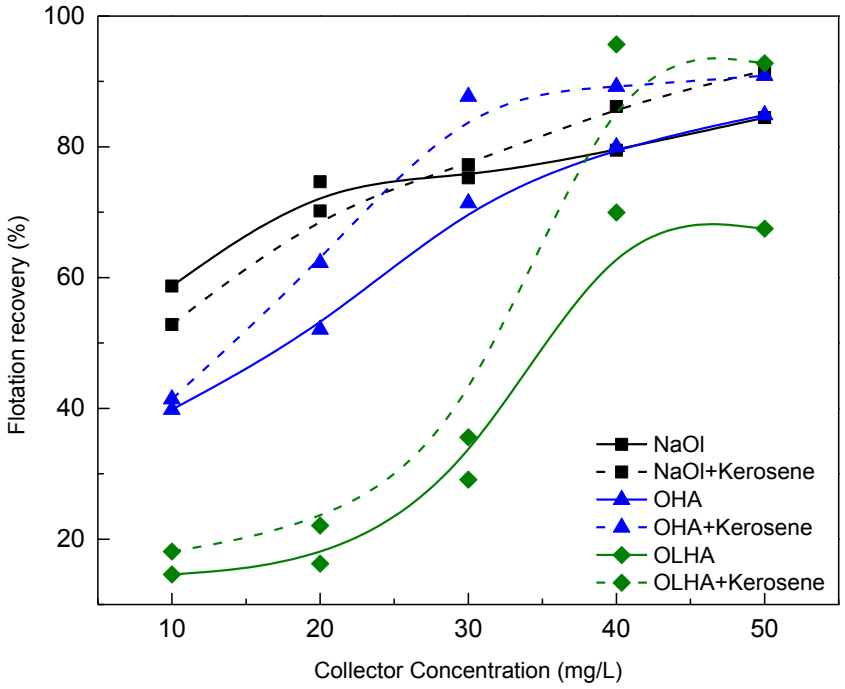

Figure 5.3 Micro-flotation recovery of -20 μm hematite as a function of collector concentration at pH 7 with or without 100 mg/L kerosene.

5.2.3 The Effect of Kerosene Concentration

The influence of kerosene concentration on hematite flotation at pH 7 is shown in Figure 5.4, at a fixed collector concentration of 40 mg/L. It can be seen that the recovery of hematite increases gradually with kerosene concentration at a fixed collector concentration of 40 mg/L. When the concentration of kerosene increased from 0 to 300 mg/L, hematite recovery increased from 80% to 91% for NaOl, 80% to 96% for OHA, and 70% to 97% for OLHA, respectively. The addition of kerosene improved the flotation of hematite more when the hydroxamic acids were used.

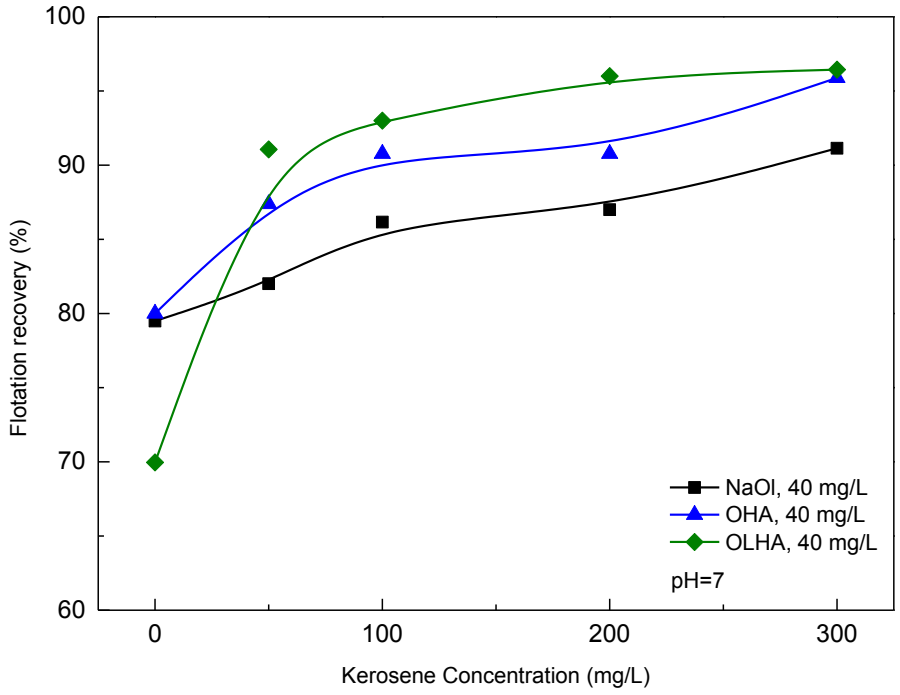

Figure 5.4 Micro-flotation recovery of -20 μm hematite as a function of kerosene concentration at pH 7.

5.2.4 The Effect of Kerosene Adding Manner

Oil-assisted micro-flotation tests were carried out to study the effect of kerosene adding manner on fine -20 μm hematite flotation recovery. Collector concentration was maintained at 40 mg/L and kerosene concentration at 100 mg/L. The kerosene was added either as an immiscible liquid or as an oil-in-water emulsion. The results were shown in Figure 5.5.

As can be seen, the intensifying effect of kerosene in the form of an immiscible liquid was consistently inferior to emulsion, regardless of the types of collectors used. When kerosene was added in the form of an emulsion, the addition sequence of kerosene before, after or together with collector was examined and the results are also shown in Fig. 5.5. It appeared that the best flotation recovery was achieved when the hematite was rendered hydrophobic by a collector first, followed by the addition of the kerosene emulsion. Adding the kerosene emulsion prior to collector,

or adding the kerosene emulsion together with the collector resulted in slightly inferior results.

Therefore, in the following micro-flotation tests, kerosene was added in the form of an emulsion after collector addition.

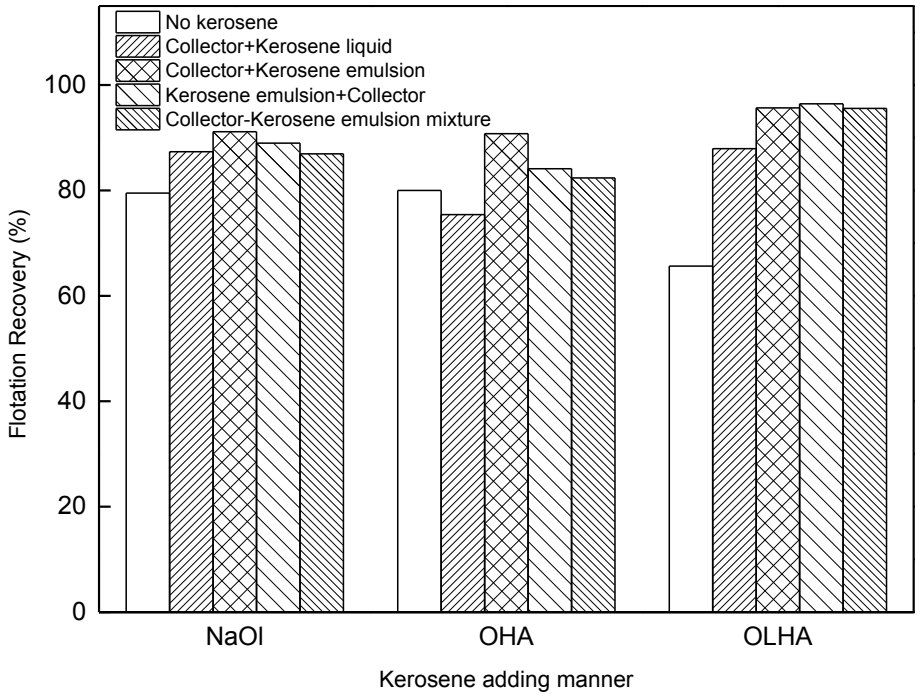

Figure 5.5 Micro-flotation recovery of -20 μm hematite at pH 7 when 40 mg/L NaOl, OLHA or OHA was used as a collector. Legend shows addition sequence. "Kerosene liquid" was bulk kerosene that was not emulsified. Kerosene liquid or emulsion was added at a concentration of 100 mg/L.

In conclusion, kerosene showed beneficial effects in the microflotation of fine hematite using a custom-made glass tube where a froth layer did not exist, which was consistent with other oil-assisted flotation reports using a similar flotation procedure (Liu et al., 2014; Song et al., 2012).

5.3 Oil-assisted Batch Flotation

5.3.1 Reproducibility of Flotation Tests

In the current study, four replicate tests were performed on single hematite mineral under the same test conditions as described in Section 4.4.2 to determine the reproducibility of the flotation tests. The results are shown in Table 5.2. The standard error was 0.567 and the flotation recovery was reproducible within ±1%.

Table 5.2 Reproducibility of batch flotation of hematite single mineral

Test No.	OHA, g/t	Recovery, %	Deviation from mean, %
1	750	80.10	-0.59
2	750	80.96	+0.27
3	750	80.34	-0.35
4	750	81.34	+0.65
Average		80.69	

5.3.2 Effect of Kerosene on Batch Flotation of Single Minerals

5.3.2.1 Comparison between Conventional Flotation, Shear Flocculation Flotation and Agglomeration Flotation

As described in previous sections, due to the inefficiency of collecting fine mineral particles using conventional batch flotation, shear flocculation flotation or agglomeration flotation are often employed to improve the recovery of fine particles by hydrophobic aggregation or oil-assisted agglomeration (Coleman et al., 1995; Jiangang et al., 2012). In both cases, sufficient mechanical energy input, desired amount of bridging oil and selective wetting of particles are the major controlling parameters that determine the size and the strength of flocs/agglomerates, and will influence the follow-up flotation efficiency (Mehrotra et al., 1983).

Therefore, conventional batch flotation, shear flocculation flotation and agglomeration flotation were carried out to observe their differences (Note that the "shear flocculation flotation" was a control test in which the flotation pulp was subjected to the same shear as in agglomeration flotation but without the addition of kerosene). The batch flotation results of hematite single mineral using the three modes are shown in Figure 5.6 and Figure 5.7. Flotation was carried out with different collectors at desired dosages with or without 1 kg/t kerosene emulsion. The shear process was carried out at 1200 rpm for 20 min prior to flotation. Approximately 14.33 kJ mechanical energy dissipated into the flotation pulp during the intense agitation. Detailed operation procedures were described in Section 4.4.3.

As can be seen, the results of conventional flotation, shear flocculation flotation and agglomeration flotation using NaOl, OHA or OLHA were very different from each other.

When NaOl was used as a collector, the flotation recovery of the -20 μm hematite was essentially the same whether the procedures of the conventional flotation, shear flocculation flotation, or agglomeration flotation, were used (compare Figure 5.6and Figure 5.7). The advantages of applying intense conditioning before froth flotation was not observed. The addition of kerosene, however, showed minor adverse effects on the hematite recovery at a low dosage of NaOl (<500 g/t), and such a minor adverse effect was gradually eliminated with increasing NaOl dosages.

When OHA or OLHA was used as a collector, the intense conditioning seemed to show an adverse effect on the flotation performance of hematite minerals, as the flotation recoveries shown in Fig. 5.7 are consistently lower than those shown in Fig. 5.6 at the same OHA or OLHA dosage (the test using 100 g/t OHA is an exception but this may be an outlier). The addition of kerosene when OHA was used as a collector caused a drop in hematite recovery whether intense agitation was used (Figure 5.7) or not (Figure 5.6). This decrease in hematite recovery was gradually eliminated by higher dosages of OHA when no intensive agitation was

used (conventional batch flotation, Figure 5.6). But in agglomeration flotation where intensive agitation was used prior to flotation, the suppression effect of the kerosene was still apparent even after adding 2 kg/t OHA. This observation was in disagreement with the micro-flotation, where the recovery of hematite was enhanced in the presence of kerosene irrespective of OHA dosages (Figure 5.3).

To avoid the possible complications caused by the intensive agitation which may mask the effect of neutral oil in the flotation process, the intensive agitation step was removed from subsequent tests.

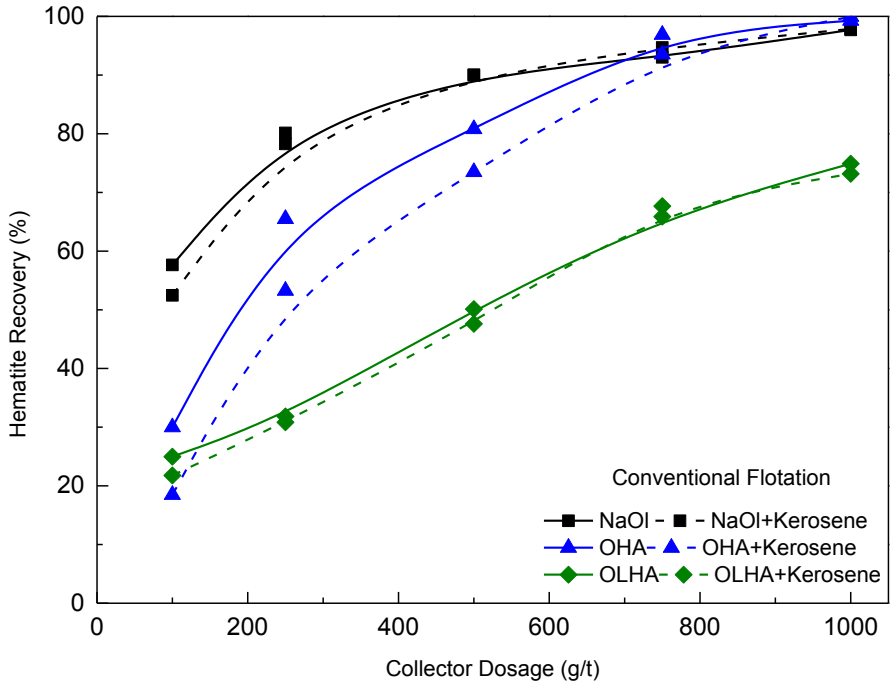

Figure 5.6 Conventional flotation recovery of fine hematite using NaOl, OHA, or OLHA as a collector with or without 1 kg/t kerosene. Kerosene emulsion was added to the flotation cell directly without intensive conditioning.

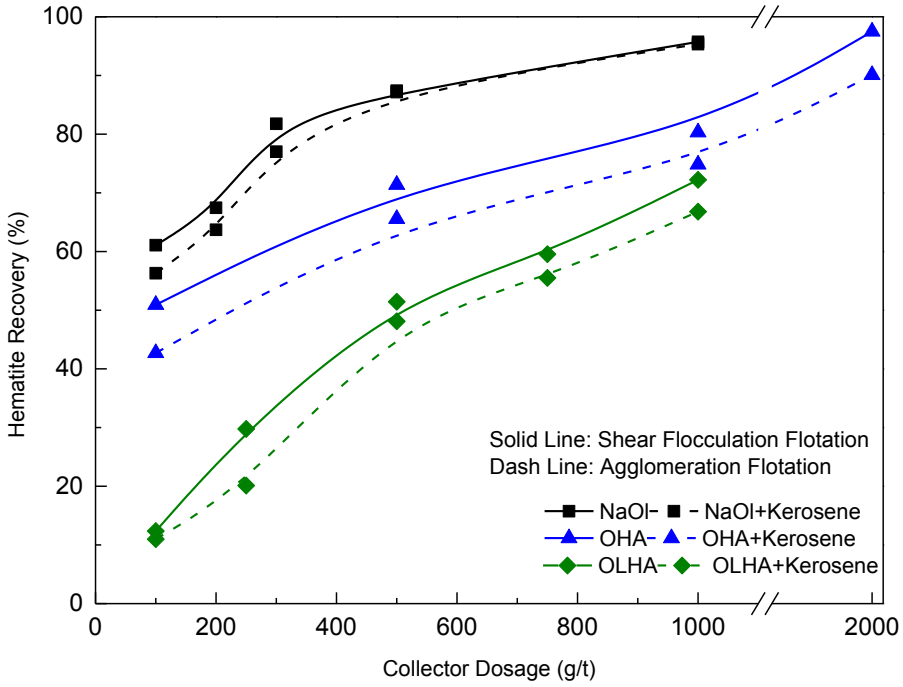

Figure 5.7 Batch flotation recovery of fine hematite using NaOl, OHA, or OLHA as a collector in the mode of shear flocculation flotation or agglomeration flotation in presence of 1 kg/t kerosene.

5.3.2.2 Effect of Kerosene on Flotation Kinetics of Fine Hematite

Figure 5.8 to Figure 5.10 show the effect of kerosene on the kinetics of flotation of the fine -20 μm hematite using NaOl, OHA or OLHA as a collector at dosages ranging from 100 g/t to 1 kg/t, respectively.

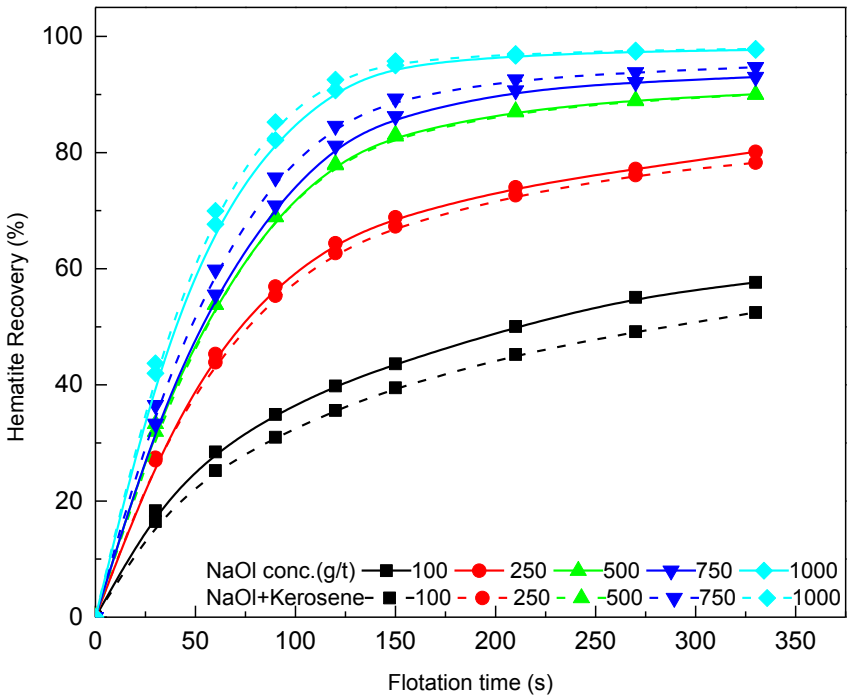

Figure 5.8 Flotation of hematite using NaOl as a collector with or without 1 kg/t kerosene.

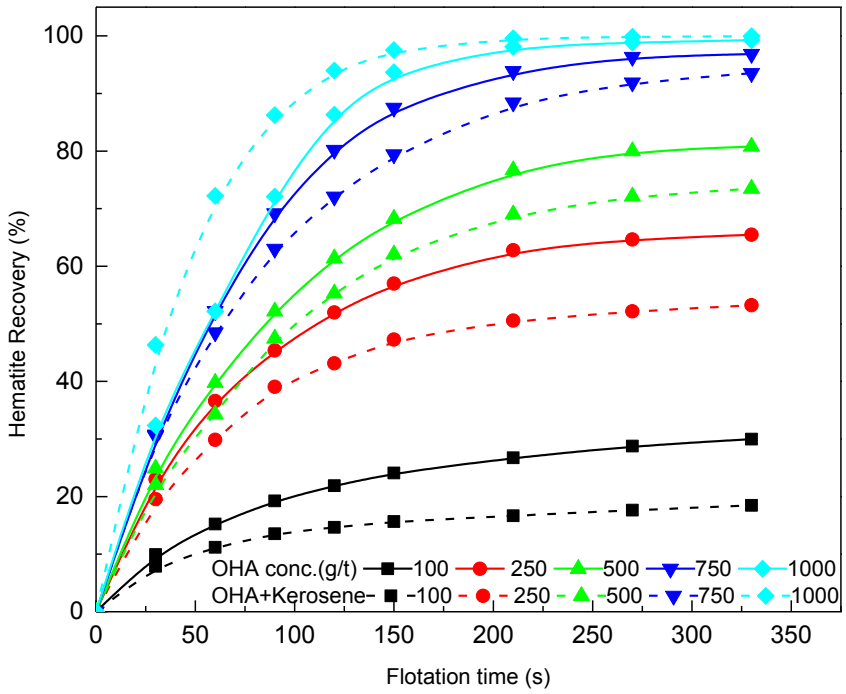

Figure 5.9 Flotation of hematite using OHA as a collector with or without 1 kg/t kerosene.

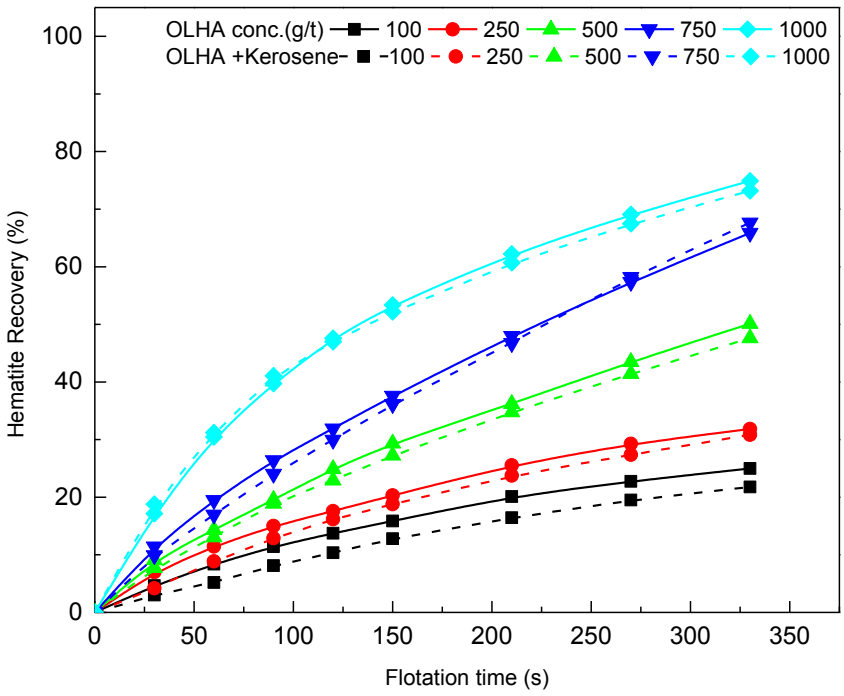

Figure 5.10 Flotation of hematite using OLHA as a collector with or without 1 kg/t kerosene.

As can be seen in Figure 5.8, at 100 g/t NaOl, the addition of 1 kg/t kerosene caused no more than 3 percentage points of cumulative hematite recovery loss. Therefore, kerosene had a detrimental effect when NaOl was used as a collector at low dosages. This limited detrimental effect was compensated and counter-balanced at higher NaOl dosages. Above 500 g/t NaOl, the addition of 1 kg/t kerosene started to show positive impacts and accelerated flotation rates of the hematite. This was consistent with past reports in the literature.

Similar trend of the effect of kerosene was also noticed with OLHA as shown in Figure 5.10. Despite its poor collecting power and reduced frothing ability caused by the low solubility of OLHA, the adverse effect of kerosene when OLHA was used as a collector was generally very small, and was offset at higher OLHA dosages.

However, when OHA was used as the collector, the detrimental effect of kerosene was obvious, especially at low OHA dosages (Figure 5.9). In fact, in the range of OHA dosages tested, from 100 to 750 g/t, the addition of 1 kg/t kerosene caused a significant reduction in hematite recovery. The magnitude of the reduction was higher at lower OHA dosages. It was observed during the flotation tests that at 100 g/t OHA, the mineralization of the froth decreased drastically after adding 1 kg/t kerosene. Bubbles were turning fragile and easily ruptured during aeration and froth scrapping. This was also observed at 250 g/t OHA. A similar phenomenon was noticed by Ni (2013) when he attempted to use 1 kg/t or higher dosages of emulsified kerosene to improve the OHA flotation of a niobium oxide ore, even when using a strong frother Dowfroth 250. Such a detrimental defrothing effect on the froth behavior, however, was not visually observed when the long chain collectors NaOl or OLHA was used as a collector.

However, at the higher OHA dosage of 1 kg/t OHA, the addition of kerosene accelerated the flotation rates of hematite (Figure 5.9), and the detrimental effect of kerosene seemed to have been reversed.

5.3.3 Effect of Kerosene on Batch Flotation of Mineral Mixtures

In froth flotation, value mineral recovery is not the only criterion to judge the performance. The grade of the floated concentrates is also important as it controls product quality. In this regards, an overly stable froth layer is in fact not desirable as it increases the chances of mechanical/hydraulic entrainment of the fine hydrophilic gangue minerals. To study the possible effect of the defrothing effect of neutral oil on concentrate grade, batch flotation tests were conducted on mixtures of -20 μm fine hematite and -15 μm fine quartz. Fine quartz was chosen as gangue minerals since it does not react with the collectors. Its recovery to the concentrate would indicate the degree of mechanical entrainment. The collector dosages were decreased by half compared with hematite single mineral flotation tests to account for the decreased amount of hematite.

5.3.3.1 Effect of Collector Dosages on Batch Flotation of Mineral Mixtures

These comparative batch flotation tests were performed at natural pH (pH 6.5~7.5), and the results are shown in Table 5.3 to Table 5.5.

Table 5.3 Batch flotation of hematite/quartz mixtures with NaOl and kerosene.

NaOl, g/t	Kerosene	Conc. weight, %	Assay		Distribution		Efficiency, %
			Fe_2O_3, %	SiO_2, %	Fe_2O_3, %	SiO_2, %	
50	0	17.1	55.69	41.48	21.3	13.5	7.8
	1 kg/t	15.3	56.94	40.22	19.6	11.6	8.0
125	0	33.1	61.20	35.77	45.4	22.6	22.8
	1 kg/t	33.2	61.92	35.35	45.4	22.5	22.9
250	0	46.2	61.52	35.60	62.6	31.6	31.0
	1 kg/t	46.4	62.75	34.48	63.9	30.9	33.0
375	0	57.7	61.62	35.44	77.6	39.7	37.9
	1 kg/t	55.3	62.50	34.61	75.6	37.0	38.6
500	0	62.4	61.59	36.67	83.4	43.9	38.9
	1 kg/t	64.4	67.61	30.50	92.5	38.3	53.1

Table 5.4 Batch flotation of hematite/quartz mixtures with OHA and kerosene.

OHA, g/t	Kerosene	Conc. weight, %	Assay		Distribution		Efficiency, %
			Fe_2O_3, %	SiO_2, %	Fe_2O_3, %	SiO_2, %	
50	0	10.9	47.12	49.94	11.5	10.4	1.1
	1 kg/t	7.4	44.90	52.12	7.4	7.3	0.1
125	0	36.8	54.57	42.67	44.4	30.0	14.4
	1 kg/t	29.3	52.06	45.32	33.9	25.2	8.7
250	0	60.6	61.47	35.72	81.6	41.8	39.8
	1 kg/t	54.7	62.20	35.11	74.5	37.1	37.4
375	0	66.0	62.93	34.15	91.1	43.4	47.7
	1 kg/t	65.8	62.88	34.23	90.6	43.5	47.1
500	0	72.0	61.57	36.66	94.1	51.5	41.9
	1 kg/t	71.1	63.42	34.78	94.8	48.7	45.2

Table 5.5 Batch flotation of hematite/quartz mixtures with OLHA and kerosene.

OLHA, g/t	Kerosene	Conc. weight, %	Assay		Distribution		Efficiency, %
			Fe_2O_3, %	SiO_2, %	Fe_2O_3, %	SiO_2, %	
50	0	8.2	52.76	43.96	9.5	7.0	2.5
	1 kg/t	5.3	56.75	39.64	6.7	4.0	2.7
125	0	21.2	53.85	42.92	24.8	17.7	7.1
	1 kg/t	20.3	55.48	41.14	24.5	16.3	8.2
250	0	28.0	64.15	32.48	39.5	17.4	22.1
	1 kg/t	25.5	67.09	29.48	37.2	14.7	22.5
375	0	35.1	69.60	26.72	52.2	18.6	33.6
	1 kg/t	31.4	71.35	25.13	49.1	15.2	33.9
500	0	42.3	80.77	17.48	72.7	14.4	57.3
	1 kg/t	44.7	87.08	11.34	83.2	9.8	72.4

As can be seen from Table 5.3 to Table 5.5, in the absence of kerosene, NaOl, OHA and OLHA acted as hematite collectors as both the Fe_2O_3 grade and recovery increased with increasing collector dosages. The SiO_2 recovery also increased with increasing collector dosage despite its lower grade in the floated concentrate at the higher collector dosages, a result caused by the higher concentrate weight yield due to the higher froth stability at the high collector dosages. Different from NaOl and OHA, the flotation response using OLHA was not satisfactory despite its long hydrocarbon chain, which was likely caused by its low solubility in water. Interestingly, the short chain hydroxamic acid OHA was not only better than OLHA but also better than NaOl.

The addition of 1 kg/t kerosene, however, resulted in different responses using the three collectors. Table 5.3 and Table 5.5 showed the beneficial effects of kerosene

in promoting the flotation performance of the fine hematite when NaOl or OLHA was used as a collector. Within the range of collector dosages tested, the assayed Fe_2O_3 grades of the concentrates were consistently higher than those without kerosene. This could be due to the higher surface hydrophobicity of the hematite induced by the kerosene, and/or by the lower entrainment of quartz due to the defrothing effect of kerosene.

On the other hand, when the short chain hydroxamic acid OHA was used as a collector, the addition of kerosene had a detrimental effect (Table 5.4). Hematite recovery was not improved but rather, was reduced when 1 kg/t kerosene was added at low OHA dosages (50-250 g/t). Starting from OHA dosage of 375 g/t, the detrimental effect of kerosene seemed to have been eliminated and the hematite grade and recovery were similar or slightly higher than when no kerosene was used. At low OHA dosages, the addition of 1 kg/t kerosene caused a reduction on concentrate weight yield, Fe_2O_3 grades and Fe_2O_3 recovery. While the reduction in concentrate weight yield was likely the result of the defrothing effect of kerosene, the slight reduction of concentrate Fe_2O_3 grade was puzzling. It seemed that the surface hydrophobicity of the hematite was not improved following kerosene addition when it was made hydrophobic by low dosages of OHA.

5.3.3.2 Effect of Kerosene Dosages on Batch Flotation of Mineral Mixtures

The effect of kerosene dosage on batch flotation of fine hematite and quartz was studied with a high dosage of collectors (500 g/t). The results are shown in Table 5.6 to Table 5.8. Due to the stable and rich frothing layers at high collector dosage, the flotation responses in terms of concentrate Fe_2O_3 grade and recovery improved dramatically with increasing addition of kerosene. This positive effect was very strong, leading to a much higher separation efficiency, which may be attributed to a higher surface hydrophobicity and the formation of larger hydrophobic flocs when kerosene was added. At low kerosene dosages, the defrothing effect of kerosene was not obvious judging by the stable mineralized froth. Once oil addition reached

a “critical dosage” (3 kg/t with NaOl, 2 kg/t with OHA, and 0.5 kg/t with OLHA), further increase in kerosene dosage resulted in a decrease in separation efficiency – most likely as the kerosene droplets were starting to play a role in lowering froth stability. For instance, when 10 kg/t kerosene was added in the flotation pulp where 500 g/t NaOl was used as a collector, the concentrate weight yield, grade and recovery as well as entrained quartz decreased significantly, implying unstable froths due to excessive oil in the flotation pulp.

Table 5.6 Batch flotation of hematite/quartz mixtures with NaOl and kerosene.

NaOl, g/t	Kerosene, kg/t	Conc. weight, %	Assay		Distribution		Efficiency, %
			Fe_2O_3, %	SiO_2, %	Fe_2O_3, %	SiO_2, %	
500	0	62.4	61.59	36.67	83.4	43.9	38.9
	0.5	64.2	65.42	32.97	88.3	41.6	45.9
	1	64.4	67.61	30.50	92.5	38.3	53.1
	2	62.2	68.85	29.35	90.8	35.7	54.1
	3	59.2	70.98	27.09	89.0	31.4	56.5
	10	53.0	58.76	37.81	66.8	39.8	25.8

Table 5.7 Batch flotation of hematite/quartz mixtures with OHA and kerosene.

OHA, g/t	Kerosene, kg/t	Conc. weight, %	Assay		Distribution		Efficiency, %
			Fe_2O_3, %	SiO_2, %	Fe_2O_3, %	SiO_2, %	
500	0	72.0	61.57	36.66	94.1	51.5	41.9
	0.5	73.5	61.90	35.36	95.9	51.7	42.7
	1	71.1	63.42	34.78	94.8	48.7	45.2
	2	71.4	64.46	33.72	97.1	47.4	48.8
	3	70.1	62.32	35.81	95.1	47.8	46.3
	10	66.5	63.20	33.57	92.4	43.0	47.6

Table 5.8 Batch flotation of hematite/quartz mixtures with OLHA and kerosene.

OLHA g/t	Kerosene kg/t	Conc. weight, %	Assay		Distribution		Efficiency, %
			Fe_2O_3, %	SiO_2, %	Fe_2O_3, %	SiO_2, %	
500	0	42.3	80.77	17.48	72.7	14.4	57.3
	0.5	48.6	84.94	13.20	87.9	12.5	74.1
	1	44.7	87.08	11.34	83.2	9.8	72.4
	2	43.6	82.55	15.55	76.6	13.2	62.2
	3	42.5	82.55	15.68	74.4	13.0	60.3
	10	40.0	81.07	17.01	68.9	13.3	54.6

Therefore, the foregoing description of the flotation test results shows that in froth flotation, the benefits of adding neutral oil as an auxiliary collector could only be achieved when the oil's ability to enhance mineral surface hydrophobicity

outweighed its detrimental effect of defrothing. In the absence of a frother, collectors with a longer hydrocarbon chain, such as the oleoyl group, or collectors with a short hydrocarbon chain but used at high dosages, can benefit from the use of a neutral oil as an auxiliary collector. Using collectors with short hydrocarbon chains and low dosages, the addition of neutral oil was detrimental.

It was observed during the flotation testing that the addition of kerosene also seemed to have caused the growth of the sizes of the hydrophobic aggregates. This was likely caused by the increased hydrophobicity of the particles rendering them more capable to form aggregate by hydrophobic association in the aqueous flotation pulp. The large sized hydrophobic aggregates were also the reason for improved flotation recovery of the hematite. A detailed study was carried out and reported in the next section on the aggregation of the fine hematite particles.

5.4 Interactions of Oil Droplets and Hematite Particles

5.4.1 Oil-assisted Aggregation of Hematite Particles

The results of fine -20 μm hematite flocculation as a function of collector concentration with or without 100 mg/L kerosene addition is shown in Figure 5.11. The "Flocculation Efficiency" of -20 μm hematite particles is calculated as the percent reduction in the number of hematite particles below D_{90} (-10 μm), provided by FBRM particle size analyzer, after 5-min conditioning followed by collector or kerosene addition.

As can be seen, the effectiveness of NaOl, OHA or OLHA for the flocculation of fine hematite was very evident. OLHA acted as the strongest flocculants, followed by NaOl. OHA showed the least flocculation ability even at high concentrations where about 90% flotation recovery can be achieved (refer to Figure 5.3). Upon kerosene addition, the flocculation efficiency was further enhanced as the particle number below 10 μm was decreased further. It was worth noting that despite the

observation that the addition of OHA and 100 mg/L kerosene caused about 10 percentage point increase in flocculation efficiency, the "absolute" flocculation efficiency of OHA with kerosene addition was still low (about 25%) compared with NaOl (90%) and OLHA (99%). In addition, due to the strong flocculation ability of OLHA itself, the flocculation efficiency was extremely high. The effect of kerosene addition was masked and cannot be simply reflected by fine particle number reduction.

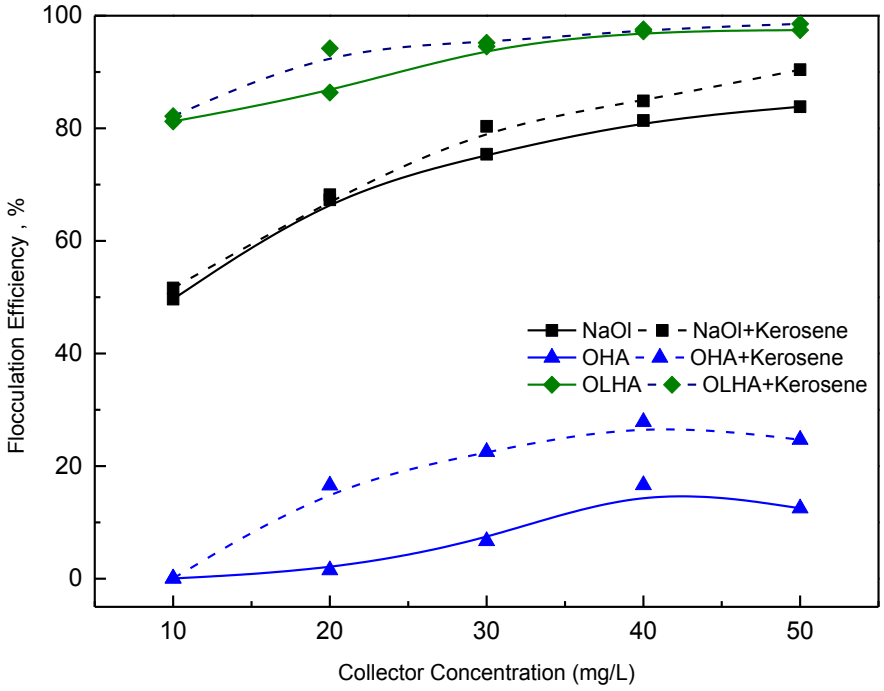

Figure 5.11 The flocculation efficiency of fine -20 μm hematite particles as a function of collector concentration with or without 100 mg/L kerosene at pH 7.

Therefore, oil-assisted aggregation study by evaluating in-situ floc growth of -20 μm hematite was performed by combining FBRM particle size analysis and optical microscopic observations. Chord length counts were recorded in real time in different channels of the FBRM controller and were considered to be related to the number of particles within the different size ranges. Chord length distribution (CLD) data were also acquired simultaneously after reagent addition. The "no weight" CLD provided enhanced number-sensitive information of the counts of fine

particles, while the "square weighted" CLD provided volume-sensitive information of aggregated coarse particles. The FBRM particle size analysis results are shown in Figure 5.12 to Figure 5.14, together with the corresponding optical microscopic images.

Figure 5.12 shows the aggregation status of the -20 μm hematite sample before and after NaOl and kerosene addition. The hematite suspension was initially stirred for 5 min at pH 7. Figure 5.12a shows that the particle counts were predominantly in the -10 μm and the 10-50 μm channels of the FBRM (Figure 5.12a, green and red curves), and the corresponding square weighted chord length was about 29 μm (Figure 5.12a, black curve). The no weight count curve at time point 04:58 (Figure 5.12b) shows that the particles were indeed predominantly below 20 μm. At time point 05:00, 50 mg/L NaOl was added to the hematite suspension. This caused a sharp decrease in the counts of fine particles below a chord length of 50 μm, especially the particle counts below a chord length of 10 μm (Figure 5.12a, red curve). In the meantime, the particle count curves for chord lengths larger than 50 μm increased, showing particle aggregation (Figure 5.12a, dark blue and light blue curves). The square weighted chord length increased sharply from 29 μm to above 70 μm upon the addition of 50 mg/L NaOl, followed by a slow increase and reached 80 μm after 5 min (Figure 5.12a, black curve). The optical microscopic image of hematite aggregates in the presence of NaOl is shown in Figure 5.12c. Most of the aggregates were about 30×70 μm, which was in good agreement with the aggregation endpoint observed in the FBRM.

When kerosene emulsion was added subsequently at time point 10:00, the fine particle counts (less than 50 μm) were decreased further. The square weighted chord length jumped from about 80 μm to above 150 μm (Figure 5.12a and b), clearly showing further growth of the aggregates. The double peaks near 1 mm chord length (Figure 5.12b) were likely due to the interfering air bubbles attached to the lens of the probe during stirring. The optical microscope image (Figure 5.12d) also shows that the aggregates were much larger, about 170×220 μm in dimension,

after adding kerosene. In addition, the particle counts below 50 μm dropped significantly in exchange for a significant increase in particle counts with chord length larger than 150 μm (Figure 5.12a, light blue curve). In other word, the observed large aggregates were mainly made of oil-bridged small aggregates. The large size of the aggregates obviously benefited the flotation recovery of the fine hematite.

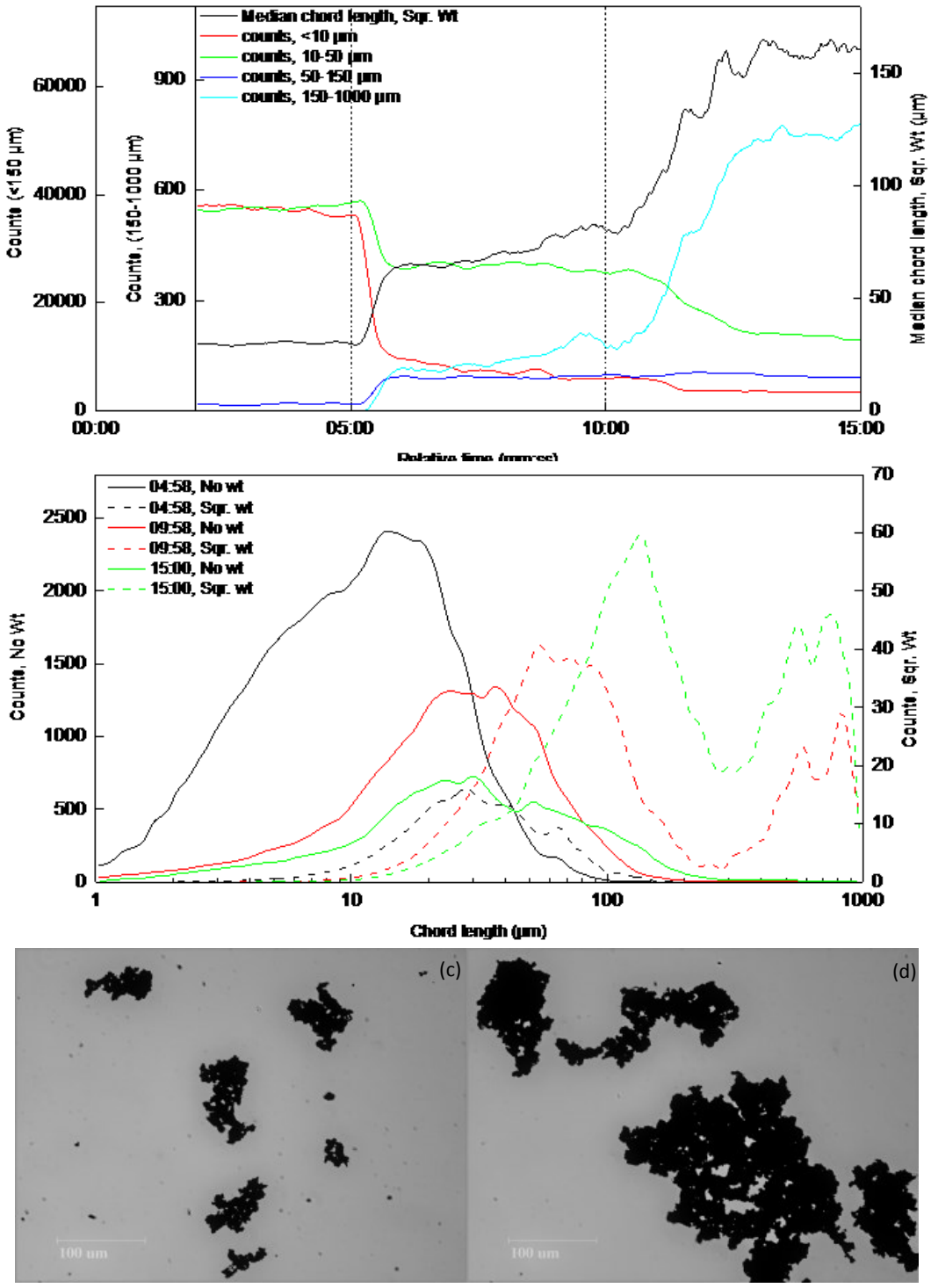

Figure 5.12 Aggregation of hematite by NaOl and kerosene at pH 7. (a) Counts and square weighted median chord length of hematite suspension as a function of time. NaOl (50 mg/L) was added at 05:00 min and kerosene (100 mg/L) was added at 10:00 min. (b) No weighted and square weighted counts chord length distribution of hematite suspension at 04:58, 09:58 and 15:00; (c) Optical microscope image of hematite at 09:58; (d) Optical microscope image of hematite at 15:00.

Figure 5.13 illustrates the oil-assisted aggregation of -20 μm hematite when OHA was used as a collector. Different from NaOl, the aggregation by short-chain OHA was not obvious. The addition of OHA at time point 05:00 only caused a minor decrease in the particle counts with a chord length less than 10 μm. The peak next to 05:00 was due to the dispersion effect as a result of an increase in pH after hydroxamate addition. The particle counts of other size ranges remain unchanged. A similar phenomenon was also observed at time point 10:00 when kerosene was added. The weighted chord length at time point 15:00 only increased by 4 μm compared with that before OHA addition, which was negligible. The optical images of the hematite suspension after kerosene addition did not show a significant degree of aggregate dimensions, indicating a less efficient adhesion effect of kerosene on hematite particles when OHA was used as a collector.

To make a comparison, a longer chain hydroxamic acid, OLHA, was added to the hematite suspension to investigate the effect of kerosene. The results are shown in Figure 5.14. In order to minimize the influence of undissolved OLHA, a lower dosage of 30 mg/L was used. As can be seen, the aggregation behavior shown in Figure 5.14 was similar to that shown in Figure 5.12, where NaOl, with the same hydrocarbon chain, was used. After adding the OLHA, a sharp peak in the particle count of the -10 μm chord length was observed. This was similar to OHA and likely caused by the increase in pH. Once the suspension pH was readjusted to neutral, the counts of fine particles (chord length less than 50 μm) decreased significantly from 42,000 to 2990 (Figure 5.14a, red curve). At the same time, the particle count between chord length 50 and 150 μm increased from near zero to 220 (Figure 5.14a, dark blue curve). However, particle counts larger than chord length 150 μm (Figure 5.14a, light blue curve) went through a rapid increase from 0 to as high as 860 but followed by a quick drop to below 300, signaling the breakage of the aggregates. Despite the apparent decrease in the count of large aggregate size, the median chord length at 09:58, at about 70-80 μm, was still several times larger than the chord length in the original suspension (Figure 5.14a, black curve and Figure 5.14b, red dashed curve).

The addition of kerosene at time point 10:00 in the OLHA system also caused a further increase in the degree of aggregation, which was similar to NaOl. The peak of square weighted CLD shifted from 80 to 150 μm (Figure 5.14b, green dashed curve), representing a significant growth of hematite aggregates. The sizes of hematite aggregates observed from optical microscope images also increased from about 60×90 μm to 180×280 μm, which was consistent with the FBRM results. Therefore, kerosene had a beneficial effect in hematite aggregation using OLHA.

The results shown in Figure 5.12 to Figure 5.14 indicated that the limited effect of kerosene in hematite aggregation when OHA was used was mainly due to a weaker interaction associated with the shorter hydrocarbon chain length of OHA, rather than its hydroxamate group. The findings were also consistent with the conclusions by Ozkan et al. (2016), who compared the flocculation enhancement of a talc suspension with kerosene promoted by surfactants with different hydrocarbon chain lengths.

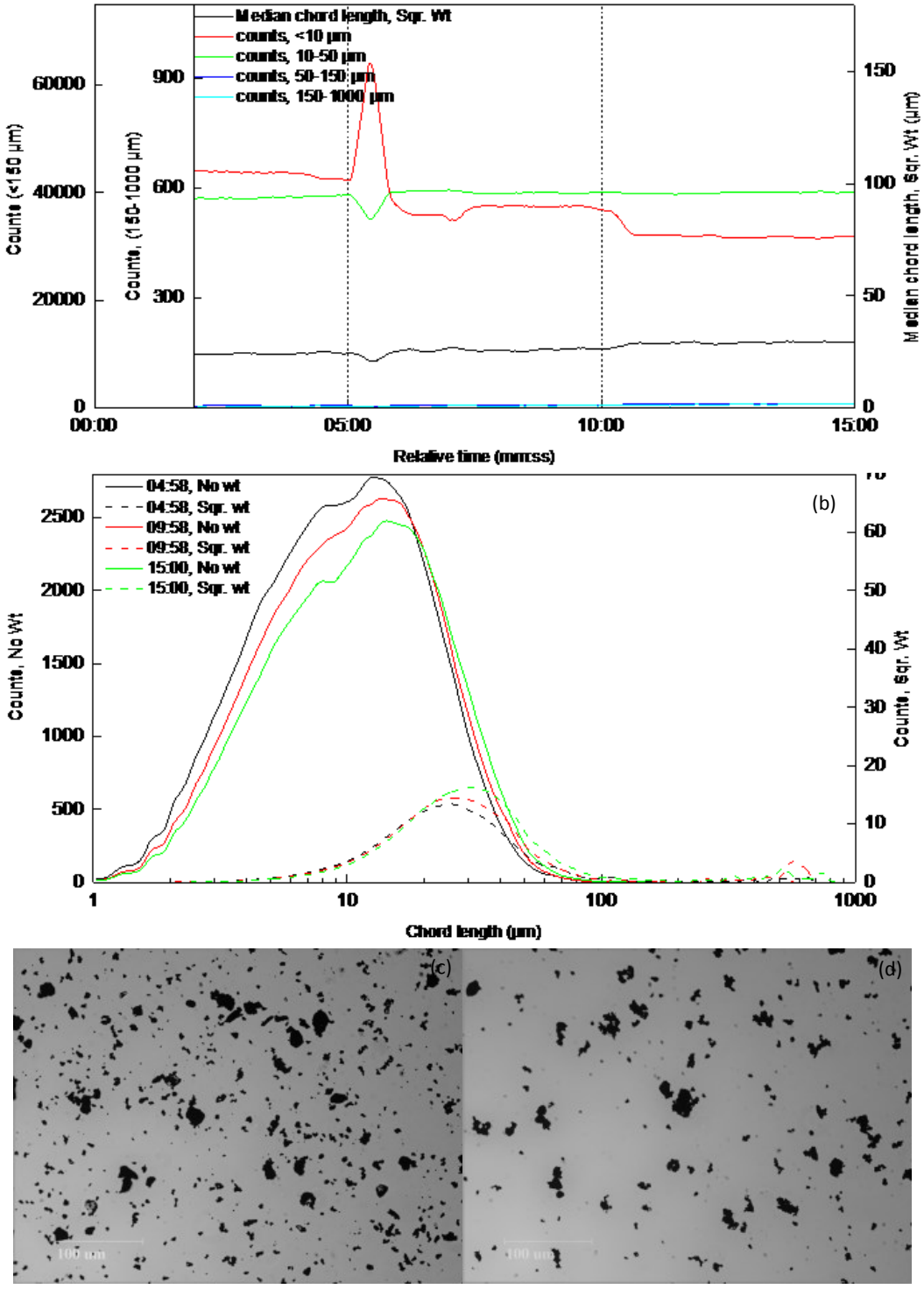

Figure 5.13 Aggregation of hematite by OHA and kerosene at pH 7. (a) Counts and square weighted median chord length of hematite suspension as a function of time. OHA (50 mg/L) was added at 05:00 and kerosene (100 mg/L) was added at 10:00. (b) No weighted and square weighted counts chord length distribution of hematite suspension at 04:58, 09:58 and 15:00; (c) Optical microscope image of hematite at 09:58; (d) Optical microscopy image of hematite at 15:00.

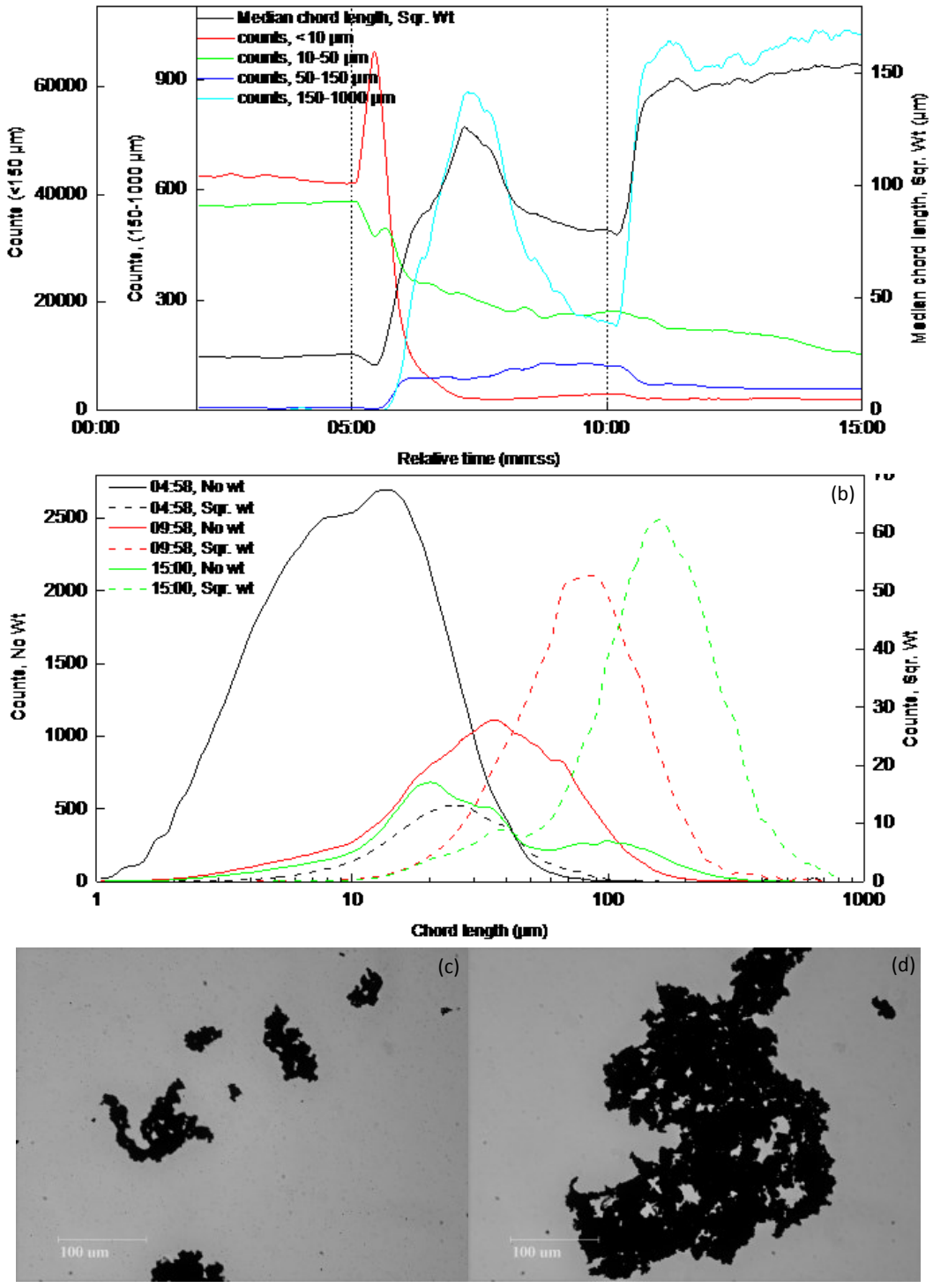

Figure 5.14 Aggregation of hematite by OLHA and kerosene at pH 7. (a) Counts and square weighted median chord length of hematite suspension as a function of time. OLHA (30 mg/L) was added at 05:00 and kerosene (100 mg/L) was added at 10:00. (b) No weighted and square weighted counts chord length distribution of hematite suspension at 04:58, 09:58 and 15:00; (c) Optical microscope image of hematite at 09:58; (d) Optical microscopy image of hematite at 15:00.

In an aqueous suspension, the aggregation or dispersion behavior of fine mineral particles is governed by the inter-particulate forces, which are quantitatively described by the classical DLVO theory, or the extended-DLVO theory when non-DLVO forces are involved. The type of inter-particulate forces were studied to understand the observed aggregation behaviors in the hematite suspensions.

5.4.2 Zeta Potential and Zeta Potential Distribution

5.4.2.1 Zeta Potentials of Hematite and Kerosene Droplets

Figure 5.15 shows the zeta potentials of hematite particles in the absence or presence of the tested collectors as a function of pH. As can be seen, the zeta potentials of hematite decreased steadily with increasing solution pH, exhibiting its isoelectric point (IEP) at around 6.4, which was identical to the IEPs of hematite compiled by Parks (1965). In the presence of OHA or OLHA, the IEP of hematite particles shifted to about 5.3 and 3.7, respectively, implying the chemisorption of hydroxamate on hematite surface at neutral pH since both hematite and the collectors were charged negatively at pH > IEP. Different from OHA and OLHA, the addition of NaOl caused a remarkable decrease in zeta potentials of hematite throughout the pH range, with a projected IEP at below 2. The maximum shift in zeta potential caused by NaOl occurred at pH near 7.0, probably related to the maximum oleic acid/oleate co-adsorption in this pH range (Kulkarni & Somasundaran, 1975).

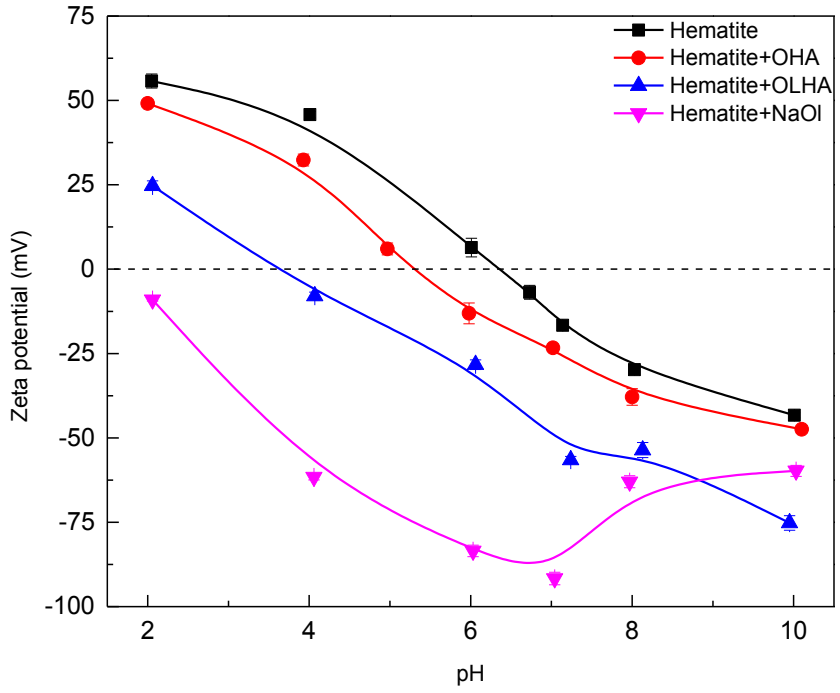

Figure 5.15 Zeta potentials of hematite particles as a function of pH in the presence of 100 mg/L of OHA, OLHA, or NaOl.

The zeta potentials of kerosene droplets as a function of pH were determined in aqueous solution with and without 100 mg/L OHA, OLHA, or NaOl, and the results are presented in Figure 5.16. As can be seen, kerosene droplets were negatively charged over the entire pH range tested (from 2 to 10). The value of zeta potential increased significantly in the negative direction with increasing pH. Adding NaOl in the kerosene emulsion did not make a noticeable difference on its zeta potential at very acidic condition, but decreased it gradually with increasing pH. The acid dissociation constant of oleic acid *p*Ka = 5.0 (Stoker, 2012), but it is speculated that it is not the ionized oleate group but the ion-molecular species of NaOl that interacted with kerosene droplets. The *p*Ka of OHA and OLHA were approximately 9.0 and 9.5, respectively (Somasundaran, 1987; Zhou et al., 2015), so that at below pH 9.5, the OHA and OLHA solutions were dominated by neutral hydroxycarbamoyl (-C(=O)NH-OH) molecules rather than hydroxamate anions (-C(=O)NH-O^-). Thus, the interaction of OHA and OLHA in the majority of the tested pH range of 2 to 10 would involve the binding of the neutral hydroxamic

acid molecules to kerosene, thus lowering the magnitude of the negative charge of kerosene.

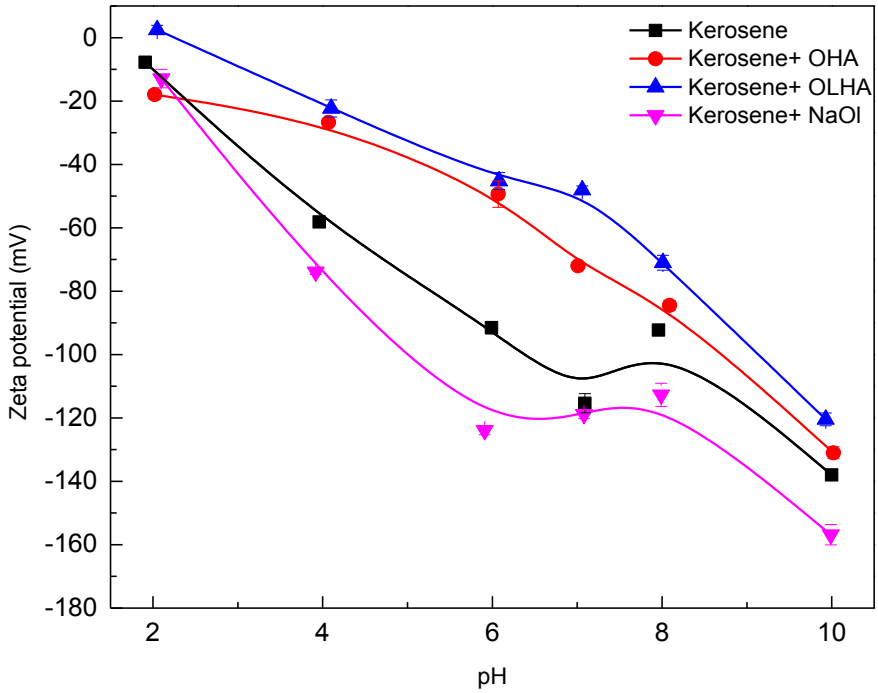

Figure 5.16 Zeta potentials of kerosene droplets as a function of pH in the absence and presence of 100 mg/L of OHA, OLHA, or NaOl

Figure 5.15 and Figure 5.16 also indicated strong negative surface charges of collector coated hematite surfaces and kerosene/collector droplets at pH 7, implying that strong electrostatic repulsion forces exist between them. Yet, the improved aggregation of hematite particles in the presence of collectors was observed, especially with the use of NaOl and OLHA. Therefore, the zeta potential distributions of hematite particles and kerosene droplets, individually or as a mixture were examined to observe their interactions.

5.4.2.2 Zeta Potential Distribution

The zeta potential distributions of hematite particles and kerosene droplets were measured individually or as a mixture (mass ratio of 1:1) in 1 mM KCl solution

containing 50 mg/L NaOl, OHA, or OLHA at pH 7. The results were shown in Figure 5.17 to Figure 5.19.

As can be seen in Figure 5.17, when 50 mg/L NaOl was added in the hematite mineral suspension or kerosene emulsion, their zeta potentials were centered around -70 mV and -125 mV, respectively. When the two suspensions were mixed, the distribution peaks of kerosene droplets disappeared and shifted significantly towards the peaks of hematite particles. The observed boarder zeta potential distribution (than hematite alone) suggested a partial attachment of hematite particles on kerosene droplets.

When OLHA was added in the suspension at pH 7, as shown in Figure 5.19, only one distribution peak centered at -33 mV was observed in binary mixture at mass ratio of 1:1, which was identical to that of hematite particles measured alone. This phenomenon may be caused by the near full coverage of kerosene droplets by hematite particles.

In the case where 50 mg/L OHA was tested under similar condition, as shown in Figure 5.18, the distribution peaks of hematite particles and kerosene droplets were centered at about -25 mV and -80 mV, respectively. However, when mixed, three distinct groups of peaks were observed. The positions of major peaks on both sides suggested that kerosene droplets and hematite particles shifted slightly towards each other, and the group of minor peaks in the center was likely due to the weak interaction between hematite particles and kerosene droplets.

The electrophoretic measurements show that the interactions of kerosene droplets and hematite particles was much stronger when NaOl or OLHA was used than when OHA was used, which must be the results of other more favorable attractive forces. The extended DLVO theory calculation was therefore carried out to understand the energetics of the studied hematite-collector-kerosene system.

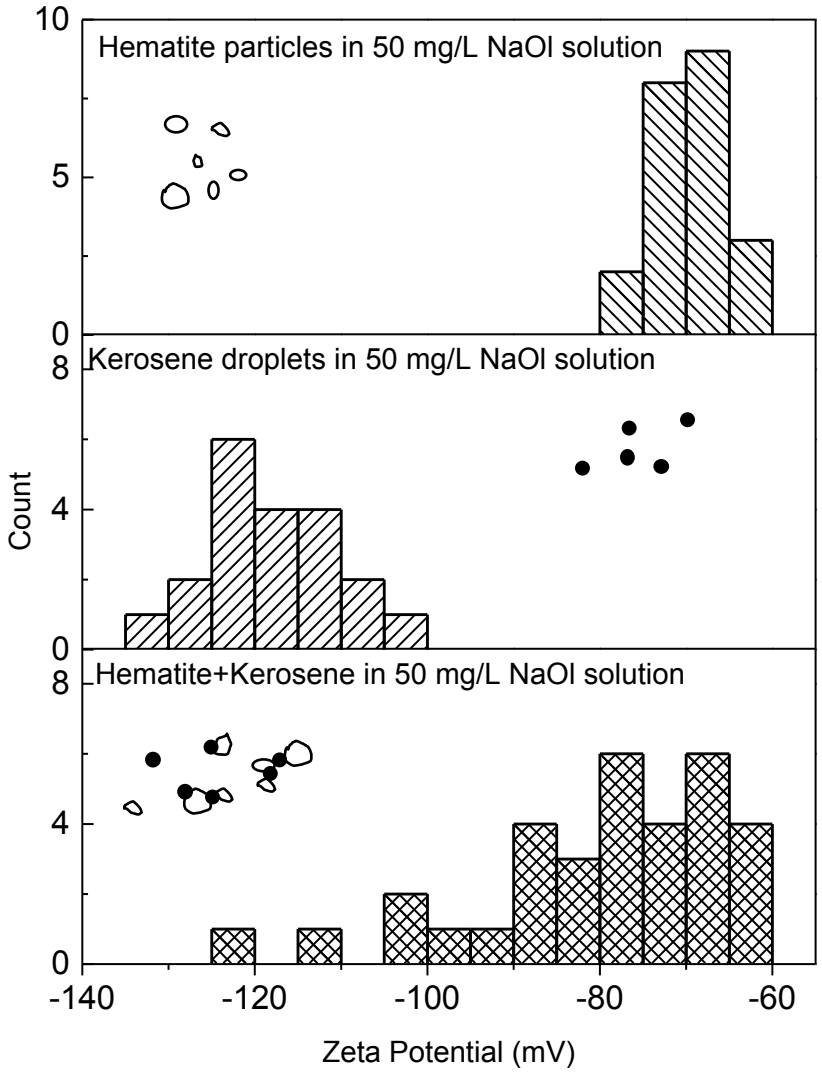

Figure 5.17 Zeta potential distribution of hematite particles, kerosene droplets and their mixture in 50 mg/L NaOl solution at pH 7.

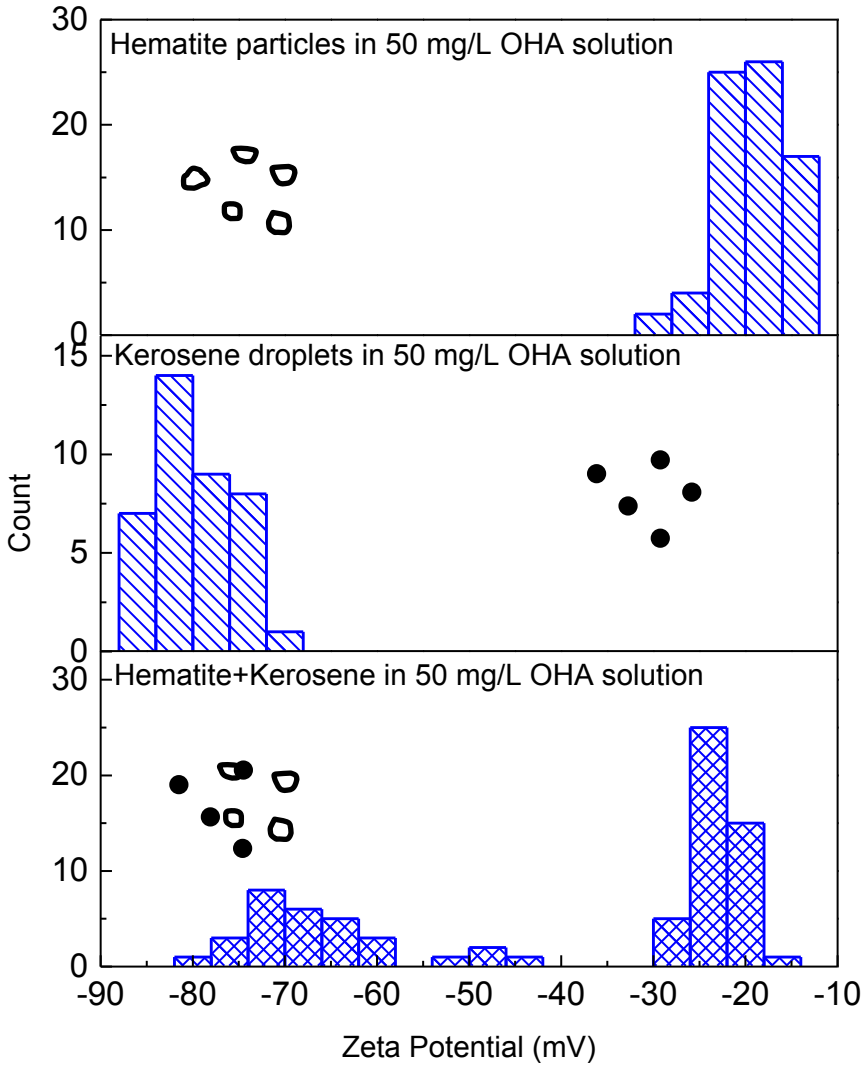

Figure 5.18 Zeta potential distribution of hematite particles, kerosene droplets and their mixture in 50 mg/L OHA solution at pH 7.

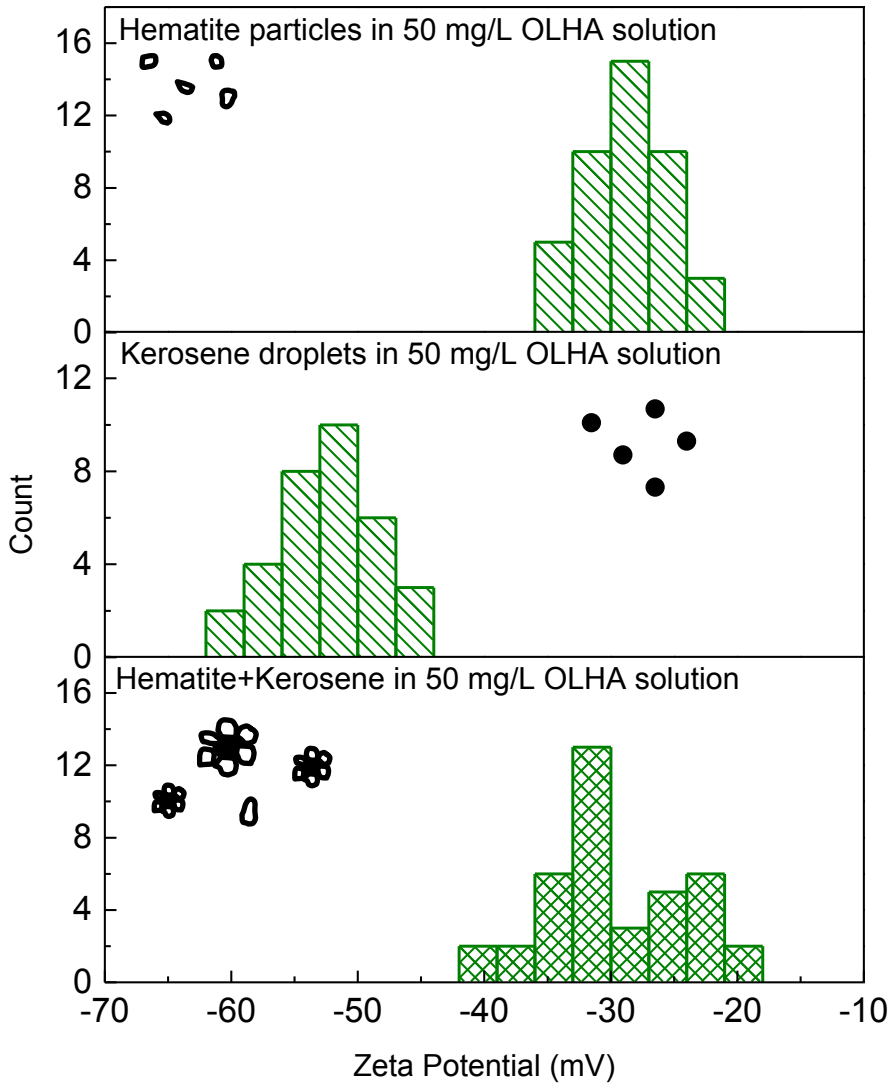

Figure 5.19 Zeta potential distribution of hematite particles, kerosene droplets and their mixture in 50 mg/L OLHA solution at pH 7.

5.4.3 Contact Angles

In order to quantify the surface hydrophobicity of hematite, the static sessile drop method was used to measure the contact angles of a water drop on a hematite slice treated with different collectors and different collector dosages at pH 7. The results are shown in

Figure 5.20. As can be seen, the hematite surface was not affected by any of the three tested collectors below a concentration of 0.01 mg/L, and exhibited its natural hydrophilic characteristics with a contact angle at about 20º. When the collector concentration was increased to above 0.2 mg/L, there was a sharp increase in the measured contact angle. The critical concentration for NaOl and OLHA was 0.2 mg/L to make a significant change in the contact angle of hematite. The critical concentration for OHA was about 5 times higher at 1 mg/L. Below the critical concentrations in the different collector solutions, it was possible that the ionized groups of the collectors adsorbed on the hematite surface, and the hydrocarbon chains sparsely lay flat on the hematite surface, as suggested by Somasundaran and Zhang (2006). As the collector concentration was increased, the collectors more and more took a head-on orientation pointing the hydrocarbon chains outwards, leading to a more hydrophobic surface and a higher contact angle. Figure 9 also shows that the sequence of contact angle increase caused by the different collectors followed the order NaOl > OLHA > OHA. Therefore, OHA induced a lower degree of hydrophobicity to the hematite surface than NaOl or OLHA at the same concentration.

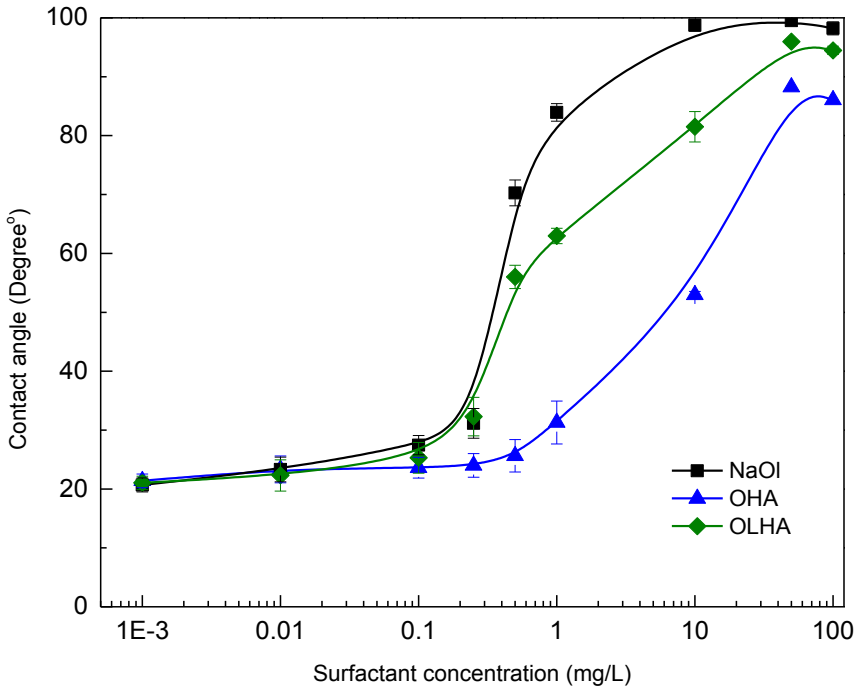

Figure 5.20 Contact angles of hematite as a function of collector concentration. The hematite slice was treated with 100 mL solutions of different collectors for 5 min at pH 7, then air dried and used for contact angle measurements using the sessile drop method.

5.4.4 Interaction Energy Calculations

5.4.4.1 Theoretical background

Based on the interpretations by Churaev and Derjaguin (1985), the validity of the classic DLVO theory was upheld when the contact angles of particles ranged from 20° to 40°. In the oil-assisted flotation, where hydrophobic particles interact with hydrophobic oil droplets, the extended-DLVO model should be used to interpret the colloidal surface interactions (Hunter, 1986). The hydrophobic interaction energy ($V_{hydrophobic}$) (Christenson & Claesson, 1988), was, therefore, applied to calculate the overall potential energy (V_{total}), in addition to van der Waals energy (V_{vdw}) and electrostatic double layer energy (V_{edl}) (Derjaguin & Landau, 1941; Overbeek & Verwey, 1948). A schematic diagram of interaction energy between

mineral particles and oil droplets is shown in Figure 5.21. Each term is a function that depends on the approaching distance (H) between two spheres.

$$V_{total} = V_{vdw} + V_{edl} + V_{hydrohobic} \quad (19)$$

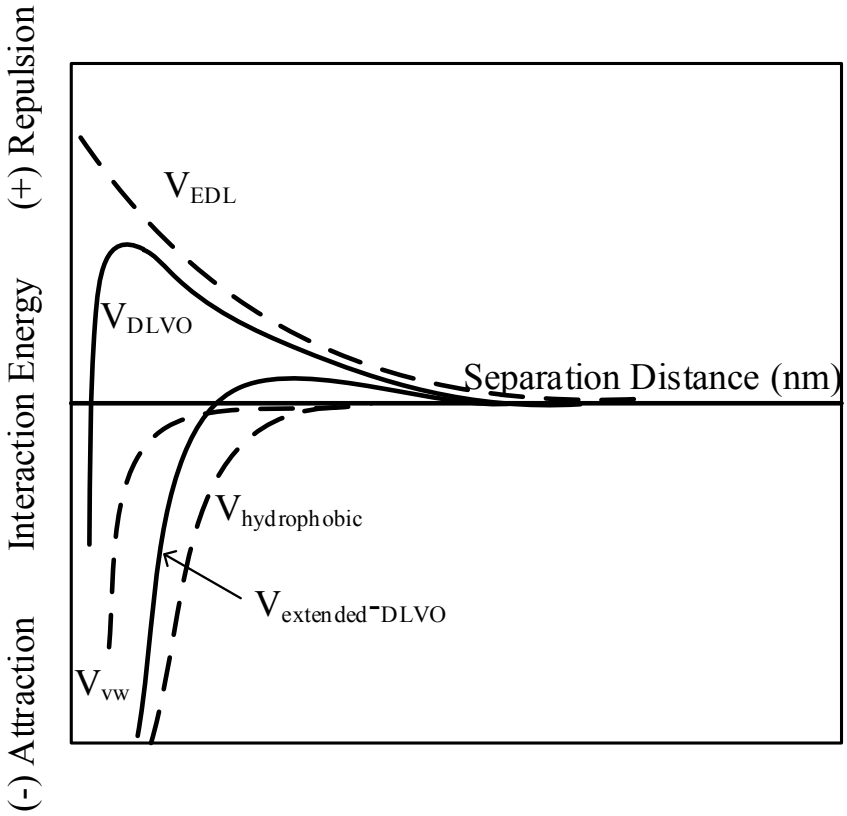

Figure 5.21 Schematic variations of potential interaction energies between oil droplets and mineral particles according to DLVO and Extended-DLVO theory.

(1) van der Waals interaction

The energy of van der Waals interaction is calculated using Equation (20) without considering the retardation effect. For hematite particles and oil droplets with an equivalent spherical radii R_1 and R_2, V_{vdw} is given as

$$V_{vdw} = -\frac{A}{6H} \cdot \frac{R_1 R_2}{(R_1 + R_2)} \quad (20)$$

The Hamaker constant A is obtained from the Lifshitz approach (Lifshitz, 1956). For hematite particle_1 and oil droplet_2 interacting in aqueous solution_3, we have

$$A_{132} = \frac{3}{4}k_B T\left(\frac{\varepsilon_1-\varepsilon_3}{\varepsilon_1+\varepsilon_3}\right)\left(\frac{\varepsilon_2-\varepsilon_3}{\varepsilon_2+\varepsilon_3}\right) + \frac{3h_p\nu_e}{8\sqrt{2}}\frac{(n_1^2-n_3^2)(n_2^2-n_3^2)}{(n_1^2+n_3^2)^{1/2}(n_2^2+n_3^2)^{1/2}\{(n_1^2+n_3^2)^{1/2}+(n_2^2+n_3^2)^{1/2}\}} \quad (21)$$

Where k_B is the Boltzmann constant (1.381×10^{-23} J/K), T is the absolute temperature, ε is the static dielectric permittivity, n is the refractive index in the visible range ($n_1 = 2.42, n_2 = 1.43, n_3 = 1.33$ for hematite paticle_1, oil droplet_2 and aqueous solution_3, respectively), h_p is Planck's constant (6.626×10^{-34} m^2kg/s), ν_e is the main electronic absorption frequency (approximately 3×10^{15} s^{-1}).

(2) Electrostatic double layer interaction

The most extensively used Hogg-Healy-Fuerstenau (HHF) formula was applied to determine the electrostatic double layer energy between hematite particles and oil droplets using the Derjaguin approximation, and is expressed as (Hogg et al., 1966):

$$V_{edl} = \frac{\pi\varepsilon_0\varepsilon_r R_1 R_2}{R_1+R_2}(\psi_1^2 + \psi_2^2)\left\{\frac{2\psi_1\psi_2}{\psi_1^2+\psi_2^2}Ln\left[\frac{1+\exp(-\kappa H)}{1-\exp(-\kappa H)}\right] + Ln[1-\exp(-2\kappa H)]\right\} \quad (22)$$

Where ε_0 is the permittivity of vacuum (8.854×10^{-12} $C^2/J/m$), ε_r is the dielectric constant of the aqueous medium (78.54 at 25°C), ψ_1 and ψ_2 are the surface potentials or the Stern layer potentials of the particles and droplets, but can be approximated by zeta potentials. κ^{-1} is the Debye length, which is related to the

thickness of the electric double layer. For a 1:1 electrolyte like KCl or NaCl, κ^{-1} is calculated as 9.6 nm in 10^{-3} M electrolyte solution using classic Debye–Hückel theory.

$$\kappa = [\frac{\sum_i C_{i,0} e^2 Z_i^2}{\varepsilon_0 \varepsilon_r k_B T}]^{1/2} \quad (23)$$

Where $C_{i,0}$ is the ionic strength in the medium, e is electronic charge (1.602×10^{-19} C), Z_i is the ion valency.

(3) Hydrophobic interaction

As an attractive structural component in an aqueous medium, a strong hydrophobic interaction was initially detected by Israelachvili and Pashley (1982) on the induced hydrophobic mica surfaces using direct force measurement techniques. Subsequently, researchers discovered that the hydrophobic interaction was a long-range attraction effective with a separation distance beyond 100 nm for induced hydrophobic surfaces (Christenson & Claesson, 1988; Claesson et al., 1986). Hence, the hydrophobic interaction was commonly expressed by an empirical double-exponential equation (Claesson et al., 1986; Pashley et al., 1985) :

$$\frac{F_{hydrohobic}}{R} = -C_1 \exp\left(\frac{H}{D_1}\right) - C_2 \exp\left(\frac{H}{D_2}\right) \quad (24)$$

Where C_1 and C_2 are pre-exponential parameters related with interfacial tensions at solid/liquid interface, D_1 and D_2 are the decay lengths of short range and long range hydrophobic forces, respectively, subject to the hydrophobicity of approaching surfaces (Mao, 1998). The measured hydrophobic forces can also be fitted by a power law in Eq. (25) (Claesson & Christenson, 1988):

$$\frac{F_{hydrophobic}}{R} = -\frac{K}{6H^2} \tag{25}$$

In which K is the hydrophobic interaction parameter. The energy of hydrophobic interaction between a mineral particle and an oil droplet can be calculated by substituting Equation (25) into Equation (26):

$$V_{hydrophobic} = -\frac{1}{2}\int_{\infty}^{H} F_{hydrophobic}\, dH \tag{26}$$

The empirical hydrophobic interaction energy equation between asymmetric spheres is therefore described as:

$$V_{hydrophobic} = -\frac{K_{132}}{6H} \cdot \frac{R_1 R_2}{(R_1 + R_2)} \tag{27}$$

An advantage of Equation (27) is its unique hydrophobic parameter and identical equation form compared with Equation (20) for the van der Waals interaction, making it possible to compare the values of hydrophobic parameter K directly with Hamaker constant A.

The hydrophobic parameter of hematite particle_1 and oil droplet_2 in aqueous medium_3, K_{132}, can be obtained with the geometric mean combining rule and expressed as follows (Yoon et al., 1997):

$$K_{132} \approx \sqrt{K_{131} K_{232}} \tag{28}$$

Where K_{131} is the hydrophobic parameter of two hematite_1 / aqueous solution_3 interfaces; Similarly, K_{232} is the hydrophobic parameter of two oil_2 / aqueous solution_3 interfaces. Mao (1998) showed that the K_{232} of oil droplets is approximately 6×10^{-18} J without surfactant, and the value of K_{232} decreased slightly when the concentration of surfactant was lower than 10^{-4} M. Therefore, the value of K_{232} was simplified as 6×10^{-18} J as an approximation in this work. The

K_{131} was calculated by adopting an empirical expression, Equation (29), from Yoon and Luttrell (1992):

$$logK_{131} = -3.194 \times cos\theta_w - 18.229 \qquad (29)$$

Where θ_w is the water contact angle of the mineral.

It is worth noting that despite the fact that the vast majority of the evidence supporting the existence of hydrophobic interactions between hydrophobic surfaces, the origin of the hydrophobic force is still under dispute. Thus, equations (24) to (29) are empirical expressions without solid theoretical basis.

5.4.4.2 The interaction energy estimation by extended DLVO theory

The interaction energies between kerosene droplets and hematite particles are shown in Figure 5.22 to Figure 5.24. The energies of van der Waals, electrical double layer and hydrophobic interaction were calculated based on Equations (19) to (29). The negative values of interaction energy indicated an attractive interaction. Conversely, a repulsive force existed when the interaction energy was positive. Therefore, the Extended-DLVO interaction energy estimation could be used to predict the adhesion of kerosene droplet onto the hydrophobic hematite particles induced by different collectors.

It is clear from Figure 5.22 to Figure 5.24 that the classic DLVO energy profile could not support the different behaviors of hematite when NaOl, OHA, or OLHA was used as a collector in aggregation and flotation. This is because the attractive van der Waals energy was very small while the electrical double layer repulsion was very strong, and the hematite and kerosene could not aggregate based only on van der Waals and electrical double layer interactions. However, the extended DLVO theory, with the inclusion of hydrophobic interaction energy, predicted an overall strongly negative total interaction energy in all three cases when OHA, OLHA or NaOl was used as the collector. This was mainly attributed to the

magnitude of the hydrophobic interaction constant, K_{132}, which was about two orders of magnitude higher than the Hamaker constant A_{132} in this case. When the hydrophobic hematite particle and kerosene droplet approached close enough, the attractive hydrophobic forces increased exponentially as a function of separation distance to overcome the repulsive electrical double layer force. The kerosene droplets would collide and adhere onto hematite particle surfaces, making the surface more hydrophobic, forming large hydrophobic aggregates, thus improving the flotation recovery of the hematite.

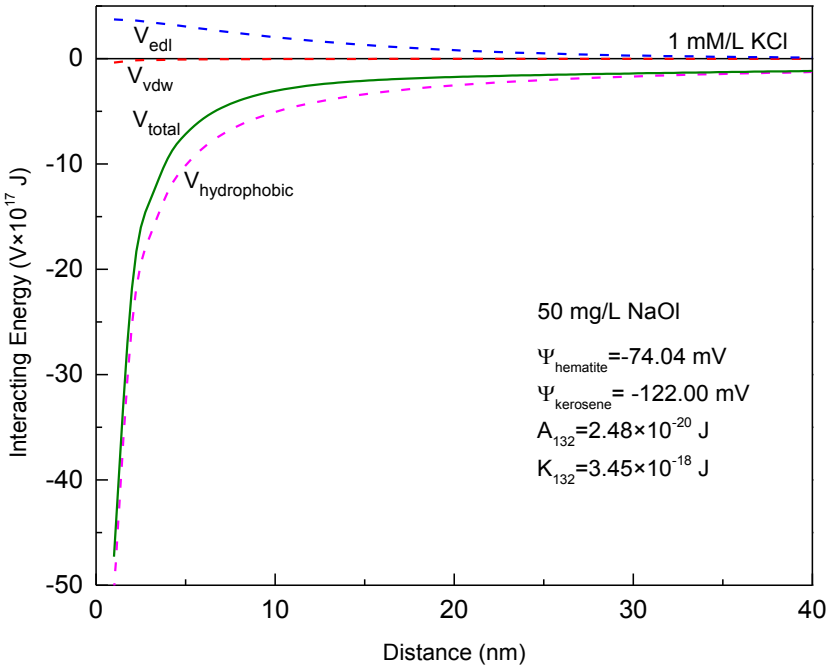

Figure 5.22 The extended DLVO interaction energy diagram as a function of separation distance between kerosene droplet of radius 1.49 μm and hematite particles of radius 2.15 μm in the presence of 50 mg/L NaOl at pH 7.

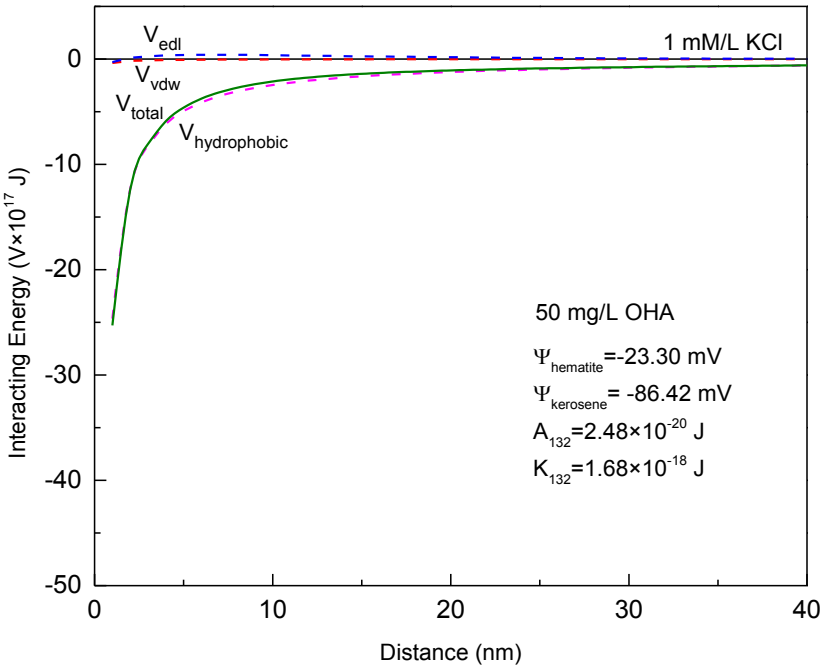

Figure 5.23 The extended DLVO interaction energy diagram as a function of separation distance between kerosene droplet of radius 1.49 μm and hematite particles of radius 2.15 μm in the presence of 50 mg/L OHA at pH 7.

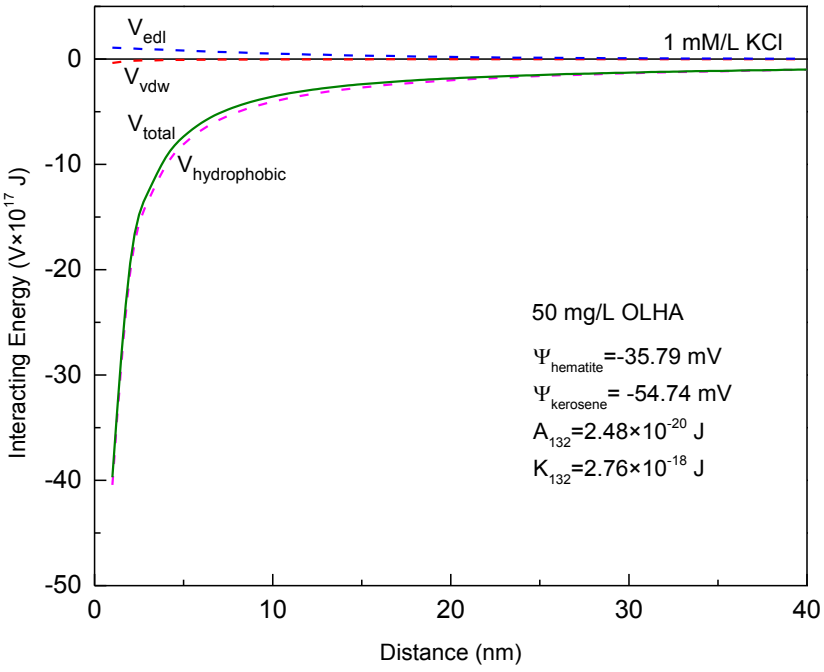

Figure 5.24 The extended DLVO interaction energy diagram as a function of separation distance between kerosene droplet of radius 1.49 μm and hematite particles of radius 2.15 μm in the presence of 50 mg/L OLHA at pH 7.

5.5 Influence of Oil Droplets on Froth Stability

5.5.1 Equilibrium Surface Tension

Surfactant adsorbs at the air/water interface and changes the interfacial properties of the bubble, making it critically important in determining the froth stability. Figure 5.25 shows the equilibrium surface tensions of NaOl, OHA and OLHA solution at pH 7.

As expected, at low concentration for all three collectors, the surface tension decreases gradually with increasing molar concentration. Starting from approximately 1.5×10^{-4} mole/L (45 mg/L), which is the critical micelle concentration (CMC) of NaOl, the surface tension of the solution with NaOl leveled off, consistent with the formation of micelles. The surface tension of OHA,

however, decreased continuously. No micelles were formed within the tested concentration range range (up to 10^{-3} mole/L). Due to the low solubility of OLHA, surfactant concentration was limited below 1×10^{-4} mole/L at pH 7 for a reliable surface tension measurement.

The equilibrium surface tensions of NaOl and OLHA solution in the tested concentration range were much lower than that of OHA solution, indicating stronger surface activity, possibly due to higher surface area occupied by longer hydrocarbon chains of NaOl or OLHA molecules (Beneventi et al., 2001).

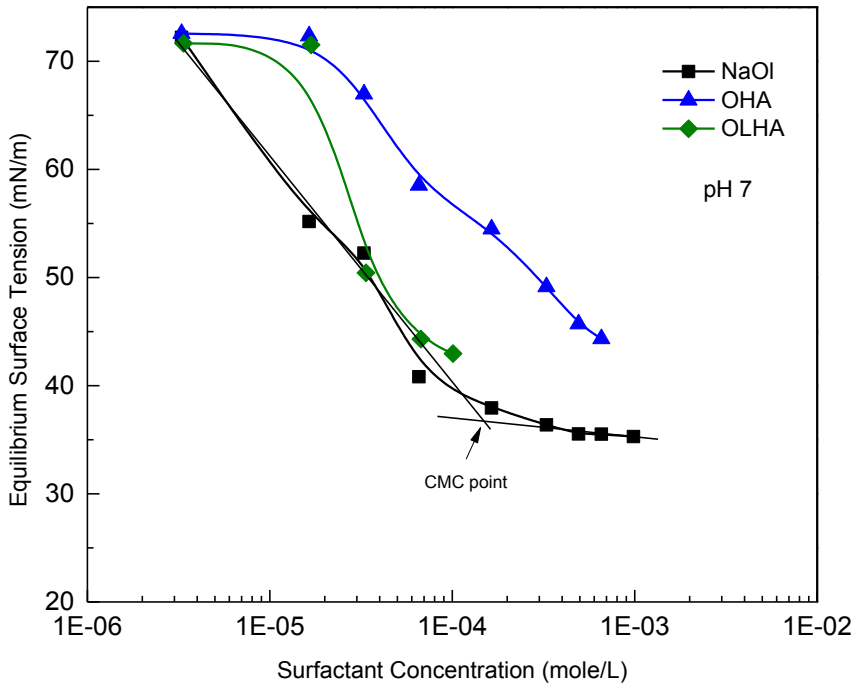

Figure 5.25 Equilibrium surface tension of NaOl, OHA and OLHA as a function of their concentration at pH 7.

5.5.2 Entry, Spreading and Bridging Coefficients (E, S, B)

The action mechanisms of kerosene on froth stability were studied by calculating the equilibrium entry, spreading and bridging coefficients E, S, and B, after measuring the relevant interfacial tensions. The results are shown in Figure 5.26 to Figure 5.28.

The entry coefficients for kerosene in different collector solutions are shown as a function of collector concentration in Figure 5.26. Apparently, all three surfactants exhibited positive entry coefficients in the tested concentration range, indicating the favorable conditions for kerosene to get into the water/air interface. Therefore, the spreading and bridging activities of kerosene droplets on the lamella of NaOl, OLHA or OHA froth depends on the signs and values of S and B (refer to Figure 3.10).

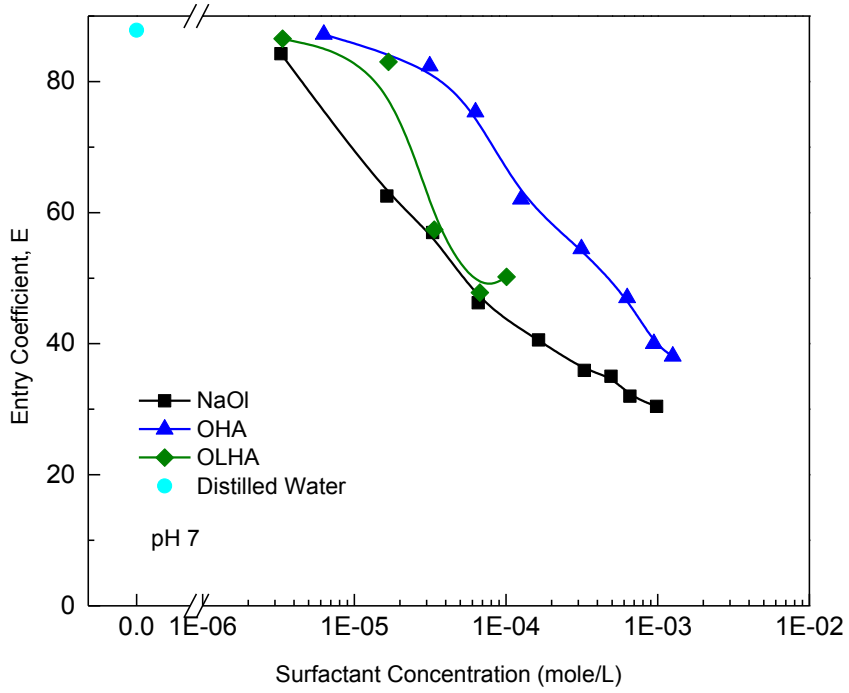

Figure 5.26 Entering coefficient calculations for NaOl, OHA or OLHA surfactant solution as a function of its concentration at pH 7 in the presence of kerosene.

The spreading coefficient S as a function of collector concentration is shown in Fig. 5.26. As can be seen, at very low concentrations, all three surfactants exhibit positive values of S, implying weak and unstable lamella in the presence of kerosene droplets, and the kerosene could spread into the lamella. With increasing surfactant concentration, NaOl and OLHA were starting to display negative values of S, therefore, the kerosene droplet would not spread on water/air interface, and the froth would be stable. On the other hand, in the intermediate concentrate range,

the values of S in the case of the OHA solution remain positive until it reached comparatively high concentration (approximately 7×10^{-4} mole/L or 100 mg/L). When OHA solution concentration was lower than 100 mg/L, kerosene droplets were highly likely to spread on water/air interface, resulting in bubble rupture; Above 100 mg/L OHA, S turned zero or negative, implying a stronger bubble lamella to resist the spreading of oil lens on water film.

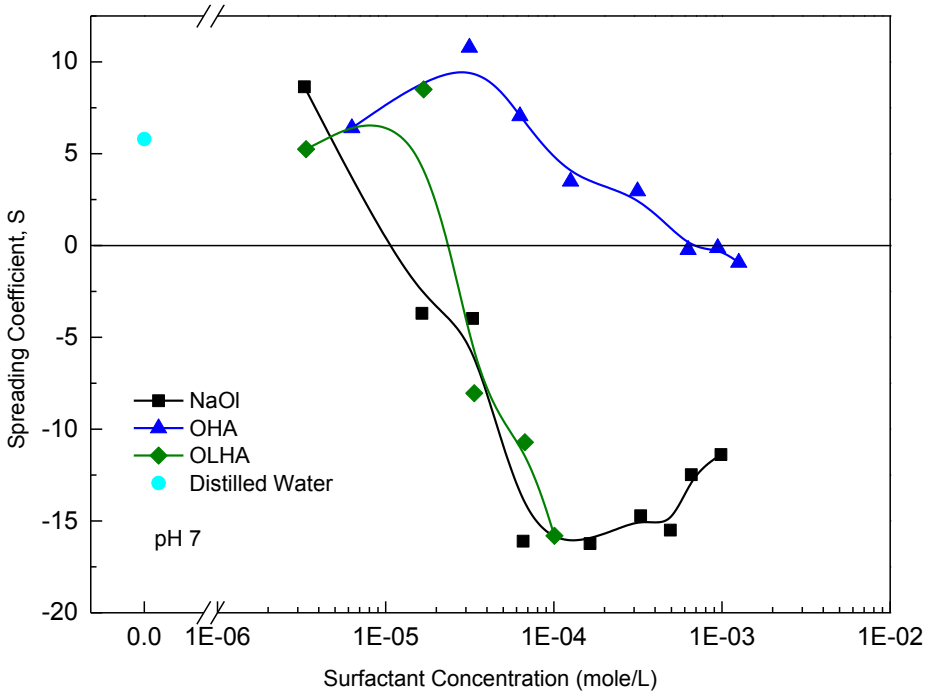

Figure 5.27 Spreading coefficient calculations for NaOl, OHA or OLHA surfactant solution as a function of its concentration at pH 7 in the presence of kerosene.

The calculated bridging coefficients of NaOl, OLHA and OHA showed positive values (Figure 5.28). Based on these values, it can be seen that the water films separating the bubbles will rupture eventually due to unstable oil bridge across the film. However, the magnitude of B for OHA was much higher than NaOl or OLHA. Thus, it can be inferred that the froth formed by OHA is less stable.

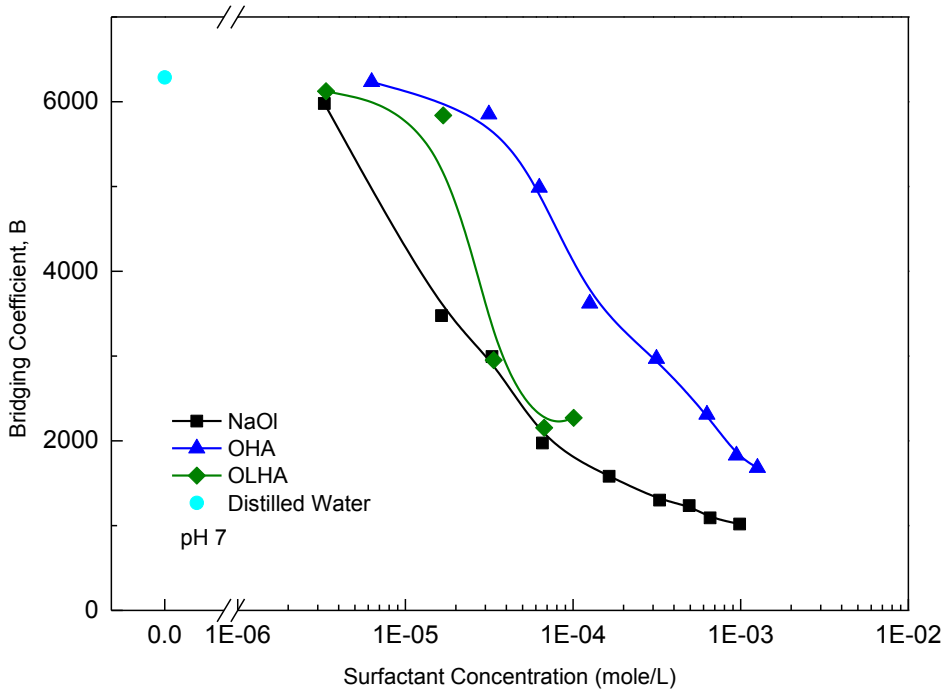

Figure 5.28 Bridging coefficient calculations for NaOl, OHA or OLHA surfactant solution as a function of its concentration at pH 7 in the presence of kerosene.

5.5.3 Foamability of NaOl and OHA

A set of dynamic foam stability tests of 100 mL NaOl or OHA solution at pH 7 were carried out as a function of time using the Bikerman method (Bikerman, 2013). Various concentrations of NaOl and OHA were evaluated and the results are presented in Figure 5.29 to Figure 5.31. Due to the poor solubility of OLHA in aqueous solution, the foam was extremely unstable for a proper comparison with NaOl and OHA, and thus OLHA was excluded from two-phase foam stability tests.

It is interesting to note that the foaming rate and final foam volume produced by NaOl solution at 25 mg/L within 1 min was quite low compared with other concentrations. Once the concentration of NaOl solution reached 50 mg/L and above, the foaming rate and foam volume increased drastically. However, further increase in NaOl concentration only resulted in a limited increase in froth volume. Also, from Figure 5.29, it is clear that the foam height from NaOl solution rose

linearly without levelling off. In fact, the foam would continue to rise until it overflowed from the top of the glass column if the gas supply lasted. A similar phenomenon was also noticed by Atrafi (2015). In other words, traditional foam stability assessment based on equilibrium foam height could not be used in the foam study of NaOl solutions. Therefore, the maximum foam height after aerating for 1 min was used as an alternative approach in the study to evaluate the foam stability.

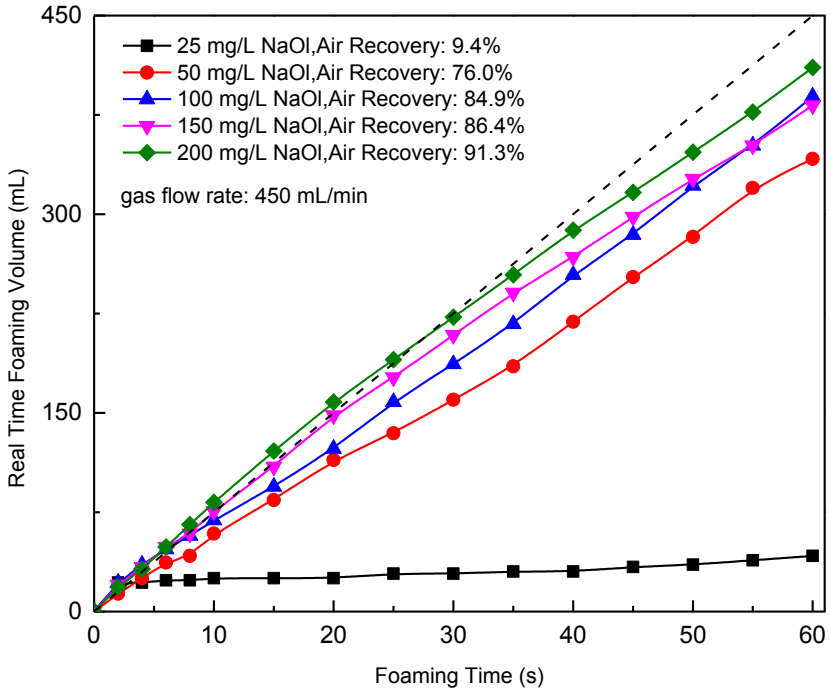

Figure 5.29 Real time foaming volume as a function of time for NaOl solution at pH 7 at 450 mL/min gas flow rate. The dashed line indicates theoretical maximum foaming volume.

The foamability of OHA solution, shown in Figure 5.30, however, was very different from NaOl. The foam growth rate and maximum foam height in 1 min increased much more slowly with higher OHA concentration, indicating weaker foamability of OHA solution at neutral pH. In addition, when the OHA solution concentration was between 25 and 100 mg/L, a peak height of the foam was reached with continuous aeration, followed by a decrease in foam height. This foam

behavior could be explained by surfactant depletion in the aqueous solution as the aeration progresses (Beneventi et al., 2001).

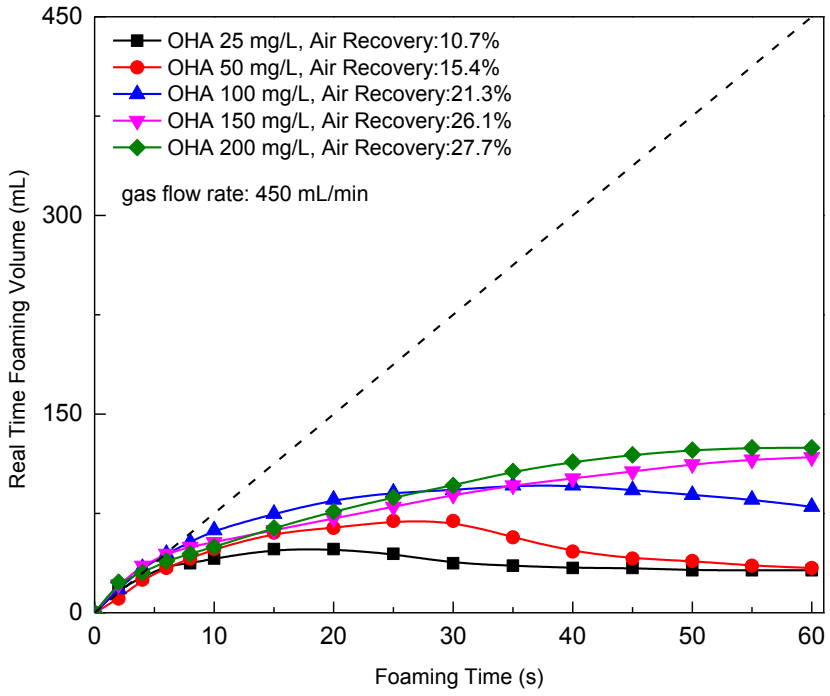

Figure 5.30 Real time foaming volume as a function of time for OHA solution at pH 7 at 450 mL/min gas flow rate. The dashed line indicates theoretical maximum foaming volume.

Apart from foam growth rate and volume, air recovery in the presence of NaOl or OHA can be qualitatively compared. Air recovery is defined as the fraction of air injected into the column as foam phase, and the results are shown in Figure 5.29 and Figure 5.30 (Hadler & Cilliers, 2009). The dashed line shows the theoretical maximum foam volume without foam burst. The foam growth rate of NaOl solution containing more than 50 mg/L NaOl only deviated slightly from the theoretical value, indicating that only a small portion of bubbles coalesced or burst within the foam phase. On the contrary, large deviations from the dashed diagonal line indicating small air recovery and apparent bubble burst showed less stabilized foam for OHA solutions (Figure 5.30). The linear correlation shown in Figure 5.31 between the maximum foam volume in 1 min aeration and gas flow rate indicates

that the air recovery of the two foam phases is dependent of air flow rate, and the foamability for NaOl solution is much better than OHA solution.

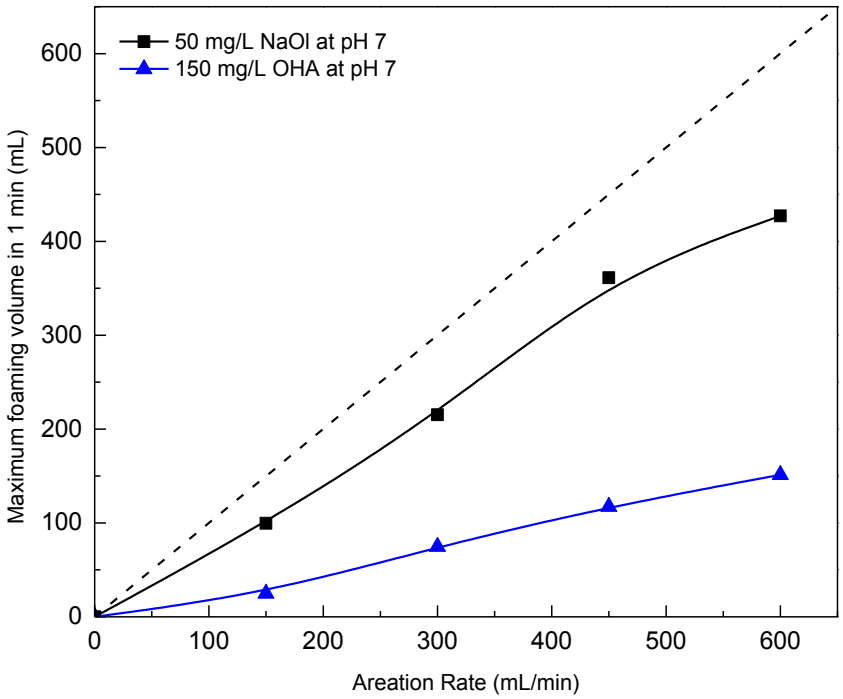

Figure 5.31 Maximum foaming volumes of NaOl (50 mg/L) and OHA (150 mg/L) as a function of gas flow rate at pH 7. The dashed line indicates theoretical maximum foaming volume.

5.5.4 Influence of Oil Droplets on the Foamability of NaOl and OHA Solution

The effect of kerosene droplets on the air/water two-phase foams of NaOl and OHA solutions is shown in Figure 5.32**Error! Reference source not found.** and Figure 5.33. It is clear that oil droplets can destabilize or stabilize foam depending on the concentration of surfactant in both solutions. At low concentration of surfactant solution, kerosene droplets drastically decreased foam stability. The more kerosene that was added to the surfactant solution, the worse the foam stability. However, at high surfactant concentrations, not only was the foam stabilized, but the addition of kerosene even generated more stable froths.

In the absence of kerosene droplets, maximum foam volume of NaOl solution was achieved starting from 50 mg/L, which is close to the CMC of NaOl solutions. Above CMC, the surfactant coverage on the water/air interface was compact, and excess surfactant molecules would form micelles in aqueous solution. Therefore, maximum foam volume in 1 min remained similar and was independent of surfactant concentration. In the presence of kerosene droplets, foam destruction was observed at 50 and 100 mg/L NaOl. The defrothing by kerosene at these NaOl concentrations contradicted the calculated spreading coefficient (Figure 5.27), implying that the spreading of the neutral oil at the bubble surface is not a necessary step for defrothing. Thus, it was speculated that the unstable pseudoemulsion film at low NaOl concentration allowed oil droplets to enter bubble films and resulted in bubble rupture by dewetting of oil bridges. At high NaOl concentration, i.e., 150 and 200 mg/L, the addition of kerosene droplets stabilized the froth. This is explained by stable pseudoemulsion film to prevent oil droplets from entering water/air interface (Koczo et al., 1992). Instead, oil droplets accumulated in the Plateau boarder and hindered water drainage; Therefore, froth stability increased.

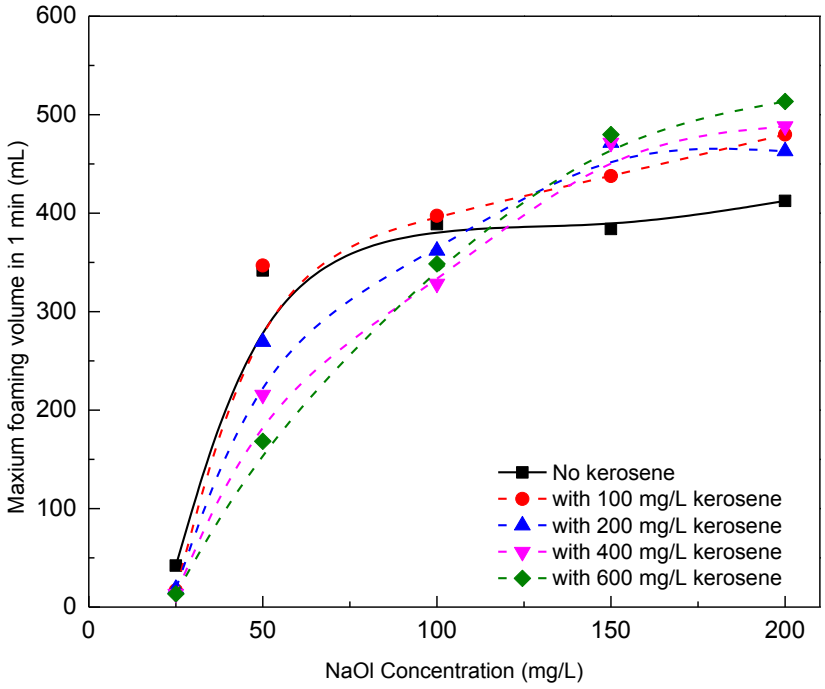

Figure 5.32 The maximum foaming volume of NaOl solution in 1 min at pH 7 at 450 mL/min gas flow rate in the presence of different concentration of kerosene emulsion.

The trend for the OHA frothing activity in the absence or presence of kerosene droplets was similar. The foam height in 1 min increased steadily with increasing OHA concentration without the presence of kerosene droplets. However, the foam height was much lower in the OHA case at the same concentrations, indicating a lower surface active property of OHA than NaOl. This is consistent with surface tension results (Figure 5.25). Moreover, the defrothing of kerosene droplets on OHA foam at low concentrations is in good agreement with the positive spreading coefficient at the same OHA concentration. The stabilization effect of kerosene on the froth was also observed at high OHA concentrations, possibly due to the similar effect caused by pseudoemulsion films.

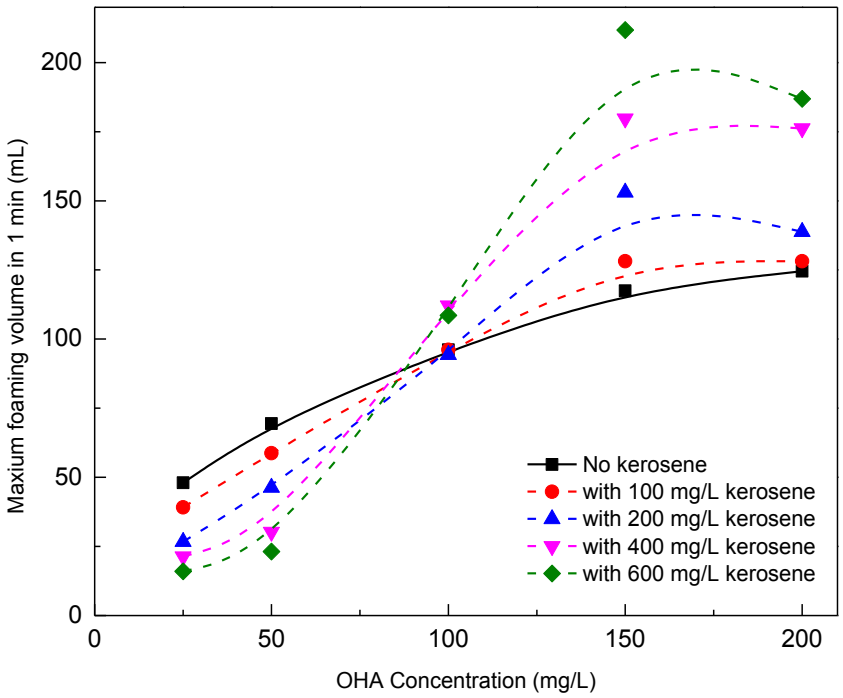

Figure 5.33 The maximum foaming volume of OHA solution in 1 min at pH 7 at 450 mL/min gas flow rate in the presence of different concentration of kerosene emulsion.

5.5.5 Influence of Neutral Oil on the Water Recovery during Hematite Flotation

Mineral flotation recovery depends not only on the collector concentration, but also on water recovery (Boylu & Laskowski, 2007). The amount of water transferred to the froth product is generally linked to froth stability.

Figure 5.34 shows water recovery before and after adding 1 kg/t kerosene in the batch flotation of -20 μm hematite. Water recovery decreased significantly from 33.4% to 17.7% after adding 1 kg/t kerosene when 100 g/t OHA was used, which coincided with a reduction in hematite recovery (Figure 5.9). This large difference in water recovery was gradually reduced with increasing OHA dosage. However, when NaOl or OLHA was used as a collector, the water recovery was not significantly affected after adding the 1 kg/t kerosene at all dosages of the collectors tested from 100 g/t to 1 kg/t.

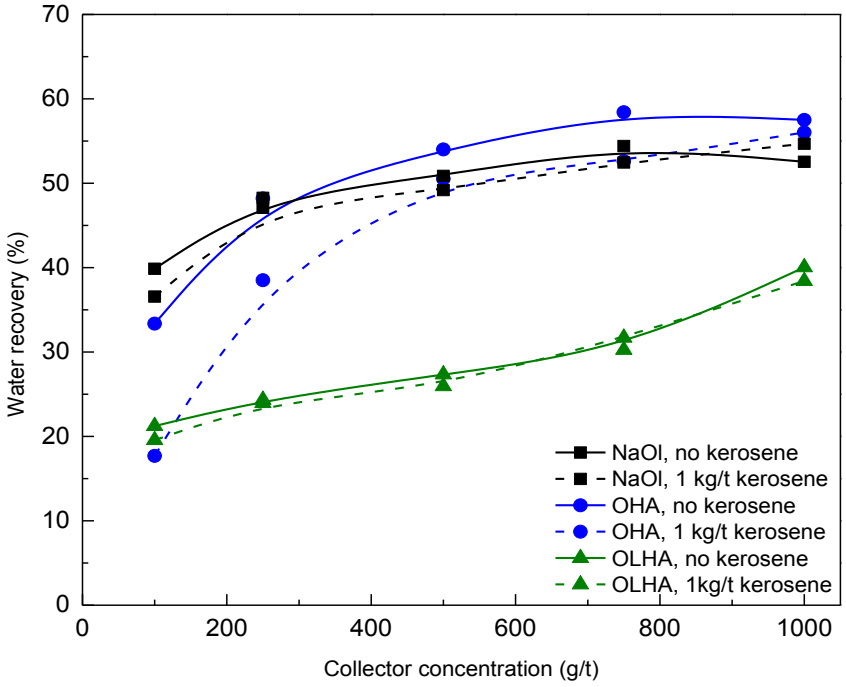

Figure 5.34 The effect of 1 kg/t kerosene on water recovery in the batch flotation of -20 μm hematite using different dosages of NaOl, OHA and OLHA.

Froth flotation is a complex process in which the additives have various functions. Some of these functions may lead to poor flotation results. It is obvious that the stability of froth is a primary requirement for good flotation performance. Froth stabilization was controlled by the adsorbed surfactants at the gas/water interface which modulate the mechanical and dynamic properties of bubble surface layer (Leja, 1982; Pugh, 1996). For successful froth flotation, a stable froth layer needs to be formed; Thus a high surface tension gradient is required (Pugh, 1996).

In this study, as no frother was used in the flotation tests, apart from the adsorbed collectors on mineral surfaceS, the remaining collectors in suspension would act as frothers. When collector dosage was low, the bubbles were unstable and sensitive to the surfactant concentration. This was especially true in the case of OHA where defrothing phenomenon was obvious when kerosene was used, causing lower water recovery and lower hematite recovery (Figure 5.9 and Figure 5.34). On the contrary, the addition of kerosene did not have significant influence on the water recovery

when NaOl or OLHA was used as a collector, even at low dosages. This difference was probably caused by the different hydrocarbon chain lengths of the collectors. The longer hydrocarbon chain gave the collectors such as NaOl and OLHA a higher surface activity than the short chain collector such as OHA (Figure 5.25). The higher surface activity in turn leads to higher surface modulus and faster water migration kinetics, to delay water drainage and strengthen the froth stability (Beneventi et al., 2001). Therefore, NaOl and OLHA, with longer hydrocarbon chains, were expected to delay the water drainage rate. A larger gradient in surface tension of both NaOl and OLHA also tended to induce a flow of water that helps to heal the thin spot caused by kerosene and hinder rupture, even at low collector concentration. Therefore, kerosene can only exert limited water drainage effect during aeration and froth collection. When the short hydrocarbon chain collector such as OHA was used, water migration kinetics in the intervening water films in the froth was comparatively slow. Once neutral oil entered and spread on the bubble surface, it gradually eliminates the surface tension gradient and elasticity, leading to faster water drainage and bubble rupture.

In addition, hematite fines help froth stabilization during flotation (Johansson & Pugh, 1992). The hematite surface is expected to be more hydrophobic with long chain NaOl and OLHA than short chain OHA (Figure 5.20). Once the surface of hematite particles achieved a critical degree of hydrophobicity, the stabilizing effect of hematite particles would compensate the detrimental defrothing effect caused by kerosene, leading to a relatively minor detrimental effect of kerosene in the batch flotation when long chain NaOl or OLHA was used as a collector. However, at high collector concentrations, regardless of the collector type, the froth layer was stable because of the stable pseudoemulsion film and the Marangoni effect plays critical roles and provides a strong restoring force to film thinning caused by kerosene. Therefore, the water drainage caused by kerosene droplets was counter-balanced by the surface tension gradient.

The frothing test results seem to show that the effect of non-polar oil on froth stability was far more complicated than our current understanding. In a real flotation system, multiple parameters such as mineral particle size, hydrophobicity, surfactant concentration, dissolved ions, etc., all have direct influence on the frothing behavior upon oil addition. It is a subject that is worthy of further study.

Chapter 6 Conclusions, Contributions and Recommendations

6.1 Summary and Conclusions

The roles of kerosene in froth flotation of fine -20 μm hematite were studied systematically using sodium oleate or hydroxamic acids as a collector. By carrying out flotation tests with and without the presence of a froth layer, oil-particle interaction mechanism study and froth stability study, the following conclusions were drawn:

- Sodium oleate (NaOl), oleoyl hydroxamic acid (OLHA) and octyl hydroxamic acid (OHA) were effective collectors in the flotation of fine hematite. The optimum flotation pH was observed to be 6.5 to 8.5 for NaOl, 6 to 8 for OHA, and 6 to 7 for OLHA. The flotation recovery using OLHA was lower than that using NaOl or OHA, possibly due to its low solubility in water.

- In laboratory frothless flotation of single mineral hematite, the flotation recovery was enhanced with the addition of kerosene regardless of the type of collectors used. Kerosene in the form of an oil-in-water emulsion added after the collector showed the best flotation performance. It was shown that the flotation-promotion effect of kerosene increased steadily with increasing collector concentration and increasing kerosene concentration.

- In batch flotation of single hematite mineral in a conventional mechanical flotation machine where a froth layer existed (the froth layer was generated by the collector alone), the addition of kerosene adversely affected flotation recovery only when a short hydrocarbon-chain collector (OHA) was used at a low dosage. This was due to the defrothing effect of the kerosene. When long hydrocarbon-chain collectors were used, or when the short-chain

collector was used at high dosages, the addition of kerosene was beneficial to hematite flotation recovery.

- The beneficial role of kerosene in the flotation of fine hematite was found to be due to the enhanced surface hydrophobicity, which by itself improved flotation recovery. The higher hydrophobicity also promoted hydrophobic aggregation of the fine hematite resulting in the formation of large hydrophobic flocs, which also benefitted flotation recovery.

- The batch flotation tests of mixtures of hematite and quartz (1:1 weight ratio) revealed the complicated effects of neutral oil on hematite recovery and its grade in the floated concentrate. When the long-chain collectors (NaOl or OLHA) were used as a collector, the addition of kerosene improved both hematite recovery and Fe_2O_3 grade in the floated concentrate. This was due to the hydrophobicity-enhancing effect of kerosene which benefited hematite flotation, and the defrothing effect of kerosene which lowered quartz entrainment. When OHA was used as a collector, the addition of kerosene lowered both hematite recovery and concentrate grade at low OHA dosages (< 375 g/t). The detrimental defrothing effect dominated at the low OHA dosages. At high OHA dosages (> 375 g/t), the detrimental effect of kerosene seemed to have been eliminated and the hematite recovery and concentrate grade were both improved.

- Real-time in-situ monitoring of particle aggregation by using a focused beam reflectance measurement particle size analyzer coupled with optical microscopy showed that significant aggregate size growth occurred when kerosene was added to the -20 μm hematite suspension previously treated with NaOl or OLHA. However, the aggregation was not as strong when OHA was used to treat the hematite, and there was virtually no formation of large aggregates under the test conditions using OHA and kerosene.

The aggregation behavior was explained by electrophoretic measurements, contact angles, and interaction energy estimation according to the extended-DLVO theory where van der Waals, electrical double layer and hydrophobic interactions were considered. It was shown that a strong attractive interaction was dominated between the hydrophobicized hematite particles and kerosene droplets when long chain NaOl or OLHA, rather than short chain OHA, was used as a collector.

- The relevant interfacial tensions of the NaOl, OLHA and OHA solutions in the presence of kerosene were measured and the classical entry coefficient E, spreading coefficient S, and bridging coefficients B were calculated using the measured interfacial tensions. The signs and magnitude of the calculated spreading and bridging coefficients indicated that an oil droplet was more likely to induce bubble rupture in an OHA solution than in NaOl or OLHA solutions.

  The froth stability of NaOl and OHA solutions was studied with or without kerosene droplets using a frothing column. NaOl was observed to have stronger frothing power than OHA. The addition of kerosene destabilized the froth at low concentrations of NaOl and OHA. Interestingly, at high NaOl and OHA concentration, the addition of kerosene in fact caused more stable froths. This was thought to be due to a stable pseudoemulsion film that prevented the spreading of kerosene onto the bubble surface.

- In conclusion, non-polar oil has simultaneous beneficial roles (surface hydrophobicity enhancement, and oil-assisted aggregation) and detrimental roles (defrothing) in froth flotation. This study revealed a delicate balance between the two conflicting roles when different collectors, with different polar groups and hydrocarbon chain lengths, were used in fine particle

flotation. The defrothing effect of kerosene was found to be significant with a shorter chain collector such as octyl hydroxamic acid, especially at low dosages, than longer chain collectors such as sodium oleate, which led to poor flotation results. However, this detrimental defrothing effect was gradually counter-balanced by higher collector dosages, resulting in higher concentrate grade and recovery.

6.2 Original Contributions

- Demonstrated that neutral oil is not a universal flotation promoter as conventional wisdom perceives. In froth flotation, neutral oil can benefit fine mineral recovery by rendering the mineral more hydrophobic and promoting hydrophobic flocculation thus enlarging the apparent size of the fine mineral. On the other hand, neutral oil can destroy froths, which adversely affects froth flotation.

- Revealed that the balance of the beneficial and detrimental roles of neutral oil depends on the hydrocarbon chain length (surface activity) of flotation collectors. Long hydrocarbon-chain collectors tend to make the mineral more hydrophobic and can also generate more stable froths so that the simultaneous use of neutral oil is beneficial. Where the addition of neutral oil deteriorates flotation performance is usually when a short hydrocarbon-chain collector is used.

- When flotation collectors and neutral oil are both used, there is a critical dosage (concentration) of the collector, below which the neutral oil has either no effect (long hydrocarbon-chain collector) or detrimental effect (short hydrocarbon-chain collector). Above the critical dosage, the addition of neutral oil is beneficial for the promotion of mineral flotation.

6.3 Suggestions for Future Work

The role of frothers has not been studied in this work. Further research should focus on the roles of different types of frothers in countering the defrothing effects of neutral oil. This can be done by using a naturally hydrophobic mineral such as coal, graphite, talc, or molybdenite, where only the neutral oil and a frother will be used. Such studies can eliminate the interference from the collectors.

The froth stability study of this work is preliminary and has not dealt with the presence of minerals, their hydrophobicity and particle size. Enhanced hydrophobicity and larger aggregate size upon oil addition make the flotation system more complicated because they all affect froth stability. Follow-up research can be carried out by focusing on the effects of the mineral particles (particle size and hydrophobicity) on froth stability with and without the neutral oil, as well as with and without a collector or frother.

Most commonly used non-polar oil, such as kerosene, diesel, truck oil or fuel oil, is a hydrocarbon mixture. These hydrocarbons may have straight or branched hydrocarbon chains with different chain lengths and/or unsaturated bonds. Flotation performance may vary significantly due to different physicochemical properties of different types of hydrocarbon oils. Further study is need by testing different types of oils, including heavy oils that may contain heavy atoms such as P, S, etc.

The intensive agitation tested in this work seemed to have no effect in fine hematite flotation when sodium oleate was used as a collector. When octyl hydroxamic acid was used, the intensive agitation caused a drop in hematite recovery. These observations were contradictory to literature reports which indicated that shear flocculation flotation was beneficial in fine minerals recovery. The reason is unknown at this point. It was possible that the particles were relatively coarse for effective shear flocculation. It was also possible that the shear rate was excessive and the shear time was too long, which resulted in floc breakage or reagent

desorption from mineral surfaces. More in-situ aggregation studies as a function of agitation parameters and reagent adsorption measurements are necessary.

Reference

[1] Ananthapadmanabhan, K., & Somasundaran, P. (1984). The role of dissolved mineral species in calcite-apatite flotation. *Minerals and Metallurgical Processing, 1*(1), 36.

[2] Aruna, V., & Shende, S. (2006). *Floc-Flotation of Chalcopyrite from a Low Grade Cu-Zn Ore.* Paper presented at the International Seminar on Mineral Processing Technology, Chennai, India.

[3] Ata, S., & Yates, P. D. (2006). Stability and flotation behaviour of silica in the presence of a non-polar oil and cationic surfactant. *Colloids and Surfaces A: Physicochemical and Engineering Aspects, 277*(1), 1-7. doi:10.1016/j.colsurfa.2005.10.062

[4] Atrafi, A. (2015). *Frothing properties of fatty acid collectors*. (Ph.D.), University of British Columbia.

[5] Attia, Y. (1977). Synthesis of PAMG chelating polymers for the selective flocculation of copper minerals. *International Journal of Mineral Processing, 4*(3), 191-208.

[6] Attia, Y., & Kitchener, J. (1975). *Development of complexing polymers for the selective flocculation of copper minerals.* Paper presented at the Proc. 11th Int. Mineral Processing Congress.

[7] Attia, Y. A. (1982). Fine particle separation by selective flocculation. *Separation Science and Technology, 17*(3), 485-493.

[8] Aveyard, R., & Haydon, D. (1965). Thermodynamic properties of aliphatic hydrocarbon/water interfaces. *Transactions of the Faraday Society, 61*, 2255-2261.

[9] Beneventi, D., Carre, B., & Gandini, A. (2001). Role of surfactant structure on surface and foaming properties. *Colloids and Surfaces A: Physicochemical and Engineering Aspects, 189*(1), 65-73.

[10] Bera, A., Ojha, K., & Mandal, A. (2013). Synergistic effect of mixed surfactant systems on foam behavior and surface tension. *Journal of Surfactants and Detergents, 16*(4), 621-630.

[11] Bhaskar Raju, G., & Khangaonkar, P. (1984). Electroflotation-A critical review. *Transactions of the Indian Institute of Metals, 37*(1), 59-66.

[12] Bikerman, J. J. (1973). *Foams* (Vol. 10). Berlin: Springer-Verlag New York Inc.

[13] Bikerman, J. J. (2013). *Surface chemistry: Theory and applications*: Elsevier.

[14] Bos, J., & Quast, K. (2000). Effects of oils and lubricants on the flotation of copper sulphide minerals. *Minerals Engineering, 13*(14), 1623-1627.

[15] Botsaris, G. D., & Glazman, Y. M. (1989). *Interfacial phenomena in coal technology* (Vol. 4). New York: M. Dekker.

[16] Boylu, F., & Laskowski, J. S. (2007). Rate of water transfer to flotation froth in the flotation of low-rank coal that also requires the use of oily collector. *International Journal of Mineral Processing, 83*(3), 125-131.

[17] Capes, C., & Germain, R. (1982). Selective oil agglomeration in fine coal beneficiation *Physical cleaning of coal* (pp. 293-351): Marcel Dekker New York.

[18] Capes, C. E., & Darcovich, K. (1997). *Size enlargement*: Wiley Online Library.

[19] Carissimi, E., & Rubio, J. (2005). *Advances in particulates aggregation–flotation separation.* Paper presented at the Proceedings in Centenary of Flotation Symposium, Brisbane, Australia.

[20] Carman, P. (1941). CAPILLARY RISE AND CAPILLARY MOVEMENT OF MOISTURE IN FINE SANDS. *Soil science, 52*(1), 1-14.

[21] Cebeci, Y., & Sönmez, I. b. (2004). Investigation of spherical oil agglomeration properties of celestite. *Journal of colloid and interface science, 273*(1), 198-204.

[22] Christenson, H. K., & Claesson, P. M. (1988). Cavitation and the interaction between macroscopic hydrophobic surfaces. *Science, 239*(4838), 390-393.

[23] Churaev, N. (1995). Contact angles and surface forces. *Advances in colloid and interface science, 58*(2-3), 87-118.

[24] Churaev, N., & Derjaguin, B. (1985). Inclusion of structural forces in the theory of stability of colloids and films. *Journal of colloid and interface science, 103*(2), 542-553.

[25] Churaev, N., & Zorin, Z. (1992). Wetting films. *Advances in Colloid and Interface Science, 40*, 109-146.

[26] Claesson, P. M., Blom, C. E., Herder, P. C., & Ninham, B. W. (1986). Interactions between water—stable hydrophobic Langmuir—Blodgett monolayers on mica. *Journal of colloid and interface science, 114*(1), 234-242.

[27] Claesson, P. M., & Christenson, H. K. (1988). Very long range attractive forces between uncharged hydrocarbon and fluorocarbon surfaces in water. *J. Phys. Chem.;(United States), 92*(6).

[28] Clauss, C., Appleton, E., & Vink, J. (1976). Selective flocculation of cassiterite in mixtures with quartz using a modified polyacrylamide flocculant. *International Journal of Mineral Processing, 3*(1), 27-34.

[29] Coleman, R. D., Sparks, B. D., Majid, A., & Toll, F. N. (1995). Agglomeration-flotation: recovery of hydrophobic components from oil sands fine tailings. *Fuel, 74*(8), 1156-1161.

[30] Collins, D., & Read, A. (1971). The treatment of slimes. *Mineral Science and Engineering, 3*, 19-31.

[31] Collins, G., & Jameson, G. (1976). Experiments on the flotation of fine particles: the influence of particle size and charge. *Chemical Engineering Science, 31*(11), 985-991.

[32] Colombo, A. (1980). Selective flocculation and flotation of iron-bearing materials *Fine particles processing* (Vol. 2, pp. 1034-1056): SEM/AIME New York.

[33] Cooper, F. D. (1980). *Mining and quarrying trends in the metals and nonmetal industries* (*Minerals Yearbook, Volume 1*). Retrieved from Washington, DC.

[34] Cornell, R. M., & Schwertmann, U. (2003). *The iron oxides: structure, properties, reactions, occurrences and uses*: John Wiley & Sons.

[35] Cotnoir, D., Liu, Q., Ourriban, M., Peng, P., & Richard, D. (2005). *Some solutions to the problems in fine particle flotation.* Paper presented at the Centenary of Flotation Symposium.

[36] Creux, P., Lachaise, J., Graciaa, A., Beattie, J. K., & Djerdjev, A. M. (2009). Strong specific hydroxide ion binding at the pristine oil/water and air/water interfaces. *The Journal of Physical Chemistry B, 113*(43), 14146-14150.

[37] Dai, Z., Fornasiero, D., & Ralston, J. (2000). Particle–bubble collision models—a review. *Advances in Colloid and Interface Science, 85*(2), 231-256.

[38] Dai, Z., & Lu, S. (1991). Hydrophobic interaction in flocculation and flotation 2. Interaction between non-polar oil drop and hydrophobic mineral particle. *Colloids and Surfaces, 57*(1), 61-72.

[39] Demond, A. H., & Lindner, A. S. (1993). Estimation of interfacial tension between organic liquids and water. *Environmental science & technology, 27*(12), 2318-2331.

[40] Denkov, N. D., Cooper, P., & Martin, J.-Y. (1999). Mechanisms of action of mixed solid− liquid antifoams. 1. Dynamics of foam film rupture. *Langmuir, 15*(24), 8514-8529.

[41] Denkov, N. D., Marinova, K. G., & Tcholakova, S. S. (2014). Mechanistic understanding of the modes of action of foam control agents. *Advances in Colloid and Interface Science, 206*, 57-67.

[42] Derjaguin, & Landau. (1941). Theory of the stability of strongly charged lyophobic sols and the adhesion of strongly charged particles in solutions of electrolytes. *Acta Physicochim. USSR, 14*, 633-662.

[43] Derjaguin, B., & Churaev, N. (1989). The current state of the theory of long-range surface forces. *Colloids and Surfaces, 41*, 223-237.

[44] Derjaguin, B., & Dukhin, S. (1961). Theory of flotation of small and medium-size particles. *Progress in Surface Science, 43*(1), 241-266.

[45] Derjaguin, B., Dukhin, S., & Rulyov, N. (1984). Kinetic theory of flotation of small particles *Surface and colloid science* (pp. 71-113): Springer.

[46] Dippenaar, A. (1982a). The destabilization of froth by solids. I. The mechanism of film rupture. *International Journal of Mineral Processing, 9*(1), 1-14.

[47] Dippenaar, A. (1982b). The destabilization of froth by solids. II. The rate-determining step. *International Journal of Mineral Processing, 9*(1), 15-22.

[48] Dobby, G., & Finch, J. (1986). Flotation column scale-up and modelling. *CIM Bulletin, 79*(889), 89-96.

[49] Duong, C., Choung, J., Xu, Z., & Szymanski, J. (2000). A novel process for recovering clean coal and water from coal tailings. *Minerals Engineering, 13*(2), 173-181.

[50] El-Shall, H., Abdel-Khalek, N., & Svoronos, S. (2000). Collector–frother interaction in column flotation of Florida phosphate. *International Journal of Mineral Processing, 58*(1), 187-199.

[51] Engelbrecht, J., & Woodburn, E. (1975). Effects of froth height, aeration rate, and gas precipitation on flotation. *Journal of the South African Institute of Mining and Metallurgy, 76*, 125-132.

[52] Ennis, B. J., Li, J., Gabriel I, T., & Robert, P. (1990). The influence of viscosity on the strength of an axially strained pendular liquid bridge. *Chemical Engineering Science, 45*(10), 3071-3088. doi:https://doi.org/10.1016/0009-2509(90)80054-I

[53] Falutsu, M., & Dobby, G. (1989). Direct measurement of froth drop back and collection zone recovery in a laboratory flotation column. *Minerals Engineering, 2*(3), 377-386.

[54] Farrokhpay, S. (2011). The significance of froth stability in mineral flotation — A review. *Advances in Colloid and Interface Science, 166*(1), 1-7. doi:https://doi.org/10.1016/j.cis.2011.03.001

[55] Fenske, D. H. (1959). US.Flotation of mica from silt deposits, U. S. P. Office:International Minerals & Chemical Corporation.

[56] Finch, J., & Dobby, G. (1994). Column flotation, 1990: Pergamon Press.

[57] Finkelstein, N. (1979). Oil flotations—discussion *Beneficiation of Mineral Fines—Problems and Research Needs* (pp. 331-340): AIME USA.

[58] Finkelstein, N. (1997). The activation of sulphide minerals for flotation: a review. *International Journal of Mineral Processing, 52*(2), 81-120.

[59] Finkelstein, N., & Allison, S. (1976). Chemistry of Activation, Deactivation and Depression in the Flotation of Zinc Sulfide--Review. *Flotation--A. M. Gaudin Memorial*.

[60] Fornasiero, D., & Ralston, J. (2005). Cu (II) and Ni (II) activation in the flotation of quartz, lizardite and chlorite. *International Journal of Mineral Processing, 76*(1), 75-81.

[61] Fuerstenau, D. (1980). *Fine particle flotation.* Paper presented at the International Symposium on Fine Particles Processing New York.

[62] Fukui, Y., & Yuu, S. (1980). Collection of submicron particles in electro-flotation. *Chemical Engineering Science, 35*(5), 1097-1105.

[63] Garrett, P. (1992). *Defoaming: theory and industrial applications* (Vol. 45): CRC Press.

[64] Gaudin, A. M. (1957). Flotation: McGraw-Hill Book Company. Inc.

[65] Gaudin, A. M., Schuhmann Jr, R., & Schlechten, A. (1942). Flotation Kinetics. II. The Effect of Size on the Behavior of Galena Particles. *The Journal of Physical Chemistry, 46*(8), 902-910.

[66] Glembotskii, V., Mamakov, A., Romanov, A., & Nenno, V. (1975). *Selective separation of fine mineral slimes using the method of electric flotation.* Paper presented at the XI th International Mineral Processing Congress.

[67] Glembotsky, V. (1953). Rate of adhesion of air bubbles to mineral particles during flotation and methods for its measurement. *Izv. Akad. Nauk. SSSR*, 1524-1531.

[68] Good, R. (2012). *Surface and Colloid Science: Volume 11: Experimental Methods*: Springer Science & Business Media.

[69] Greaves, D., Boxall, J., Mulligan, J., Montesi, A., Creek, J., Sloan, E. D., & Koh, C. A. (2008). Measuring the particle size of a known distribution using the focused beam reflectance measurement technique. *Chemical Engineering Science, 63*(22), 5410-5419.

[70] Hadler, K., & Cilliers, J. J. (2009). The relationship between the peak in air recovery and flotation bank performance. *Minerals Engineering, 22*(5), 451-455. doi:https://doi.org/10.1016/j.mineng.2008.12.004

[71] Hancock, R. (1918). The rating of concentration tests. *Mining Magazine, 19*, 144-145.

[72] Harkins, W. D., & Feldman, A. (1922). Films. The spreading of liquids and the spreading coefficient. *Journal of the American Chemical Society, 44*(12), 2665-2685.

[73] Harris, G., DIAO, J., & Fuerstenau, D. (1995). Coal flotation with nonionic surfactants. *Coal Perparation, 16*(3-4), 135-147.

[74] He, T., Wan, H., Song, N., & Guo, L. (2011). The influence of composition of nonpolar oil on flotation of molybdenite. *Minerals Engineering, 24*(13), 1513-1516.

[75] Hemmings, C. E. (1980). An alternative viewpoint on flotation behavior of ultrafine particles. *Transactions of the Institution of Mining and Metallurgy Section C-Mineral Processing and Extractive Metallurgy, 89*(SEP), C113-C120.

[76] Hewitt, D., Fornasiero, D., & Ralston, J. (1995). Bubble–particle attachment. *Journal of the Chemical Society, Faraday Transactions, 91*(13), 1997-2001.

[77] Higgins, F. S., Magliocco, L. G., & Colthup, N. B. (2006). Infrared and Raman spectroscopy study of alkyl hydroxamic acid and alkyl hydroxamate isomers. *Applied spectroscopy, 60*(3), 279-287.

[78] Hobson, G. D., & Pohl, W. (1973). Modern petroleum technology.

[79] Hogan, P., Kuhn, A., & Turner, J. (1979). Electroflotation studies based on cassiterite ores. *Trans. Inst. Min. Metall. C, 88*.

[80] Hogg, R., Healy, T. W., & Fuerstenau, D. (1966). Mutual coagulation of colloidal dispersions. *Transactions of the Faraday Society, 62*, 1638-1651.

[81] Honaker, R., & Mohanty, M. (1996). Enhanced column flotation performance for fine coal cleaning. *Minerals Engineering, 9*(9), 931-945.

[82] Hoover, R., & Malhotra, D. (1976). Emulsion flotation of molybdenite. *Flotation--A. M. Gaudin Memorial*.

[83] Hu, W., Wang, D., & Qu, G. (1987). Principle and application of carrier flotation. *J. Cent. South. Inst. Min. metall., 4*, 408-414.

[84] Hu, W., Wang, D., & Qu, G. (1988). Autogenous carrier flotation *Proc. XVI Int. Miner. Process. Congr.* (pp. 445-452): Elsevier Amsterdam.

[85] Hughes, T. C. (2006). Hydroxamate composition and method for froth flotation: Google Patents.

[86] Hunter, R. (1986). *Foundations of Colloid Science* (Vol. 1,2): Oxford, New York.

[87] Iler, R. K. (1955). *The Colloid Chemistry of Silica and Silicates* (Vol. 80): LWW.

[88] Iler, R. K. (1979). The chemistry of silica, 1979. *Ed. J. Wiley and Sons, New York*.

[89] Israelachvili, J., & Pashley, R. (1982). The hydrophobic interaction is long range, decaying exponentially with distance. *Nature, 300*(5890), 341-342.

[90] Israelachvili, J., & Pashley, R. (1984). Measurement of the hydrophobic interaction between two hydrophobic surfaces in aqueous electrolyte solutions. *Journal of colloid and interface science, 98*(2), 500-514.

[91] Israelachvili, J. N. (2011). *Intermolecular and surface forces* (3rd ed.): Academic press.

[92] Jiangang, F., Kaida, C., Hui, W., Chao, G., & Wei, L. (2012). Recovering molybdenite from ultrafine waste tailings by oil agglomerate flotation. *Minerals Engineering, 39*, 133-139.

[93] Johansson, G., & Pugh, R. (1992). The influence of particle size and hydrophobicity on the stability of mineralized froths. *International Journal of Mineral Processing, 34*(1-2), 1-21.

[94] Johnson, N., McKee, D., & Lynch, A. (1974). Flotation rates of nonsulfide minerals in chalcopyrite flotation processes. *TRANS SOC MIN ENG, AIME, 256*(3), 204-209.

[95] Kail, N., Marquardt, W., & Briesen, H. (2009). Process analysis by means of focused beam reflectance measurements. *Industrial & engineering chemistry research, 48*(6), 2936-2946.

[96] Ketkar, D., Mallikarjunan, R., & Venkatachalam, S. (1991). Electroflotation of quartz fines. *International Journal of Mineral Processing, 31*(1), 127-138.

[97] Kirjavainen, V., Laapas, H., & Heiskanen, K. (1991). *The effect of some factors on the entrainment mechanism in froth flotation.* Paper presented at the Preprints of the XVII International Mineral Processing Congress, Dresden, FRG.

[98] Klassen, V. I., & Mokrousov, V. A. (1963). *An introduction to the theory of flotation*: Butterworths.

[99] Knecht, V., Levine, Z. A., & Vernier, P. T. (2010). Electrophoresis of neutral oil in water. *Journal of colloid and interface science, 352*(2), 223-231.

[100] Koczo, K., Koczone, J. K., & Wasan, D. T. (1994). Mechanisms for antifoaming action in aqueous systems by hydrophobic particles and insoluble liquids. *Journal of colloid and interface science, 166*(1), 225-238.

[101] Koczo, K., Lobo, L., & Wasan, D. (1992). Effect of oil on foam stability: aqueous foams stabilized by emulsions. *Journal of colloid and interface science, 150*(2), 492-506.

[102] Koh, P., & Warren, L. (1980). A pilot plant test of the shear-flocculation of ultrafine scheelite.

[103] Kulkarni, R., & Somasundaran, P. (1975). *Kinetics of oleate adsorption at the liquid/air interface and its role in hematite flotation.* Paper presented at the AIChE Symposium Series.

[104] Lai, R., & Fuerstenau, D. (1968). Liquid-liquid extraction of ultrafine particles. *Trans. AIME, 241*, 549-556.

[105] Laskowski, J. (1992). Oil assisted fine particle processing *Colloid Chemistry in Mineral Processing* (pp. 361-394): Elsevier Amsterdam.

[106] Laskowski, J., & Dai, Q. (1993). *Collector-extender flotation in the processing of coarse fractions of potash ores.* Paper presented at the Proc XVIII International Mineral Processing Congress.

[107] Laskowski, J., & Wang, Q. (1997). *Amine-containing oils as extenders in the flotation of sylvinite ores.* Paper presented at the Proc XX International Mineral Processing Congress.

[108] Laskowski, J. S., & Yu, Z. (2000). Oil agglomeration and its effect on beneficiation and filtration of low-rank/oxidized coals. *International Journal of Mineral Processing, 58*(1), 237-252.

[109] Lee, J., Nikolov, A., & Wasan, D. (2016). Stratification of a Foam Film Formed from a Nonionic Micellar Solution: Experiments and Modeling. *Langmuir, 32*(19), 4837-4847. doi:10.1021/acs.langmuir.6b00561

[110] Lee, L.-H. (2013). *Fundamentals of adhesion*: Springer Science & Business Media.

[111] Leja, J. (1982). Surface Chemistry of Froth Flotation (pp. 559-576): Plenum: New York, NY.

[112] Lidstrom, L. (1968). Surface and bond-forming properties of quartz and silicate minerals and their application in mineral processing techniques.

ACTA POLYTECHNICA SCANDINAVICA-CHEMISTRY INCLUDING METALLURGY SERIES(75), 7-&.

[113] Lifshitz, E. (1956). The theory of molecular attractive forces between solids. *Journal of Experimental Theoretical Physics, USSR, 29*, 94-110.

[114] Liu, A., Fan, M., & Fan, P. (2014). Interaction mechanism of miscible DDA–Kerosene and fine quartz and its effect on the reverse flotation of magnetic separation concentrate. *Minerals Engineering, 65*, 41-50.

[115] Liu, G., Zhang, H., Zhong, H., Liu, S., Zhao, G., & Xiao, J. (2015). China.CN 201410189143.Preparation method of hydroxamic acid or hydroxamic acid salt, Google Patents.

[116] Liu, J., Zhou, Z., & Xu, Z. (2002a). Electrokinetic study of hexane droplets in surfactant solutions and process water of bitumen extraction systems. *Industrial & engineering chemistry research, 41*(1), 52-57.

[117] Liu, J., Zhou, Z., Xu, Z., & Masliyah, J. (2002b). Bitumen–clay interactions in aqueous media studied by zeta potential distribution measurement. *Journal of colloid and interface science, 252*(2), 409-418.

[118] Liu, Q., Wannas, D., & Laskowski, J. (2004). *The role of polymeric-depressant-induced flocculation in fine particle flotation.* Paper presented at the Particle Size Enlargement in Mineral Processing, Proceedings of the UBC-McGill Biennial International Symposium on Fundamentals of Mineral Processing 5th, Hamilton, Canada.

[119] Llerena, C., Ho, J., & Piron, D. (1996). Effects of pH on electroflotaion of sphalerite. *Chemical Engineering Communications, 155*(1), 217-228.

[120] Lobo, L., Nikolov, A., & Wasan, D. (1989). Foam stability in the presence of oil: on the importance of the second virial coefficient. *JOURNAL OF DISPERSION SCIENCE ANDTECHNOLOGY, 10*(2), 143-161.

[121] Lobo, L., & Wasan, D. (1993). Mechanisms of aqueous foam stability in the presence of emulsified non-aqueous-phase liquids: structure and stability of the pseudoemulsion film. *Langmuir, 9*(7), 1668-1677.

[122] Lu, S., Zhou, Q., Xu, H., Zou, J., & Duan, Q. (1997). *Surfactant-synergy in fatty acid flotation.* Paper presented at the Proc. XX Int. Min. Process. Congress, Aachen.

[123] Luzar, A., Svetina, S., & Žekš, B. (1983). The contribution of hydrogen bonds to the surface tension of water. *Chemical Physics Letters, 96*(4), 485-490.

[124] Mamakov, A., Sorokina, V., Avvakumov, M., & Bureau, C. (1970). *Electroflotability of cassiterite*: Consultants Bureau.

[125] Mao, L. (1998). *Application of Extended DLVO Theory: Modeling of Flotation and Hydrophobicity of Dodecane.* Virginia Tech.

[126] Mathur, S., Singh, P., & Moudgil, B. (2000). Advances in selective flocculation technology for solid-solid separations. *International Journal of Mineral Processing, 58*(1), 201-222.

[127] Matis, K., & Backhurst, J. (1984). *Laboratory studies of electrolytic flotation as a separation technique.* Paper presented at the Solid–Liq Sep.(ap.-Symp. Adv. Solid–Liq. Sep.).

[128] Matis, K. A. (1994). *Flotation science and engineering*: CRC Press.

[129] McKay, J., Foot, D., & Huiatt, J. (1986). Column flotation of Montana chromite ore. *Miner. Metall. Process., 2*, 170.

[130] Mehrotra, V., Sastry, K., & Morey, B. (1983). Review of oil agglomeration techniques for processing of fine coals. *International Journal of Mineral Processing, 11*(3), 175-201.

[131] Michaud, D. (2016). Column Cells. Retrieved from https://www.911metallurgist.com/blog/column-cells.

[132] Miettinen, T., Ralston, J., & Fornasiero, D. (2010). The limits of fine particle flotation. *Minerals Engineering, 23*(5), 420-437.

[133] Mishchuk, N., Ralston, J., & Fornasiero, D. (2002). Influence of dissolved gas on van der Waals forces between bubbles and particles. *The Journal of Physical Chemistry A, 106*(4), 689-696.

[134] Mishchuk, N., Ralston, J., & Fornasiero, D. (2006). Influence of very small bubbles on particle/bubble heterocoagulation. *Journal of colloid and interface science, 301*(1), 168-175.

[135] Mitchell, B. S. (2004). *An introduction to materials engineering and science for chemical and materials engineers*: John Wiley & Sons.

[136] Mitchell, T. K., Nguyen, A. V., & Evans, G. M. (2005). Heterocoagulation of chalcopyrite and pyrite minerals in flotation separation. *Advances in Colloid and Interface Science, 114*, 227-237.

[137] Morris, T. (1950). Measurement of equilibrium forces between an air bubble and an attached solid in water. *Trans. AIME, 187*, 91-95.

[138] Moudgil, B., Shah, B., & Soto, H. (1987). Loss of selectivity in apatite-dolomite flocculation. *Minerals and Metallurgical Processing, 4*(2), 27-31.

[139] Narasimhan, K., Rao, S., & Choudhury, G. (1972). Column flotation improves graphite recovery. *Eng. Min. J., 163*, 84-85.

[140] Natarajan, R. (2013). Hydroxamic Acids as Chelating Mineral Collectors *Hydroxamic Acids* (pp. 281-307): Springer.

[141] Newitt, D. (1958). M. & CONWAY-JONES, J. *Trans. Inst. Chem. Engrs*.

[142] Nguyen, A., & Schulze, H. (2004). Colloidal Science of Flotation Marcel Dekker. *New York, 840pp*.

[143] Nguyen, A. V., George, P., & Jameson, G. J. (2006). Demonstration of a minimum in the recovery of nanoparticles by flotation: theory and experiment. *Chemical Engineering Science, 61*(8), 2494-2509.

[144] Ni, X. (2013). *Direct Flotation of Niobium Oxide Minerals from Carbonatite Niobium Ores*: University of Alberta.

[145] Niewiadomski, M., Hupka, J., Nalaskowski, J., & Miller, J. (2001). Dispersed oil impact on froth stability in flotation. *Physicochemical Problems of Mineral Processing, 35*, 5-19.

[146] Nikolov, A., Kralchevsky, P., Ivanov, I., & Wasan, D. (1989). Ordered micelle structuring in thin films formed from anionic surfactant solutions: II. Model development. *Journal of colloid and interface science, 133*(1), 13-22.

[147] Nikolov, A., & Wasan, D. (1989). Ordered micelle structuring in thin films formed from anionic surfactant solutions: I. Experimental. *Journal of colloid and interface science, 133*(1), 1-12.

[148] O'Connor, C., & Dunne, R. (1994). The flotation of gold bearing ores—a review. *Minerals Engineering, 7*(7), 839-849.

[149] Overbeek, & Verwey. (1948). *Theory of the Stability of Lyophobic Colloids: The interaction of Sol Particles Having an Electric Double Layer*.

[150] Owen, J. J., Morse, D. E., Morse, W., & Jovine, R. (1999). New developments in flotation equipment for water treatment systems. *Advances in Flotation Technology*, 381-389.

[151] Ozkan, A., Dudnik, V., & Esmeli, K. (2016). Hydrophobic flocculation of talc with kerosene and effects of anionic surfactants. *Particulate Science and Technology, 34*(2), 235-240.

[152] Öztürk, F., & Temel, H. A. (2013). Reverse flotation in Muş-Elmakaya lignite beneficiation. *Energy Sources, Part A: Recovery, Utilization, and Environmental Effects, 35*(8), 695-705.

[153] Parfitt, G. (1973). Fundamental aspects of dispersion *Dispersion of powders in liquids* (pp. 31): Applied Science.

[154] Parks, G. A. (1965). The isoelectric points of solid oxides, solid hydroxides, and aqueous hydroxo complex systems. *Chemical Reviews, 65*(2), 177-198.

[155] Parsonage, P. (1984). Effects of slime and colloidal particles on the flotation of galena. *Flotation of sulphide minerals*, 111-139.

[156] Pascoe, R., & Doherty, E. (1997). Shear flocculation and flotation of hematite using sodium oleate. *International Journal of Mineral Processing, 51*(1-4), 269-282.

[157] Pashley, R. M., McGuiggan, P. M., Ninham, B. W., & Evans, D. F. (1985). Attractive forces between uncharged hydrophobic surfaces: direct measurements in aqueous solution. *Science, 229*, 1088-1090.

[158] Pattanaik, M., Biswal, S., & Bhaumik, S. (2000). A comparative physicochemical study of hematite with hydroxamic acid and sodium oleate. *Separation Science and Technology, 35*(6), 919-930.

[159] Pavez, O., Brandao, P., & Peres, A. (1996). Adsorption of oleate and octyl-hydroxamate on to rare-earths minerals. *Minerals Engineering, 9*(3), 357-366.

[160] Philippoff, W. (1952). Some dynamic phenomena in flotation. *Trans. Amer. Inst. Min. Enggrs. Min. Engng, 193*, 386-390.

[161] Prud'homme, R. K. (1995). *Foams: Theory: Measurements: Applications* (Vol. 57): CRC Press.

[162] Pugh, R. (1996). Foaming, foam films, antifoaming and defoaming. *Advances in Colloid and Interface Science, 64*, 67-142.

[163] Pyke, B., Fornasiero, D., & Ralston, J. (2003). Bubble particle heterocoagulation under turbulent conditions. *Journal of colloid and interface science, 265*(1), 141-151.

[164] Qu, X., Wang, L., & Nguyen, A. V. (2013). Correlation of air recovery with froth stability and separation efficiency in coal flotation. *Minerals Engineering, 41*(Supplement C), 25-30. doi:https://doi.org/10.1016/j.mineng.2012.10.013

[165] Raghavan, S., & Fuerstenau, D. W. (1975). The adsorption of aqueous octylhydroxamate on ferric oxide. *Journal of colloid and interface science, 50*(2), 319-330. doi:https://doi.org/10.1016/0021-9797(75)90235-0

[166] Rajagopalan, R., & Hiemenz, P. C. (1997). Principles of colloid and surface chemistry. *Marcel Dekker, New-York, 3e édition, ISBN 0, 8247*(9397), 8.

[167] Raju, G. B., & Khangaonkar, P. (1982). Electro-flotation of chalcopyrite fines. *International Journal of Mineral Processing, 9*(2), 133-143.

[168] Raju, G. B., & Khangaonkar, P. (1984). Electroflotation of chalcopyrite fines with sodium diethyldithiocarbamate as collector. *International Journal of Mineral Processing, 13*(3), 211-221.

[169] Rao, G. (1997). Spherical agglomeration of scheelite fines with amphoteric collector. *METALS MATERIALS AND PROCESSES, 9*(1), 57-63.

[170] Rao, K. H., Cases, J., De Donato, P., & Forssberg, K. (1991). Mechanism of oleate interaction on salt-type minerals: IV. Adsorption, electrokinetic, and diffuse reflectance FT-IR studies of natural fluorite in the presence of sodium oleate. *Journal of colloid and interface science, 145*(2), 314-329.

[171] Read, A. (1972). The use of high molecular weight polyacrylamides in the selective flocculation separation of a mineral mixture. *British Polymer Journal, 4*(3), 253-264.

[172] Reay, D., & Ratcliff, G. (1973). Removal of fine particles from water by dispersed air flotation: effects of bubble size and particle size on collection efficiency. *The Canadian Journal of chemical engineering, 51*(2), 178-185.

[173] Rubin, A. J. (1972). Removal and use of hydrolyzable metals in foam separations *Adsorptive bubble separation techniques* (pp. 199-217): Academic Press New York, NY.

[174] Rubin, A. J., & Haberkost, D. C. (1973). Coagulation and flotation of colloidal titanium dioxide. *Separation Science, 8*(3), 363-373.

[175] Rubio, J. (1996). Modified column flotation of mineral particles. *International Journal of Mineral Processing, 48*(3), 183-196.

[176] Rubio, J., Capponi, F., Matiolo, E., Nunes, D., Guerrero, C., & Berkowitz, G. (2003). *Advances in flotation of mineral fines.* Paper presented at the Proceedings of the XXII International Mineral Processing Congress, Cape-Town, Africa do Sul.

[177] Rubio, J., Capponi, F., Rodrigues, R., & Matiolo, E. (2007). Enhanced flotation of sulfide fines using the emulsified oil extender technique. *International Journal of Mineral Processing, 84*(1), 41-50.

[178] Rubio, J., & Kitchener, J. (1977). New basis for selective flocculation of mineral slimes. *Transactions of the Institution of Mining and Metallurgy Section C-Mineral Processing and Extractive Metallurgy, 86*(SEP), C97-C100.

[179] Rubio, J., & Marabini, A. (1987). Factors affecting the selective flocculation of hydroxyapatite from quartz and/or calcite mixtures. *International Journal of Mineral Processing, 20*(1), 59-71.

[180] Rubio, J., Souza, M., & Smith, R. (2002). Overview of flotation as a wastewater treatment technique. *Minerals Engineering, 15*(3), 139-155.

[181] Sadowski, Z. (1998). Hydrophobic Agglomeration of Fine Particles *Mineral Processing and the Environment* (pp. 3-24): Springer.

[182] Sahinoglu, E., & Uslu, T. (2008). Amenability of Muzret bituminous coal to oil agglomeration. *Energy Conversion and Management, 49*(12), 3684-3690.

[183] Sayed, S. A., & Zayed, A. M. (2006). Investigation of the effectiveness of some adsorbent materials in oil spill clean-ups. *Desalination, 194*(1), 90-100. doi:https://doi.org/10.1016/j.desal.2005.10.027

[184] Schulze, H. J., & Gottschalk, G. (1981). Experimental investigation of hydrodynamic interaction of particles with a gas buble. *Colloid Journal of the USSR, 43*(5), 757-765.

[185] Schwarz, S., & Grano, S. (2005). Effect of particle hydrophobicity on particle and water transport across a flotation froth. *Colloids and Surfaces A: Physicochemical and Engineering Aspects, 256*(2), 157-164.

[186] Seitz, R., & Kawatra, S. (1986). The role of nonpolar oils as flotation reagents. *Chapter, 19*, 171-180.

[187] Sen, S., Seyrankaya, A., & Cilingir, Y. (2005). Coal–oil assisted flotation for the gold recovery. *Minerals Engineering, 18*(11), 1086-1092.

[188] Shaw, D. (1992). Introduction to surface and colloid chemistry: Butterworth-Heinemann: London.

[189] Shergold, H., & Stratton-Crawley, R. (1981). Extraction of titanium dioxide into oil from anionic surfactant solutions. *Colloids and Surfaces, 3*(3), 253-265.

[190] Shi, J. C. (1986). Method of beneficiating kaolin clay utilizing ammonium salts: Google Patents.

[191] Sis, H. (2001). *Enhancing flotation recovery of phosphate ores using nonionic surfactants.* (Ph.D.), The Pennsylvania State University.

[192] Siwek, Zembala, M., & Pomianowski, A. (1981). A method for determination of fine-particle flotability. *International Journal of Mineral Processing, 8*(1), 85-88.

[193] Smit, F., & Bhasin, A. (1985). Relationship of petroleum hydrocarbon characteristics and molybdenite flotation. *International Journal of Mineral Processing, 15*(1-2), 19-40.

[194] Smith, P., & Warren, L. (1989). Entrainment of particles into flotation froths. *Mineral Procesing and Extractive Metallurgy Review, 5*(1-4), 123-145.

[195] Solari, J. (1980). Selective dissolved air flotation of fine minerals particles. *Doctor thesis, University of London–Imperial College, 292p*.

[196] Solari, J. A., & Gochin, R. J. (1992). Fundamental aspects of microbubbles flotation. *Colloid Chemistry in Mineral Processing. Development in Mineral Processing, 12*, 395-418.

[197] Somasundaran, P. (1980a). *Fine particles processing*: American Institute of Mining, Metallurgical, and Petroleum Engineers.

[198] Somasundaran, P. (1980b). Role of surface chemistry of fine sulphides in their flotation. *Complex Sulphide Ores*, 38.

[199] Somasundaran, P. (1986). An overview of the ultrafine problem *Mineral Processing at a Crossroads* (pp. 1-36): Springer.

[200] Somasundaran, P. (1987). *Reagents in mineral technology* (Vol. 27): CRC Press.

[201] Somasundaran, P., & Wang, D. (2006). *Solution chemistry: minerals and reagents* (Vol. 17): Elsevier.

[202] Somasundaran, P., & Zhang, L. (2006). Adsorption of surfactants on minerals for wettability control in improved oil recovery processes. *Journal of Petroleum Science and Engineering, 52*(1), 198-212.

[203] Song, Lopez-Valdivieso, A., & Ding, Y. (1999a). Effects of nonpolar oil on hydrophobic flocculation of hematite and rhodochrosite fines. *Powder Technology, 101*(1), 73-80.

[204] Song, Lopez-Valdivieso, A., Reyes-Bahena, J., & Lara-Valenzuela, C. (2001a). Floc flotation of galena and sphalerite fines. *Minerals Engineering, 14*(1), 87-98.

[205] Song, Lopez-Valdivieso, A., Reyes-Bahena, J. L., Bermejo-Perez, H. I., & Trass, O. (2000). Hydrophobic flocculation of galena fines in aqueous suspensions. *Journal of colloid and interface science, 227*(2), 272-281.

[206] Song, Zhang, X., Yang, B., & Lopez-Mendoza, A. (2012). Flotation of molybdenite fines as hydrophobic agglomerates. *Separation and Purification Technology, 98*, 451-455.

[207] Song, S., Lopez-Valdivieso, A., & Ding, Y. (1999b). Effects of nonpolar oil on hydrophobic flocculation of hematite and rhodochrosite fines. *Powder Technology, 101*(1), 73-80.

[208] Song, S., Lopez-Valdivieso, A., Reyes-Bahena, J., & Lara-Valenzuela, C. (2001b). Floc flotation of galena and sphalerite fines. *Minerals Engineering, 14*(1), 87-98.

[209] Song, S., Lu, S., & Lopez-Valdivieso, A. (2002). Magnetic separation of hematite and limonite fines as hydrophobic flocs from iron ores. *Minerals Engineering, 15*(6), 415-422.

[210] Sönmez, I., & Cebeci, Y. (2003a). Fundamental aspects of spherical oil agglomeration of calcite. *Colloids and Surfaces A: Physicochemical and Engineering Aspects, 225*(1), 111-118.

[211] Sönmez, I., & Cebeci, Y. (2003b). A study on spherical oil agglomeration of barite suspensions. *International Journal of Mineral Processing, 71*(1), 219-232.

[212] Soto, H., & Iwasaki, I. (1986). Selective flotation of phosphates from dolomite using cationic collectors. I. Effect of collector and nonpolar hydrocarbons. *International Journal of Mineral Processing, 16*(1), 3-16.

[213] Sparks, R. G., & Dobbs, C. L. (1993). The use of laser backscatter instrumentation for the on‐line measurement of the particle size distribution of emulsions. *Particle & particle systems characterization, 10*(5), 279-289.

[214] Speight, J. G. (2014). *The chemistry and technology of petroleum*: CRC press.

[215] Srdjan, M. B. (2007). *Handbook of Flotation Reagents Chemistry, Theory and Practice: Flotation of Sulfide Ores*: Elsevier Science & Technology Books.

[216] Sresty, G., & Somasundaran, P. (1977). Beneficiation of mineral slimes using modified polymers as selective flocculants. *12th International Mineral Processing Congr., Sao Paulo, Brazil*.

[217] Stachurski, J., & MichaŁek, M. (1985). The zeta potential of emulsion droplets of the aliphatic hydrocarbons in aqueous solutions. *Colloids and Surfaces, 15*, 255-259.

[218] Stratton-Crawley, R., & Shergold, H. (1981). Extraction of titanium dioxide into oil from cationic surfactant solutions. *Colloids and Surfaces, 2*(2), 145-154.

[219] Subrahmanyam, T. V., & Forssberg, E. (1988). Froth stability, particle entrainment and drainage in flotation — A review. *International Journal of Mineral Processing, 23*(1), 33-53. doi:https://doi.org/10.1016/0301-7516(88)90004-X

[220] Sutherland, K. (1948). Physical chemistry of flotation. XI. Kinetics of the flotation process. *The Journal of Physical Chemistry, 52*(2), 394-425.

[221] Termes, S. C., & Wilfong, R. L. (1985). *Flocculation of metal oxide and hydroxide minerals with cross-linked starches containing chelating groups*: US Department of the interior, Bureau of Mines.

[222] Tian, J., Gao, H., Guan, J., & Ren, Z. (2017). Modified floc-flotation in fine sericite flotation using polymethylhydrosiloxane. *Separation and Purification Technology, 174*(Supplement C), 439-444. doi:https://doi.org/10.1016/j.seppur.2016.10.051

[223] Trahar, W., & Warren, L. (1976). The flotability of very fine particles—a review. *International Journal of Mineral Processing, 3*(2), 103-131.

[224] Tummons, E. N. (2016). *Oil droplet behavior at the membrane surface during filtration of oil-water emulsions.* Michigan State University.

[225] Varley, T. (1928). *Reports of Investigation* (Serial No. 2852). Retrieved from Washington, DC.

[226] Vaysse, L., Dubreucq, E., Pirat, J.-L., & Galzy, P. (1997). Fatty hydroxamic acid biosynthesis in aqueous medium in the presence of the lipase-acyltransferase from Candida parapsilosis. *Journal of biotechnology, 53*(1), 41-46.

[227] Walton, A. G., Füredi, H., Elving, P. J., & Kolthoff, I. M. (1967). The formation and properties of precipitates.

[228] Wang, D. (2016a). Collectors for Nonsulfide Minerals *Flotation Reagents: Applied Surface Chemistry on Minerals Flotation and Energy Resources Beneficiation* (pp. 69-113): Springer.

[229] Wang, D. (2016b). *Flotation Reagents: Applied Surface Chemistry on Minerals Flotation and Energy Resources Beneficiation: Volume 2: Applications*: Springer.

[230] Wang, Q., & Heiskanen, K. (1992). Dispersion selectivity and heterocoagulation in apatite-hematite-phlogopite fine particle suspensions II. Dispersion selectivities of the mineral mixtures. *International Journal of Mineral Processing, 35*(1), 133-145.

[231] Wang, Y.-H. C., & Somasundaran, P. (1980). A study of carrier flotation of clay *Fine particles processing* (Vol. 2, pp. 1112-1128): SME of AIME Denver, Co.

[232] Warren, L. (1984). *Ultrafine particles in flotation.* Paper presented at the Principles of Mineral Flotation-The Wark Symposium.

[233] Warren, L. (1992). Shear flocculation *Colloid Chemistry in Mineral Processing* (Vol. 12, pp. 309-329): Elsevier Amsterdam.

[234] Welch, A. (1953). The relation of crystal lattice discontinuities in mineral dressing *Recent Development in Mineral Dressing* (pp. 192-387): IMM London.

[235] Whelan, P., & Brown, D. (1956). Particle-bubble attachment in froth flotation. *Bulletin of the Institute of Mining and Metallurgy*(591), 181-192.

[236] Williams, D. L., Gantt, G. E., Behl, S., & Willis, M. J. (1997). Method for separating mixture of finely divided minerals: Google Patents.

[237] Wills, B. A. (2011). *Wills' mineral processing technology: an introduction to the practical aspects of ore treatment and mineral recovery* (7 ed.): Butterworth-Heinemann.

[238] Wojcik, W., & Al Taweel, A. (1984). Beneficiation of coal fines by aggregative flotation. *Powder Technology, 40*(1), 179-185.

[239] Wong, J. (2013). Clarifying Treatment: Dissolved air flotation provides alternative for treating raw water with light particles. *WaterWorld, 29*(8).

[240] Xu, Z., Liu, J., Choung, J., & Zhou, Z. (2003). Electrokinetic study of clay interactions with coal in flotation. *International Journal of Mineral Processing, 68*(1-4), 183-196.

[241] Xu, Z., & Yoon, R.-H. (1989). The role of hydrophobia interactions in coagulation. *Journal of colloid and interface science, 132*(2), 532-541.

[242] Yalcin, T., Byers, A., & Ughadpaga, K. (2002). Dissolved gas method of generating bubbles for potential use in ore flotation. *Mineral Processing and Extractive Metallurgy Review, 23*(3-4), 181-197.

[243] Yamaji, T., Saito, T., Hayamizu, K., Yanagisawa, M., Yamamoto, O., Wasada, N., . . . Tamura, T. (2014). Spectral database for organic compounds, SDBS. *National Institute of Advanced Industrial Science and technology (AIST),(14 Oct 2011). http://riodb01. ibase. aist. go. jp/sdbs/cgi-bin/cre_index. cgi*.

[244] Yang, S.-M., Han, S. P., & Hong, J. J. (1995). Capture of small particles on a bubble collector by Brownian diffusion and interception. *Journal of colloid and interface science, 169*(1), 125-134.

[245] Ye, Y., & Miller, J. (1988). Bubble/particle contact time in the analysis of coal flotation. *Coal Perparation, 5*(3-4), 147-166.

[246] Ying, L., Li, H., & Feng, Q. (2015). Entrainment behavior and control of sericite. *Journal of Central South University: natural science edition, 46*(1), 20-26.

[247] Yoon, R.-H., Flinn, D. H., & Rabinovich, Y. I. (1997). Hydrophobic interactions between dissimilar surfaces. *Journal of colloid and interface science, 185*(2), 363-370.

[248] Yoon, R.-H., & Mao, L. (1996). Application of extended DLVO theory, IV: derivation of flotation rate equation from first principles. *Journal of colloid and interface science, 181*(2), 613-626.

[249] Yoon, R., & Luttrell, G. (1989). The effect of bubble size on fine particle flotation. *Mineral Procesing and Extractive Metallurgy Review, 5*(1-4), 101-122.

[250] Yoon, R., & Luttrell, G. (1992). *Development of the selective hydrophobic coagulation process* (DOE/PC/91164-T1). Retrieved from Virginia Center for Coal and Minerals Processing, Blacksburg, VA (United States).

[251] Yoon, R., Luttrell, G., Adel, G., & Mankosa, M. (1989). Recent advances in fine coal flotation. *Advances in Coal and Mineral Processing Using Flotation*, 211-218.

[252] YOON, R., & SHI, J. (1986). *Processing of kaolin clay. Advance in Mineral Processing.* Paper presented at the Proceedings of the Arbiter Symposium, ed. AIME, New York.

[253] Yotsumoto, H., & Yoon, R.-H. (1993). Application of extended DLVO theory: I. Stability of rutile suspensions. *Journal of colloid and interface science, 157*(2), 426-433.

[254] Yu, S., & Attia, Y. (1988). Entrapment and entrainment in selective flocculation process, part 2: possible methods for minimization of entrapment and entrainment. *Interfacial Phenomena in Biotechnology and Materials Processing. Elsevier, Amsterdam*, 503-514.

[255] Zanin, M., Ametov, I., Grano, S., Zhou, L., & Skinner, W. (2009). A study of mechanisms affecting molybdenite recovery in a bulk copper/molybdenum flotation circuit. *International Journal of Mineral Processing, 93*(3), 256-266.

[256] Zeppieri, S., Rodríguez, J., & López de Ramos, A. (2001). Interfacial tension of alkane+ water systems. *Journal of Chemical & Engineering Data, 46*(5), 1086-1088.

[257] Zhou, F., Wang, L., Xu, Z., Liu, Q., Deng, M., & Chi, R. (2014). Application of reactive oily bubbles to bastnaesite flotation. *Minerals Engineering, 64*, 139-145.

[258] Zhou, F., Yan, C., Wang, H., Sun, Q., Wang, Q., & Alshameri, A. (2015). Flotation behavior of four C18 hydroxamic acids as collectors of rhodochrosite. *Minerals Engineering, 78*, 15-20.

[259] Zhou, Z., Xu, Z., Finch, J., Hu, H., & Rao, S. (1997). Role of hydrodynamic cavitation in fine particle flotation. *International Journal of Mineral Processing, 51*(1), 139-149.

[260] Zollars, R. L., & Ali, S. I. (1986). Shear coagulation in the presence of repulsive interparticle forces. *Journal of colloid and interface science, 114*(1), 149-166.